

**NASA  
Technical  
Paper  
2615**

July 1986

*Ames*

# General Equilibrium Characteristics of a Dual-Lift Helicopter System

L. S. Cicolani  
and G. Kanning

(NASA-TP-2615) GENERAL EQUILIBRIUM  
CHARACTERISTICS OF A DUAL-LIFT HELICOPTER  
SYSTEM (NASA) 86 p CSCL 01B

N88-19407

Unclas  
H1/01 0131749

**NASA**

**NASA  
Technical  
Paper  
2615**

1986

# General Equilibrium Characteristics of a Dual-Lift Helicopter System

L. S. Cicolani  
and G. Kanning

*Ames Research Center  
Moffett Field, California*

**NASA**

National Aeronautics  
and Space Administration

Scientific and Technical  
Information Branch

TABLE OF CONTENTS

	Page
SYMBOLS.....	v
SUMMARY.....	1
1. INTRODUCTION.....	2
2. NOTATION AND ASSUMPTIONS.....	5
3. FORCE-BALANCE EQUATIONS.....	12
4. ACCELERATIONS AND AERODYNAMICS.....	17
Accelerations.....	17
Helicopter Aerodynamic Forces.....	19
Load Aerodynamic Forces.....	21
5. RESULTS FROM THE LOAD EQUATION.....	24
6. BRIDLE TRIANGLE ATTITUDE.....	26
7. SPREADER-BAR AND HELICOPTER EQUATIONS: GENERAL RESULTS.....	34
8. SPREADER-BAR AND HELICOPTER EQUATIONS: TETHER-ANGLE OPTIMIZATION.....	41
A Suboptimum Configuration.....	43
Minimum Thrust-Sum Configuration.....	44
Results for Identical Helicopters and Equal Load Sharing.....	47
Results for Parallel Apparent Loads.....	50
General Results for Minimum Thrust-Sum Configuration.....	53
9. LOAD DISTRIBUTION.....	58
10. GENERAL EQUILIBRIUM CONFIGURATIONS.....	62
11. CONCLUSIONS.....	71
APPENDIX.....	74
REFERENCES.....	76

PRECEDING PAGE BLANK NOT FILMED

## SYMBOLS

A	magnitude of mutually canceling components of bridle cable forces along spreader bar
<u>a</u> ; <u>a<sub>l</sub></u> , <u>a<sub>b</sub></u> , <u>a<sub>1</sub></u> , <u>a<sub>2</sub></u>	c.g. accelerations; appended symbols <u>l</u> , <u>b</u> , <u>1</u> , <u>2</u> , indicate the body as load, spreader bar, helicopter no. 1 or 2, respectively
B	modified spreader-bar compression, $F_{34} + A$
D	helicopter rotor diameter or drag force
d	drag force per unit weight
<u>F<sub>a</sub></u>	aerodynamic force; appended symbol ( <u>l</u> , <u>b</u> , <u>1</u> , <u>2</u> ) indicates body
F <sub>ij</sub>	forces transmitted by cables and spreader bar; F <sub>ij</sub> is enumerated as F <sub>13</sub> , F <sub>34</sub> , etc., to specify the system link (see fig. 1.1); F <sub>ij</sub> is positive (negative) for tension (compression)
<u>f<sub>a</sub></u> ; <u>f<sub>a<sub>l</sub></sub></u> , <u>f<sub>a<sub>b</sub></sub></u> , <u>f<sub>a<sub>1</sub></sub></u> , <u>f<sub>a<sub>2</sub></sub></u>	aerodynamic force per unit weight (specific force); appended symbol indicates body
<u>f<sub>l</sub></u> , <u>f<sub>b</sub></u> , <u>f<sub>1</sub></u> , <u>f<sub>2</sub></u>	specific apparent loads ( $g + \underline{f_a} - \underline{a}$ ) owing to the component masses of the system
f <sub>l</sub> , f <sub>b</sub> , f <sub>1</sub> , f <sub>2</sub>	magnitudes of <u>f<sub>l</sub></u> , <u>f<sub>b</sub></u> , <u>f<sub>1</sub></u> , <u>f<sub>2</sub></u>
<u>f<sub>3</sub></u> , <u>f<sub>4</sub></u>	equivalent apparent loads for the spreader-bar endpoints, $\underline{f_b} - \underline{\Delta f}$ , $\underline{f_b} + \underline{\Delta f}$ (eq. 3.1)
g, g	gravity vector and magnitude
<u>H<sub>b</sub></u>	spreader-bar angular momentum
<u>i</u> , <u>j</u> , <u>k</u>	axes defining an orthogonal right-handed reference frame; subscripts H, N, t indicate the frame as level-heading, level-north axes, or body axes for the triangle, respectively
J	inertia matrix; appended symbol indicates body
L <sub>ij</sub>	cables and spreader bar lengths; L <sub>ij</sub> is enumerated as L <sub>13</sub> , L <sub>34</sub> , etc., to specify the link

$\underline{\ell}_1, \underline{\ell}_2, \underline{\ell}_3, \underline{\ell}_4$	apparent load difference nondimensionalized by $m_{\ell} f_{\ell}$ ; e.g., $\underline{\ell}_2 = m_2(f_2 - f_{\ell})/m_{\ell} f_{\ell}$
$M_a$	aerodynamic moment; appended symbol ( $\ell, b, 1, 2$ ) indicates body
$M_1, M_2, M_T$	thrust margins of helicopters and dual-lift system
$m$	mass; subscripts $\ell, b, 1, 2$ indicate mass of load, spreader bar, helicopter no. 1 or 2
$P$	power
$PL_1, PL_2$	helicopter payloads
$p$	locus of required optimum thrust combinations ( $T_1^*, T_2^*$ ) as $\epsilon_{\ell}$ varies over its range
$Q$	dynamic pressure, $0.5 \rho V a^2$ ; subscript indicates the body
$R_{ij}$	directed line segment between two connected points on the configuration, $R_j - R_i$ ; $R_{ij}$ is enumerated as $R_{13}, R_{34}$ , etc., to specify the link
$\underline{R}_o(t), \underline{V}_o(t), \underline{a}_o(t)$	reference trajectory position, velocity, acceleration time-histories
$\underline{R}_1, \underline{R}_2, \underline{R}_3, \underline{R}_4, \underline{R}_5$	points on the dual-lift configuration (helicopter and load attachment points and spreader-bar endpoints) (see fig. 1.1)
$T_{a,b}$	transformation of vector coordinates from reference frame "b" to frame "a"; the subscripts can be any of H, N, t for the frames used here
$\underline{T}_1, \underline{T}_2, T_1, T_2$	helicopter thrust force vectors and magnitudes
$T_{1_{\max}}, T_{2_{\max}}$	helicopter thrust limits
$\mathcal{S}$	available thrust combinations ( $T_1, T_2$ ) for $T_1 \leq T_{1_{\max}}, T_2 \leq T_{2_{\max}}$
$\underline{u}_{\ell}, \underline{u}_1, \underline{u}_2, \underline{u}_{ij}$	unit vectors along $\underline{f}_{\ell}, -\underline{T}_1, -\underline{T}_2, \underline{R}_{ij}$
$(u_{\ell_x}, u_{\ell_y}, u_{\ell_z})$	components of $\underline{u}_{\ell}$ in level-heading axes
$\underline{V}, \underline{V}_a, V, V_a, V_e$	inertial and air velocity vectors and magnitudes, and equivalent airspeed; appended letters indicate the body
$\dot{v}$	speed rate

$W$	weight; subscript ( $l, b, 1, 2$ ) indicates body
$\dot{w}_f$	fuel rate
$(\alpha, \beta)$	aerodynamic angles defining direction of air velocity vector in body axes: $\underline{V}_a = V_a(\cos \alpha \cos \beta \underline{i} + \sin \beta \underline{j} + \sin \alpha \sin \beta \underline{k})$ ; subscripts indicate body
$\alpha_1, \alpha_2, \alpha_3, \alpha_4$	$\alpha = [\underline{v} \cdot \underline{j}_t^2 + \underline{v} \cdot \underline{k}_t^2]^{1/2}$ where $\underline{v}$ is $\underline{T1}^\circ, \underline{T2}^\circ, \underline{F13}^\circ, \underline{F24}^\circ$ in $\alpha_1, \alpha_2, \alpha_3, \alpha_4$ , respectively
$\beta_b, \beta_h$	weight-to-payload ratios $(W_b, W_1 + W_2)/(PL1 + PL2)$
$\beta_t$	spreader-bar heading relative to the ground track
$(\gamma, \psi_V)$	direction angles (flightpath and heading angles) of a velocity vector in level north axes: $\underline{V} = V(\cos \gamma \cos \psi_V \underline{i}_N + \cos \gamma \sin \psi_V \underline{j}_N - \sin \gamma \underline{k}_N)$
$\delta$	bridle cable angle (fig. 1.1)
$(\epsilon, \lambda)$	direction angles of a vector in triangle axes: $\underline{u} = -\sin \epsilon \underline{i}_t + \cos \epsilon \sin \lambda \underline{j}_t + \cos \epsilon \cos \lambda \underline{k}_t$ ; subscripts indicate the corresponding vector
$\mu$	fraction of $\underline{f1}$ carried by helicopter No. 1 in the configuration with $F34 = -A$
$(\xi_\ell, \beta_{u\ell})$	direction angles (angle from vertical and heading) of $\underline{u\ell}$ in level heading axes: $\underline{u\ell} = \sin \xi_\ell \cos \beta_{u\ell} \underline{i}_H + \sin \xi_\ell \sin \beta_{u\ell} \underline{j}_H + \cos \xi_\ell \underline{k}_N$
$\rho_b, \rho_T, \rho_{Tx}$	force ratios for bridle cables (F35/F45), thrust (T1/T2) and thrust limits $(T1_{max}/T2_{max})$
$\Sigma$	angle defined in context (sec. 6)
$\Sigma T, \Sigma T_{max}, \Sigma \dot{w}_f$	scalar sums of thrust magnitudes, thrust limits, and fuel rates, respectively
$\underline{\Sigma L}, \Sigma L$	sum of apparent loads, $m_\ell \underline{f\ell} + m_b \underline{fb} + m_1 \underline{f1} + m_2 \underline{f2}$ , and its magnitude
$(\phi, \theta, \psi)$	Euler angles of transformation from level-north axes to body axes; subscripts indicate the body

$(\phi_{u\ell}, \theta_{u\ell})$  direction angles (roll and pitch angles) of  $\underline{u\ell}$  in level-heading axes:  

$$\underline{u\ell} = \cos \phi_{u\ell} \sin \theta_{u\ell} \underline{i}_H - \sin \phi_{u\ell} \underline{j}_H + \cos \phi_{u\ell} \cos \theta_{u\ell} \underline{k}_H$$

$\underline{\omega}$  angular velocity

$\underline{\omega v}$  angular velocity of reference velocity relative to inertial space,  $\underline{\omega v} = \dot{\psi}_v \underline{k}_N + \dot{\gamma} \underline{j}_H$

Subscripts, superscripts, abbreviations:

$(\_)$  vectors

$(\_)_H$  a vector  $(\_)$  expressed as its components in level-heading axes

$(\_)_N$  a vector  $(\_)$  expressed as its components in level-north axes

$(\_)_t$  a vector  $(\_)$  expressed as its components in triangle body axes

$(\_)_i, (\_)_j, (\_)_k$  the subscripts  $i, j, k$  indicate the  $t$ -axis components of any vector,  $\underline{v}$ ; that is,  $\underline{v} = v_i \underline{i}_t + v_j \underline{j}_t + v_k \underline{k}_t$  and  $\underline{v}_t = (v_i, v_j, v_k)$

$(\_)*$  quantities evaluated on the minimum thrust sum configuration

$(\_)\circ$  quantities evaluated on configuration with  $F_{34} = -A$

$\underline{v1} \otimes \underline{v2}$  vector cross product of  $\underline{v1}, \underline{v2}$

$(A) \times (B)$  Cartesian product space:  $A, B$ , are sets and  $A \times B = [(a,b): a \in A, b \in B]$

$\angle(\underline{v1}, \underline{v2})$  angle between the vectors,  $\underline{v1}, \underline{v2}$

c.g. center of gravity

Units used and metric equivalents:

Length: foot, ft (1 ft = 0.304801 m)

Power: horsepower, hp (1 hp = 745.700 W)

Speed: knot (1 knot = 0.514444 m/sec)

Mass: slug (1 slug = 14.5939 kg)

Force: pound, lb (1 lb = 4.44822 N)

## SUMMARY

The characteristics of a dual-lift helicopter system in equilibrium flight along any reference trajectory are examined. The system consists of the cargo attached by cables to the endpoints of a spreader bar which is suspended by tether cables from the two helicopters. Results are given for the orientation angles of the suspension and its internal forces, and for the helicopter thrust vector requirements under general circumstances, including nonidentical helicopters, and any static or accelerating equilibrium flight condition. These results provide a basis for coordinating the system in flight.

Analytical results are derived from the force balance equations at the centers of gravity of the load and helicopter, and at the endpoints of the spreader bar. The analysis does not consider the attitude degrees of freedom of the load and helicopters, but assumes that these are stable and that the aerodynamic forces in equilibrium flight on these bodies can be calculated independently and to sufficient accuracy from aerodynamic models or that they can be measured in flight. This assumption permits closed-form solution of the equations with the equilibrium aerodynamic forces appearing parametrically. The nature and magnitude of these forces are examined for example helicopters and loads.

It is found that there are arbitrarily many equilibrium orientations of the system for any one situation (any given helicopter pair, load, and flight condition) with three angles which can be selected by the pilot or autopilot. These can be taken as (1) the spreader-bar heading relative to the ground-track direction (formation angle), (2) the spreader-bar tilt relative to the apparent gravity of the suspended load modified to include the load aerodynamic specific force (force per unit mass), and (3) the tilt of one of the tethers relative to the spreader bar. It is shown that thrust requirements vary strongly with the tether angle but are nearly invariant with the other two independent variables; hence the tether angle can be selected to minimize the sum of the required thrust magnitudes. This choice maximizes the system thrust margin and also minimizes fuel rate in the case of identical helicopters. The spreader-bar tilt controls the distribution to the two helicopters of the thrust requirements imposed by the suspended cargo. If the helicopters are identical then zero tilt results in equal distribution and, more generally, the tilt can be selected for any distribution for which no cable collapses and for which both helicopters have positive thrust margins. It is found that the thrust requirements can always be distributed in the same ratio as the helicopter thrust limits. Last, the formation angle can be selected as in conventional formation flying at some fixed value away from the longitudinal and transverse arrangements (e.g., at  $45^\circ$ ). However, with fully automatic flight control, it may be possible to select this angle from a larger range or vary it in flight. The present study does not assume a uniquely suitable choice of formation angle, but examines its considerable influence

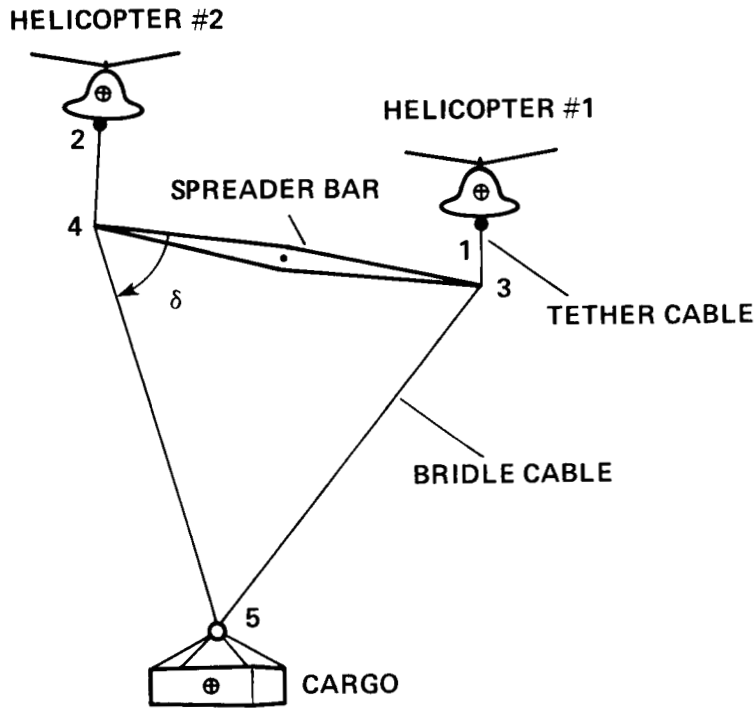
on the system's inertial orientation and the variation of this orientation with maneuvering along a reference trajectory.

## 1. INTRODUCTION

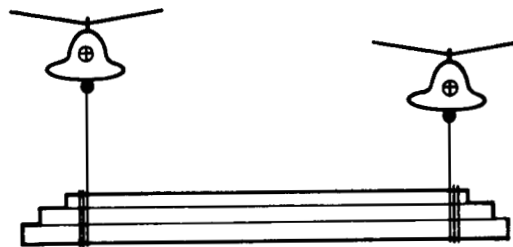
The airborne transport of loads slung beneath two or more helicopters has been considered periodically since the 1950s, following the success of single helicopter slung load operations. This technique would multiply the maximum load-carrying capacity available from existing helicopters used singly. Interest in dual-lift is represented by a few civil applications of the technique and by studies sponsored by the Department of Defense. The use of two helicopters has been a feasible and economic alternative to acquiring existing helicopters of larger payload in some commercial operations with simple load suspension requirements (described in ref. 1), and has been advocated by Carter et al. (refs. 1 and 2) as an alternative to developing new helicopters with payloads exceeding those of current helicopters.

In a 1957 feasibility study of suspension systems to couple two to six helicopters with a load, VERTOL (ref. 3) recommended a system of spreader bars suspended below the helicopters over (1) a system with rigid connection of the helicopters, or (2) a system without separation restraint in which the load was attached solely by cables to each helicopter. This study was based on tandem rotor helicopters each with a maximum payload of 2 tons. A decade later, Sikorsky Aircraft studied the feasibility of twin helicopter systems (refs. 1 and 4) and also recommended the spreader-bar suspension over several other methods of suspension. This system (fig. 1.1(a)) consists of a spreader bar hung below the helicopters by tether cables with the load attached by cables to the endpoints of the spreader-bar. The dimensions of the system are chosen to minimize spreader-bar weight while ensuring a safe helicopter separation; this results in proposed spreader bar lengths of 1.25 to 2 rotor diameters, depending on the control system, and in bridle cable angles of  $45^\circ$  to  $60^\circ$ . This study was based on the single-rotor CH-54B with a 10-ton payload, and the recommended system was subsequently demonstrated in flight tests which were confined to low speeds and within the test airfield (refs. 1 and 5).

There are also several examples of civil twin-lift operations; these have been flown over longer distances and speeds to 60 knots, but have generally been limited to loads of sufficient length (poles, logs, pipes, cables, etc.) to be suspended just below the helicopters without using a spreader bar (fig. 1.1(b)). This arrangement is inherently more stable than the system of figure 1.1(a) which accommodates more typical loads that are significantly shorter than the minimum spreader bar length. At present, interest in further development of dual-lift operations appears in proposed extensions of the flight tests reported in reference 5. Thus, dual-lift has been considered at several stages in the expansion of single helicopter payloads, but has yet to be developed into a proven operational system. A key step in achieving this goal is development and demonstration of a suitable control system, which is made feasible, in part, by today's digital flight control technology.



(a) TYPICAL LOADS



(b) LONG LOADS

Figure 1.1.- Dual-lift configuration.

The flight demonstration (ref. 5) tested the system at hover and at speeds to 20 knots and pilots encountered high work load, particularly during maneuvering when the spreader-bar tilt must be varied as necessary to maintain system equilibrium with invariant load distribution to the two helicopters. This work load indicated a potential need for coordination aids and for automatic stabilization and control to avoid excessive or even unstable transient motion during maneuvering. Indeed, it is anticipated in reference 1 that automatic control is necessary if the full operational potential of the system is to be achieved, and a master-slave stabilization and control system is proposed (refs. 1 and 6). In addition, linear system stability analyses and simulation studies are reported in references 3, 4, and 7 based on simplified system and motion models and for hover.

The present study was undertaken to explore the characteristics of the system shown in figure 1.1(a) in equilibrium flight along any reference trajectory as a basis for coordinating the system during maneuvering throughout its flight envelope. Some basic rules for appropriate tether directions and spreader-bar attitude during static equilibrium and turning flight in the case of identical helicopters and the effect of bar tilt on load distribution are already recognized in the flight tests cited above. The present paper seeks to extend these approximate rules to general maneuvering flight and to include the effects of aerodynamic forces on the system's rigid bodies. The basic assumptions are discussed in section 2, the system equations and method of solution in section 3, and the aerodynamic forces and c.g. accelerations of the system's bodies in equilibrium flight in section 4. Results are then given for the bridle cable forces (sec. 5), the inertial attitude of the spreader-bar-load triangle (sec. 6), and spreader bar and tether forces and thrust vector requirements (sec. 7), along with an analysis of the tether angle optimization (sec. 8), the distribution of the suspended load to the two helicopters (sec. 9) and the variation in system equilibrium geometry and forces with tether angle (sec. 10).

Finally, we remark that this study assumes load stability. However, the speed regime over which this assumption is satisfied for various loads with the suspension system of figure 1.1(a) is unknown; it is likely to be well below the power-limited maximum speed of the helicopters in view of the system's lack of load yaw restraint and long suspension distance. The inherent load stability at higher speeds was not considered in the present design; since this has been the most influential factor in the geometry of advanced single helicopter load suspensions, it may also strongly influence future development of dual-lift suspensions. Thus, future systems may be significantly altered from that of figure 1.1(a) and the system of the present study may be limited to low speeds and favorable loads.

## 2. NOTATION AND ASSUMPTIONS

The dual lift system is assumed to be arranged as shown in figure 1.1(a). It consists of four rigid bodies (two helicopters, a spreader bar, and a suspended load) linked by tethers and bridle cables. The bridle cables and spreader bar form a rigid isosceles triangle with angle  $\delta$  in the range of  $45^\circ$  to  $60^\circ$ . The most commonly considered system consists of identical helicopters with equal loading, but the analysis allows for unlike helicopters and unequal loading. A truncated system using two helicopters and tethers to transport sufficiently long loads (pipes, logs, bridge sections, etc.) as shown in figure 1.1(b) is also potentially useful. The arrangement in figure 1.1(a) was recommended in early studies (refs. 3 and 4), from among several choices, based on the gross properties of feasibility and thrust penalties. However, the development of suspensions for single helicopters for military cargo transport has been greatly influenced by load restraint and stabilization considerations, with the object of stabilizing all loads in a minimum-drag attitude over the power-limited speed range of the helicopter (refs. 8-10 and their reference lists). These objectives are not yet integrated in the dual-lift suspension of figure 1.1(a); as a result, future designs may differ from the arrangement assumed here.

An estimate of the suspension system dimensions can be given. The flight demonstration (ref. 5) with twin single-rotor helicopters used a system with a width (spreader-bar length) twice the rotor diameter ( $2D$ ) and load-to-helicopter height  $2D$ ; this is expected to be a maximum size. This size can be decreased through the use of reliable automatic station keeping to preclude rotor contact; a minimum size of  $1.25D$  by  $1.25D$  is predicted in reference 1. Rotor diameters of existing helicopters fall in the range of 30-125 ft (ref. 11).

The sizes of the component masses relative to the load mass can be estimated. For given helicopters and mission profile let  $PL1$  and  $PL2$  be the payloads of helicopters 1 and 2, respectively, and assume that dual-lift is both necessary (cargo weight exceeds 50% of the combined payload) and possible (suspended weight is less than the combined payload):

$$W_l > \max(PL1, PL2) > (PL1 + PL2)/2 \quad (2.1)$$
$$W_l + W_b < (PL1 + PL2)$$

where  $W_l$  and  $W_b$  are the weights of the load and spread-bar, respectively. Express  $W_b$  as a fraction of the combined payload:

$$W_b = \beta_b(PL1 + PL2) \quad (2.2)$$

For efficient use of dual-lift, the combined payload is much larger than the bar weight; e.g.,  $\beta_b < 0.1$  in reference 1. Combining equations (2.1) and (2.2) gives

$$\frac{\beta_b}{1 - \beta_b} < \frac{W_b}{W_\ell} < 2\beta_b \quad (2.3)$$

where the upper bound corresponds to the lightest load. Therefore,

$$\text{if: } \beta_b \ll 1 \quad \text{then: } m_b \ll m_\ell \quad (2.4)$$

Thus, the bar weight is an order of magnitude smaller than the cargo weight, provided that equation (2.1) and the condition of equation (2.4) are satisfied. Next, express the helicopter weights as a fraction of the payload:

$$W_1 + W_2 = \beta_h(PL1 + PL2) \quad (2.5)$$

Then, using equation (2.1),

$$\frac{\beta_h}{1 - \beta_b} < \frac{W_1 + W_2}{W_\ell} < 2\beta_h \quad (2.6)$$

Noting that helicopter gross weights are about twice their empty weight (ref. 11) it can be estimated that  $\beta_h$  is in the range of 1 to 3 for external load missions. Thus, the sum of helicopter masses is roughly the same as the load mass, provided that the previous assumptions hold and that the vehicle payload is above, say, one third of the vehicle weight,

$$\text{if: } \beta_b \ll 1 \quad \text{and} \quad 1 < \beta_h < 3 \quad \text{then: } 1 < \frac{m_1 + m_2}{m_\ell} < 6 \quad (2.7)$$

and, for twin vehicles, each mass is in the range of  $0.5 m_\ell$  to  $3 m_\ell$ . The results in equations (2.4) and (2.7) indicate the range of relative masses of the component bodies of interest for the dual-lift system.

The dual-lift configuration is defined by the positions of five points on the suspension system, which are numbered for this work as shown in figure 1.1(a). The notation for cable and spreader-bar directions and forces is based on this enumeration; i.e.,  $R_i$ ,  $R_{ij}$ ,  $L_{ij}$ ,  $u_{ij}$ , and  $F_{ij}$  refer to the position of the  $i$ th point, the link between points  $i$  and  $j$ , and its length and direction vector, and the scalar force carried by the link. The (scalar) link force  $F_{ij}$  is taken to be positive (negative) if the link is in tension (compression); it is applied to the point  $R_i$  ( $R_j$ ) in the direction  $u_{ij}$  ( $-u_{ij}$ ).

The component masses (suspended load, spreader-bar, and the two helicopters) and their accelerations and applied forces are indicated by the symbols  $\ell$ ,  $b$ ,  $1$ , and  $2$  appended to the notation; e.g.,  $m_2$ ,  $a_2$ ,  $f_{a2}$ , and  $f_2$  refer to the mass, acceleration, aerodynamic specific force, and specific apparent load vector of helicopter No. 2.

Forces appear in the analysis principally as "specific" force; that is, force per unit weight. In addition, for any component body it is useful to define the specific "apparent load"  $\underline{f}$ ; that is, the sum of the apparent gravity,  $\underline{g} - \underline{a}$ , and the applied external specific forces exclusive of control or thrust forces:

$$\underline{f} = \underline{g} + \underline{fa} - \underline{a} \quad (2.8)$$

where  $\underline{fa}$  is the aerodynamic specific force on the body. This is dominated by gravity in the present context. For the load,  $\underline{fl}$  is the specific apparent suspended load supported by the system, and, in general,  $m\underline{f}$  is the apparent load owing to the weight, aerodynamic force, and acceleration of a component mass which must be supported by the helicopter engines. Indeed, the required thrust vector sum is given by the sum of apparent loads:

$$\underline{T1} + \underline{T2} = -(m_l \underline{fl} + m_b \underline{fb} + m_1 \underline{f1} + m_2 \underline{f2})$$

and most results are given in terms of the apparent loads of the system's component bodies.

Several orthogonal right-handed reference frames are used in this work. Their axes are denoted ( $\underline{i}$ ,  $\underline{j}$ ,  $\underline{k}$ ) with a subscript (N, H, t) to indicate the frame (level-north or level-heading axes, or body axes for the triangle). Level-north and level-heading axes are both local vertical frames with  $\underline{i}_N$  and  $\underline{i}_H$  directed north along the reference trajectory ground track, respectively. The triangle formed by the spreader bar and bridle cables is a rigid body within the assumptions of this work. The triangle axes are body axes attached to the triangle (figure 2.1) and oriented with  $\underline{i}_t$  along the spreader bar (along R43) and  $\underline{k}_t$  perpendicular to the spreader bar in the plane of the triangle and pointed toward the load attachment point. Most of the analysis is carried out in this reference frame.

Subscripts are also used to indicate a vector given by its components in a reference frame. Thus, a vector  $\underline{v}$  given in reference frame "a" is denoted by  $v_a$  where

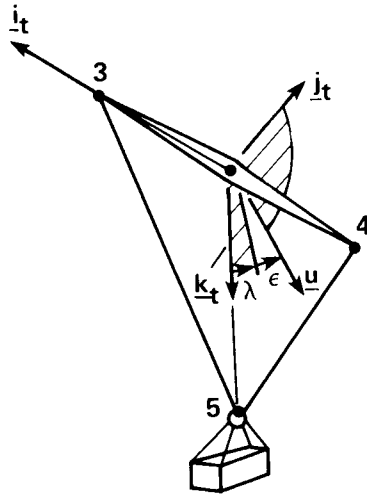
$$v_a = (v \cdot \underline{i}_a, v \cdot \underline{j}_a, v \cdot \underline{k}_a)$$

and the subscript "a" can be any of those noted in the preceding paragraph.

Transformations of vectors between orthogonal right-handed frames "a" and "b" are denoted  $T_{a,b}$ ; that is, if  $\underline{v}$  is any vector and  $v_a$  and  $v_b$  refer to its components in reference frames "a" and "b", then

$$v_a = T_{a,b} v_b \quad (2.9)$$

Transformation matrices  $T_{a,b}$  can be given as a sequence of single axis rotations,  $E_i(\sigma)$ , where  $i$  indicates the axis of rotation (see fig. 2.2). Euler-angle transformations suffice for the present work and are given by the following rotation sequence and customary aeronautics notation for the angles:



UNIT VECTORS:

$$\underline{u} = -\sin \epsilon \underline{i}_t + \cos \epsilon \sin \lambda \underline{j}_t + \cos \epsilon \cos \lambda \underline{k}_t$$

$$u_t = (-\sin \epsilon, \cos \epsilon \sin \lambda, \cos \epsilon \cos \lambda)$$

ANGLE NOTATION FOR UNIT VECTORS OF INTEREST:

VECTOR	UNIT VECTOR	$\lambda$	$\epsilon$
<u>f<sub>l</sub></u>	<u>u<sub>l</sub></u>	$\lambda_l$	$\epsilon_l$
<u>R13</u>	<u>u13</u>	$\lambda_{13}$	$\epsilon_{13}$
<u>R24</u>	<u>u24</u>	$\lambda_{24}$	$\epsilon_{24}$
<u>-T1</u>	<u>u1</u>	$\lambda_1$	$\epsilon_1$
<u>-T2</u>	<u>u2</u>	$\lambda_2$	$\epsilon_2$

Figure 2.1- Triangle body axes and direction angles  $\epsilon, \lambda$  relative to triangle axes.

### SINGLE-AXIS ROTATIONS

$$E_1(\sigma) = \begin{bmatrix} 1 & 0 & 0 \\ 0 & \cos \sigma & \sin \sigma \\ 0 & -\sin \sigma & \cos \sigma \end{bmatrix}$$

$$E_2(\sigma) = \begin{bmatrix} \cos \sigma & 0 & -\sin \sigma \\ 0 & 1 & 0 \\ \sin \sigma & 0 & \cos \sigma \end{bmatrix}$$

$$E_3(\sigma) = \begin{bmatrix} \cos \sigma & \sin \sigma & 0 \\ -\sin \sigma & \cos \sigma & 0 \\ 0 & 0 & 1 \end{bmatrix}$$

### EULER-ANGLE TRANSFORMATIONS

$$T_{a,b} = E_1(\phi) E_2(\theta) E_3(\psi)$$

$$T_{a,b} = \begin{bmatrix} \cos \theta \cos \psi & \cos \theta \sin \psi & -\sin \theta \\ \sin \phi \sin \theta \cos \psi - \cos \phi \sin \psi & \sin \phi \sin \theta \sin \psi + \cos \phi \cos \psi & \sin \phi \cos \theta \\ \cos \phi \sin \theta \cos \psi + \sin \phi \sin \psi & \cos \phi \sin \theta \sin \psi - \sin \phi \cos \psi & \cos \phi \cos \theta \end{bmatrix}$$

### SOME GENERAL TRANSFORMATION PROPERTIES

$$T_{a,b}^{-1} = T_{a,b}^T$$

$$T_{a,b} = T_{a,c} T_{c,b}$$

$$T_{a,b} = \begin{bmatrix} \mathbf{j}_a \cdot \mathbf{j}_b & \mathbf{j}_a \cdot \mathbf{k}_b & \mathbf{j}_a \cdot \mathbf{l}_b \\ \mathbf{j}_a \cdot \mathbf{j}_b & \mathbf{j}_a \cdot \mathbf{k}_b & \mathbf{j}_a \cdot \mathbf{l}_b \\ \mathbf{k}_a \cdot \mathbf{j}_b & \mathbf{k}_a \cdot \mathbf{k}_b & \mathbf{k}_a \cdot \mathbf{l}_b \end{bmatrix} = \begin{bmatrix} (\mathbf{l}_b)_a & (\mathbf{j}_b)_a & (\mathbf{k}_b)_a \end{bmatrix} = \begin{bmatrix} (\mathbf{l}_a)_b & (\mathbf{j}_a)_b & (\mathbf{k}_a)_b \end{bmatrix}^T$$

Figure 2.2.- Transformations for orthogonal right-handed axes.

$$T_{a,b} = E_1(\phi)E_2(\theta)E_3(\psi) \quad (2.10)$$

This is expanded in figure 2.2. The angles determining  $T_{t,N}$  are denoted  $(\phi_t, \theta_t, \psi_t)$ . These, together with  $\psi_v$  suffice to determine all the transformations used. Some general properties regarding inversion and invariance of the transformations, and the relation of the axes vectors with the rows and columns of the transformation are also noted in figure 2.2 for use in the text. These last are obtained by noting that the elements of a transformation matrix are direction cosines or the dot products among the axes vectors of the two frames.

The directions of vectors relative to triangle axes are given by the angles  $(\epsilon, \lambda)$ . Their definitions and appearance in the triangle axes components of a unit vector are shown in figure 2.1;  $\lambda$  is the angle out of the triangle plane and  $\epsilon$  is the angle out of the plane perpendicular to the spreader bar (a tilt angle relative to the spreader bar). Subscripts indicate the corresponding direction vector; e.g.,  $(\epsilon_2, \lambda_2)$ ,  $(\epsilon_{13}, \lambda_{13})$ ,  $(\epsilon_1, \lambda_1)$  correspond to  $\underline{u}_2$ ,  $\underline{u}_{13}$ ,  $\underline{u}_1$ .

In the analysis, it is useful to neglect sufficiently small forces and moments. These are considered negligible, provided the corresponding linear or angular accelerations are of order 0.01 g or 0.01 rps<sup>2</sup> over the operational flight envelope; that is,  $\underline{F}$  or  $\underline{M}$  is negligible provided

$$|F|/m \ll 0.1 \text{ g}$$

or

$$|J^{-1}M_b| \ll 0.1 \text{ rps}^2$$

where  $(m, J)$  are the mass and inertia matrix for the body to which  $\underline{F}$  or  $\underline{M}$  is applied.

Finally, we list the principal assumptions made in the analysis regarding the dual-lift system and the flight conditions of interest.

1. The level-north reference frame is inertial.

2. The configuration is arranged as recommended in early studies (refs. 1 and 4) using a spreader bar and cables (fig. 1.1). Typically, the bridle angle  $\delta$  is in the range 45° to 60° and masses are such that  $0 < m_b \ll m_l$  and  $m_1, m_2$  are the same order of magnitude as  $m_l$  for the range of loads considered.

3. The cables are weightless straight lines of fixed length which support only tension forces and generate no aerodynamic force. All cables are in tension.

4. The system is in equilibrium: (a) a reference point on the configuration follows the reference trajectory, (b) all redundant variables in the system have their commanded values, (c) the load is stable and in steady state attitude, (d) the helicopters are in equilibrium.

5. The maneuver domain of interest is bounded; the angular velocity of the path tangent, and the reference trajectory acceleration and jerk are much smaller

than 1 rps, 1 g, 1 g/sec, respectively. The acceleration can be written in terms of the path tangent vector and its perpendiculars in the horizontal and vertical planes:

$$\underline{\omega v} = \dot{\psi}_v \underline{k}_N + \dot{\gamma} \underline{j}_H$$

$$\underline{a} = \dot{v}(\cos \gamma \underline{i}_H - \sin \gamma \underline{k}_N) + V \dot{\psi}_v \cos \gamma \underline{j}_H - V \dot{\gamma}(\sin \gamma \underline{i}_H + \cos \gamma \underline{k}_N)$$

and we assume reasonable upper bounds:

$$|\dot{\psi}_v| < 0.06 \text{ rps} \quad \text{Heading rate}$$

$$|\dot{\gamma}| < 0.06 \text{ rps} \quad \text{Flightpath angle rate}$$

$$|\dot{v}| < 0.15 \text{ g} \quad \text{Speed rate}$$

$$V \cos \gamma |\dot{\psi}_v| < \min(0.35 \text{ g}, 0.06 V \cos \gamma) \quad \text{Centrifugal acceleration}$$

$$V |\dot{\gamma}| < \min(0.05 \text{ g}, 0.06 V) \quad \text{Normal acceleration}$$

$$|\ddot{v}| < 0.1 \text{ g/sec} \quad \text{Speed jerk}$$

$$\left| \frac{d}{dt} (V \cos \gamma \dot{\psi}_v) \right| < 0.1 \text{ g/sec} \quad \text{Centrifugal acceleration rate}$$

$$\left| \frac{d}{dt} (V \dot{\gamma}) \right| < 0.05 \text{ g/sec} \quad \text{Normal acceleration rate}$$

6. The angle between the apparent suspended load and the vertical is bounded:  $\angle(\underline{f}_l, \underline{k}_N) < \delta$ .

7. The apparent load differences are bounded:

$$|\underline{f}_b - \underline{f}_l|, |\underline{f}_1 - \underline{f}_l|, |\underline{f}_2 - \underline{f}_l| < f_l \sin \delta$$

The last two assumptions are conditions derived in sections 6 and 7 which restrict flight condition parameters (acceleration and aerodynamic force) sufficiently to ensure that equilibrium is possible with appropriate geometry; that is, with the system right side up and with the helicopters on the side of the spreader bar opposite the load with their thrust vectors directed away from the spreader bar at any  $\epsilon_l$  and  $\beta_t$ .

### 3. FORCE-BALANCE EQUATIONS

The forces applied at various points on the system are shown in figure 3.1(a). The force-balance equations at the load c.g., at the spreader-bar endpoints, and at the helicopter c.g.'s are

$$\begin{aligned}
 F_{35} \underline{u}_{35} + F_{45} \underline{u}_{45} &= m_l \underline{f}_l \\
 -F_{13} \underline{u}_{13} + F_{35} \underline{u}_{35} - F_{34} \underline{i}_t &= -0.5 m_b \underline{f}_3 \\
 -F_{24} \underline{u}_{24} + F_{45} \underline{u}_{45} + F_{34} \underline{i}_t &= -0.5 m_b \underline{f}_4 \\
 F_{13} \underline{u}_{13} - T_1 \underline{u}_1 &= -m_1 \underline{f}_1 \\
 F_{24} \underline{u}_{24} - T_2 \underline{u}_2 &= -m_2 \underline{f}_2
 \end{aligned} \tag{3.1}$$

where the apparent loads on the component bodies are

$$\begin{aligned}
 \underline{f}_l &= \underline{g} + \underline{fa}_l - \underline{a}_l \\
 \underline{f}_1 &= \underline{g} + \underline{fa}_1 - \underline{a}_1 \\
 \underline{f}_2 &= \underline{g} + \underline{fa}_2 - \underline{a}_2 \\
 \underline{f}_3 &= \underline{f}_b + \underline{\Delta f} \\
 \underline{f}_4 &= \underline{f}_b - \underline{\Delta f} \\
 \underline{f}_b &= \underline{g} + \underline{fab} - \underline{ab} \\
 \underline{\Delta f} &= \frac{2}{m_b L_{34}} \underline{i}_t \otimes (\underline{\dot{H}}_b - \underline{M}_{ab})
 \end{aligned}$$

The force-balance equations for the spreader-bar endpoints are used instead of the rigid-body equations for force-and-moment balance about the spreader-bar c.g. because the latter do not contain the spreader-bar compression. The development of these equations is given in the appendix. The remaining equations are the usual rigid-body equations for translational motion of the suspended load and helicopter c.g.'s, and they can be written by reference to figure 3.1(a).

These equations are valid provided no cable collapses (provided  $F_{13}, F_{24}, F_{35}, F_{45} > 0$ ), and this restriction coincides with the present limits of interest.

The analysis is carried out principally in triangle axes. The unit vectors in equations (3.1) can be expressed in terms of direction angles in these axes as defined in figure 2.1. For the present analysis, it is assumed that all the apparent loads on the right in equations (3.1) can be determined from the reference

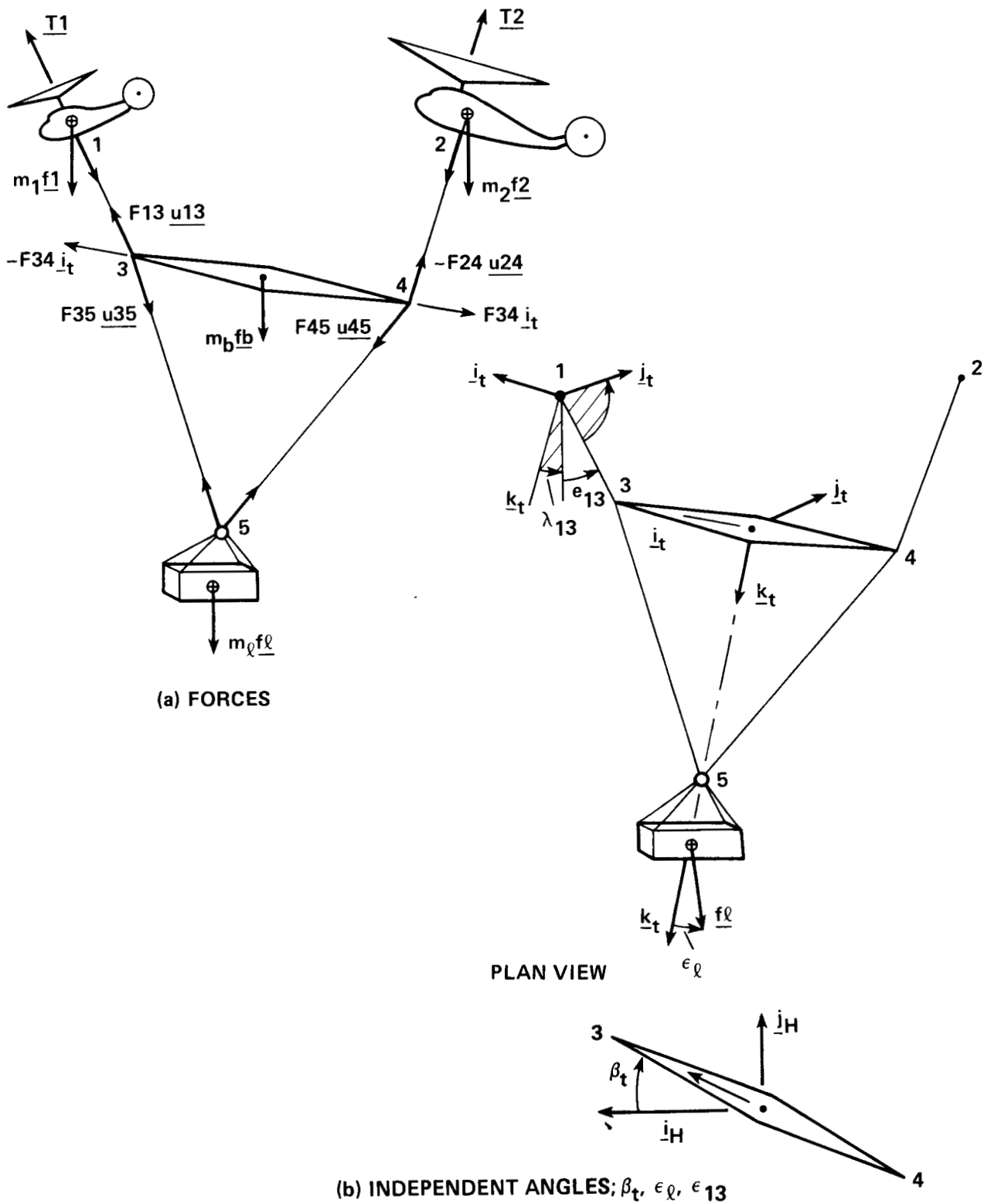


Figure 3.1.- Dual-lift system forces and independent angles.

trajectory. Then equations (3.1), expressed in triangle axes, are solved for the following unknown system variables:

$\phi_t, \theta_t, \psi_t$	Euler angles locating triangle axes relative to level-north axes	}	(3.2a)
F35, F45, F13, F24, F34, T1, T2	Suspension system tensions and trust magnitudes		
$\lambda_{13}, \epsilon_{13}, \lambda_{24}, \epsilon_{24}, \lambda_1, \epsilon_1, \lambda_2, \epsilon_2$	Tether and thrust direction angles relative to the triangle		

Equations (3.1) provide only 15 scalar equations so that 3 of the 18 variables in equation (3.2a), or functions of these variables, can be selected independently. For these we choose three angles that can be measured and controlled in flight and that are later found to be related to factors of engineering interest (see fig. 3.1(b)):

$\epsilon_{13}$	Tilt angle of No. 1 tether from spreader bar	}	(3.2b)
$\epsilon_\ell$	Spreader-bar tilt angle from apparent load vector		
$\beta_t \stackrel{\Delta}{=} \psi_t - \psi_v$	Spreader-bar heading relative to the reference ground track		

First, for any given flight condition, the thrust-sum,  $T1 + T2$ , varies with  $\epsilon_{13}$  but is very nearly independent of the other two variables. Hence, the tether direction can be selected to minimize the required thrust-sum; that is, to preclude tether directions which require the two helicopters to tug against each other along the spreader bar with mutually canceling thrust components. Second, load sharing must be set at a desired value, and this depends on  $\epsilon_\ell$  which is the tilt of the spreader bar relative to the apparent suspended load, and which is a function of  $\phi_t, \theta_t$ , and  $\psi_t$ . As will be seen, the bridle-cable load ratio, F35/F45, depends only on this angle and, assuming that  $\epsilon_{13}$  is selected to minimize the thrust-sum, then T1/T2 also depends on  $\epsilon_\ell$  only, whereas the sum  $T1 + T2$  is nearly invariant with  $\epsilon_\ell$ . Third,  $\beta_t$  orients the spreader-bar heading relative to the ground track. Thrust requirements and load sharing are virtually independent of  $\beta_t$ . In manually controlled formation flight  $|\beta_t|$  is typically maintained constant in the range of 30° to 60°; this value enhances visibility and overshoot safety for the trail helicopter which acts to maintain the relative position vector as the lead helicopter selects the flight trajectory. In many respects, the situation is similar for dual lift, and the same choice of  $\beta_t$  can be made for manually controlled flight. With automatic control, it may be possible to select or vary  $\beta_t$  over a larger range, but a fixed or slowly varying value is expected. A uniquely preferred value of  $\beta_t$  cannot be given here, and results are given for any formation angle.

Problem Statement (restricted trim): Solve equations (3.1) for the configuration variables (eq. (3.2a)) in terms of the independent variables (eq. (3.2b))

assuming the system masses ( $m_l, m_b, m_1, m_2$ ) and the apparent loads ( $f_{lN}, f_{1N}, f_{2N}, f_{3N}, f_{4N}$ ) are known, and that the assumptions of section 2 apply.

This is a restricted trim problem in which the apparent loads are treated as parameters in the analysis. This treatment yields closed-form relations for the suspension variables and thrust-vector requirements in terms of the apparent loads and indicates the general effects of maneuvering and of aerodynamic forces on the equilibrium behavior of the system.

The solution of the restricted trim problem is meaningful provided the apparent loads do not depend significantly on the unknowns to be determined from equations (3.1); that is, provided each apparent load can be given independently of solving the force-balance equation in which it appears. Calculation of the apparent loads for any specific system requires numerical solution of the general trim problem in which the system's force- and moment-balance equations and constraints are satisfied, given the reference trajectory, aerodynamic and engine descriptions of the bodies, and assuming equilibrium motion. An algorithm for this purpose is sketched in figure 3.2; it is arranged to satisfy the equations, beginning with the load and working up to the helicopters, using iteration to account for coupling with the rigid bodies higher in the system. Many of the equations required for the system below the helicopters in this algorithm are obtained in the present work, but its implementation is outside the scope of the present work.

Figure 3.2 illustrates several points relevant to the restricted trim problem. First, the load acceleration, aerodynamic force, and apparent load can be computed independently of the remaining system from its rigid-body equations (ignoring downwash), and are, therefore, functions of the reference trajectory only. In the presence of downwash, some coupling with thrust occurs, but it can be assumed to be negligible compared with load weight in the restricted trim problem. Second, the motion of the triangle is given by kinematic relations from the reference trajectory and the selected values of  $\beta_t$  and  $\epsilon_2$  after which the spreader-bar c.g. acceleration, aerodynamic force, and apparent load can be given; they are functions of these same variables. Third, the tether-force vectors can be determined from the apparent loads of the bodies below the tethers and the selected value of the tether angle,  $\epsilon_{13}$ . These forces are then used with helicopter trim routines to calculate the corresponding helicopter thrust requirements and apparent loads. Iteration is required to account for the helicopter apparent loads in selecting the tether angle for minimum thrust. In this step, helicopter aerodynamic specific forces vary with thrust, but these variations are weak so that  $fa_{1N}$  and  $fa_{2N}$  in equilibrium are principally functions of the reference trajectory. In addition, these forces are small, of the order of 0.1 g or less, so that neglecting their dependence on the unknowns of the restricted trim problem will cause little inaccuracy in the restricted trim solutions.

In the next section, the size and nature of the c.g. accelerations and aerodynamic forces in equilibrium flight over the operational envelope of interest are described before equations (3.1) are solved.

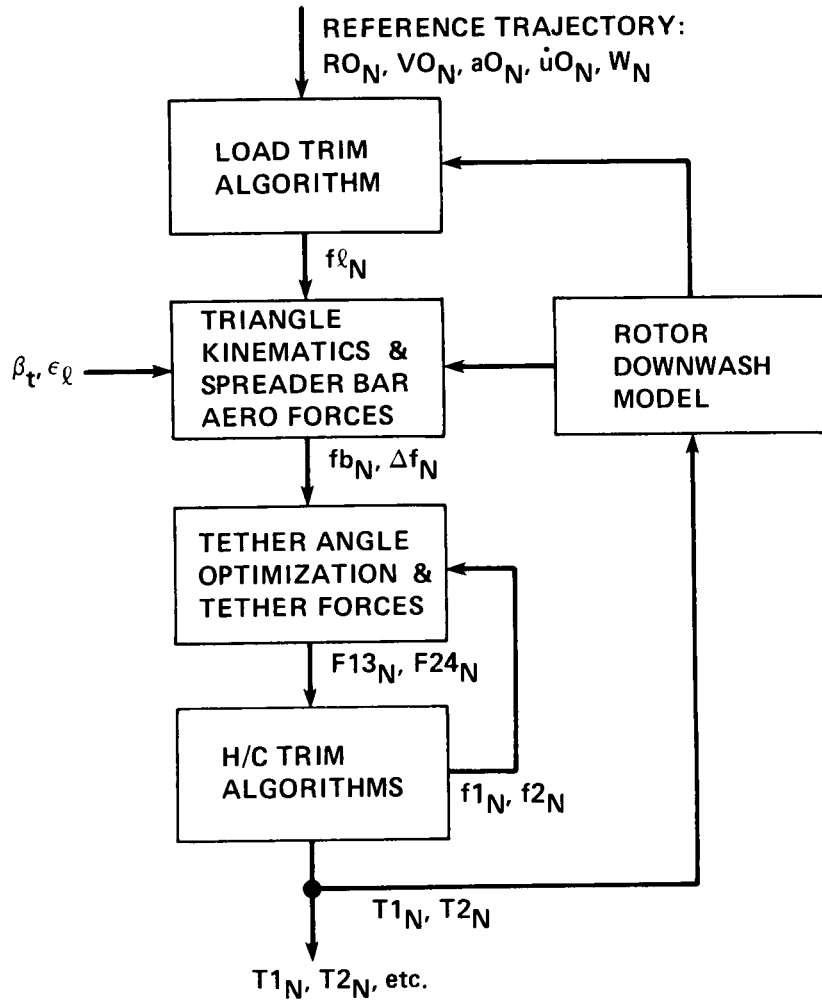


Figure 3.2- Computational flow for general dual-lift trim.

#### 4. ACCELERATIONS AND AERODYNAMICS

The c.g. accelerations and aerodynamic forces of the component bodies of the dual-lift system are necessary to the evaluation of the apparent loads in equations (3.1). Although their exact calculation from the reference trajectory, the aerodynamic descriptions of the bodies, and the assumption of equilibrium motion is not attempted in this paper, it is of interest to consider several aspects of these quantities before solving the force-balance equations. These are (1) the nature and magnitude of differences of the component body accelerations from the reference acceleration, (2) the nature and magnitude of their aerodynamic forces, and (3) the dependence of these quantities on the unknown suspension variables (eq. (3.2a)).

The analysis neglects the aerodynamic forces on the cables. Those forces acting on the spreader bar are included in the analytical results, but are not discussed below. The bar's aerodynamic force is expected to be negligible relative to load weights encountered in practice and, therefore, to have little effect on the system. It is also remarked that this force can be computed independently of solving the spreader-bar force-balance equations (eqs.(3.1)).

The dual-lift system is assumed to be in equilibrium flight at all points along a reference trajectory; that is, (1) a reference point in the system follows the reference trajectory, given as  $(R_{oN}(t), V_{oN}(t), a_{oN}(t))$  over the flight duration,  $t_0 \leq t \leq t_F$ ; (2) the redundant suspension variables  $(\beta_t, \epsilon_2, \epsilon_{13})$  have their commanded values, and their command rates are assumed small (well below 0.1 rps); (3) the load attitude and angular motion are stable and in steady state; and (4) the helicopters are in equilibrium.

##### Accelerations

In static equilibrium with fixed values of all redundant angles, all parts of the system have the same velocity and acceleration. More generally, this is not the case and we examine next the nature and magnitudes of the differences in velocity and acceleration from the reference trajectory that can occur in equilibrium flight.

The position of a point  $\underline{R}$  on a system consisting of rigid bodies and straight links of fixed length, such as those in the dual-lift system, can be given as

$$\underline{R} = \underline{R}_0 + \sum_n \underline{\Delta R}^{(n)} \quad (4.1)$$

where  $\underline{R}_0$  is a reference point in the system and  $(\underline{\Delta R}^{(n)}, n = 1, 2, \dots)$  is any sequence of fixed-length links or line segments connecting  $\underline{R}_0$  and  $\underline{R}$ . The inertial velocity and acceleration of  $\underline{R}$  can be given from Coriolis' equation specialized to this case:

$$\underline{V} = \underline{V}_0 + \sum_n \underline{\omega}^{(n)} \otimes \underline{\Delta R}^{(n)} \quad (4.2)$$

$$\underline{a} = \underline{a}_0 + \sum_n [\dot{\underline{\omega}}^{(n)} \otimes \underline{\Delta R}^{(n)} + \underline{\omega}^{(n)} \otimes (\underline{\omega}^{(n)} \otimes \underline{\Delta R}^{(n)})]$$

where  $\underline{\omega}^{(n)}$  is the angular velocity of  $\underline{\Delta R}^{(n)}$  relative to inertial space. From equation (4.2), the differences from the reference trajectory are

$$\begin{aligned} \delta V &= |\underline{V} - \underline{V}_0| = \left| \sum_n \underline{\omega}^{(n)} \otimes \underline{\Delta R}^{(n)} \right| \leq \max_n \{ |\underline{\omega}^{(n)}| |\sin \angle(\underline{\omega}^{(n)}, \underline{\Delta R}^{(n)})| \} L \\ \delta a &= |\underline{a} - \underline{a}_0| = \left| \sum_n (\dot{\underline{\omega}}^{(n)} \otimes \underline{\Delta R}^{(n)} + \underline{\omega}^{(n)} \otimes \underline{\omega}^{(n)} \otimes \underline{\Delta R}^{(n)}) \right| \\ &\leq \sum_n \left( |\dot{\underline{\omega}}^{(n)} \otimes \underline{\Delta R}^{(n)}| + |\underline{\omega}^{(n)}| |\underline{\omega}^{(n)} \otimes \underline{\Delta R}^{(n)}| \right) \\ &< \max_n \{ |\dot{\underline{\omega}}^{(n)}| + \omega^{(n)2} |\sin \angle(\underline{\omega}^{(n)}, \underline{\Delta R}^{(n)})| \} L \end{aligned} \quad (4.3)$$

where  $L$  is the maximum dimension of the system (about two rotor diameters). These differences would be zero if the system were a point mass ( $L = 0$ ) or if there were no angular motion ( $\underline{\omega}^{(n)} = 0$ ,  $n = 1, 2, \dots$ ), and they would be negligible for sufficiently small angular motion and system dimension (that is, if

$$\max_n \{ |\dot{\underline{\omega}}^{(n)}| + \omega^{(n)2} \} L \ll 0.1 g$$

We omit a detailed application of equations (4.2) to the dual-lift system, but the following are noted. The angular motion of the system is determined from the rates of the independent angles in the problem acting in the directions about which each rotation occurs. These are the direction rates of the reference velocity ( $\dot{\gamma}$ ,  $\dot{\psi}_v$ ) and apparent suspended load, the command rates of the redundant suspension variables ( $\dot{\beta}_t$ ,  $\dot{\epsilon}_l$ ,  $\dot{\epsilon}_{13}$ ), and the load and helicopter attitude rates for equilibrium flight ( $\dot{\phi}$ ,  $\dot{\alpha}$ ,  $\dot{\beta}$  for each body). On quasi-steady flight segments (constant speed or accelerating straight line and steady turn segments) all of these angles except  $\psi_v$  can be assumed invariant or to have very small rates, so that the angular motion of all parts of the dual-lift system is either negligible or dominated by the velocity heading rate in turns:

$$\underline{\omega}^{(n)} \cong \dot{\psi}_v \underline{k}_N, \quad n = 1, 2, \dots$$

For these flight segments, the system approximates a rigid body with uniform angular motion and the velocity and accelerations of its parts differ from the reference values,  $\underline{V}_0$ ,  $\underline{a}_0$ , to terms of order  $|\dot{\psi}_v|_{\max} L$ ,  $|\dot{\psi}_v|_{\max}^2 L$ , respectively, where  $L$  is the maximum system dimension and  $|\dot{\psi}_v|_{\max}$  is below 0.1 rps for the trajectory domain of interest previously stated. During brief transient maneuvering between steady-flight segments (turn entries and exits,  $\dot{v}$  and  $\gamma$  - transients), the direction rates of the apparent loads contribute to the angular motion of the system, the system's bodies change their relative positions, and the maximum angular velocity can be greater, but is still expected to be small, of the order of 0.1 rps for the acceleration and jerk limits previously stated, with corresponding maximum acceleration differences in equations (4.3) under 0.1 g.

### Helicopter Aerodynamic Forces

The nature and magnitude of the helicopter aerodynamic forces exclusive of the rotor forces can be evaluated approximately from trim solutions for the isolated helicopter. Aerodynamic models based on available wind-tunnel data (e.g., refs. 12-14 for the HO-4 and UH-1H helicopters; ref. 15 for the CH-54; ref. 16 for the UH-60; and ref. 17 for the CH-47B) along with trim-solution algorithms for isolated or externally loaded helicopters in static equilibrium flight (e.g., refs. 12,16,18) are available from simulation programs. The trim algorithm associated with the simulation described in references 13 and 16 was used to obtain data for the UH-60.

Contour plots of the aerodynamic specific force in level-heading axes aligned with the heading of the air-velocity vector are given in figure 4.1. Results are given for two weights corresponding to a helicopter weight of 12,000 lb with both light and heavy loads (2,000 and 10,000 lb) attached at the helicopter c.g. Several features can be seen. First, the load weight and thrust have a minor effect and it is principally on the vertical component. Second, the magnitude of the longitudinal component is small and under 0.1 g over the speed range shown (at low speeds it is forward (positive), and otherwise increases principally with  $V_e^2$ ), and the lateral component is virtually negligible everywhere (a discontinuity occurs in the contours at  $V_e = 60$  knots where the trim algorithm switches from selecting the helicopter's redundant variable as  $\beta = 0$  to  $\phi = 0$ ). The vertical component is also small, with similar maximum magnitude; it provides little aerodynamic lift (at higher speeds it varies principally with  $\gamma$  and is downward (positive) at higher values of  $\gamma$ ). And third, the plots of the specific force magnitude  $|\underline{f}_a|$  confirm that the helicopter's total aerodynamic specific force is generally small (below 0.1 g over most of the domain shown) and that it can, therefore, be expected to have little effect on the equilibrium rotor-thrust requirements or other system characteristics.

These data are specific to the UH-60 helicopter in static equilibrium with the load attached at the c.g. However, additional calculations for the tandem-rotor CH-47B with and without a 15,000-lb slung load, using the simulation described in

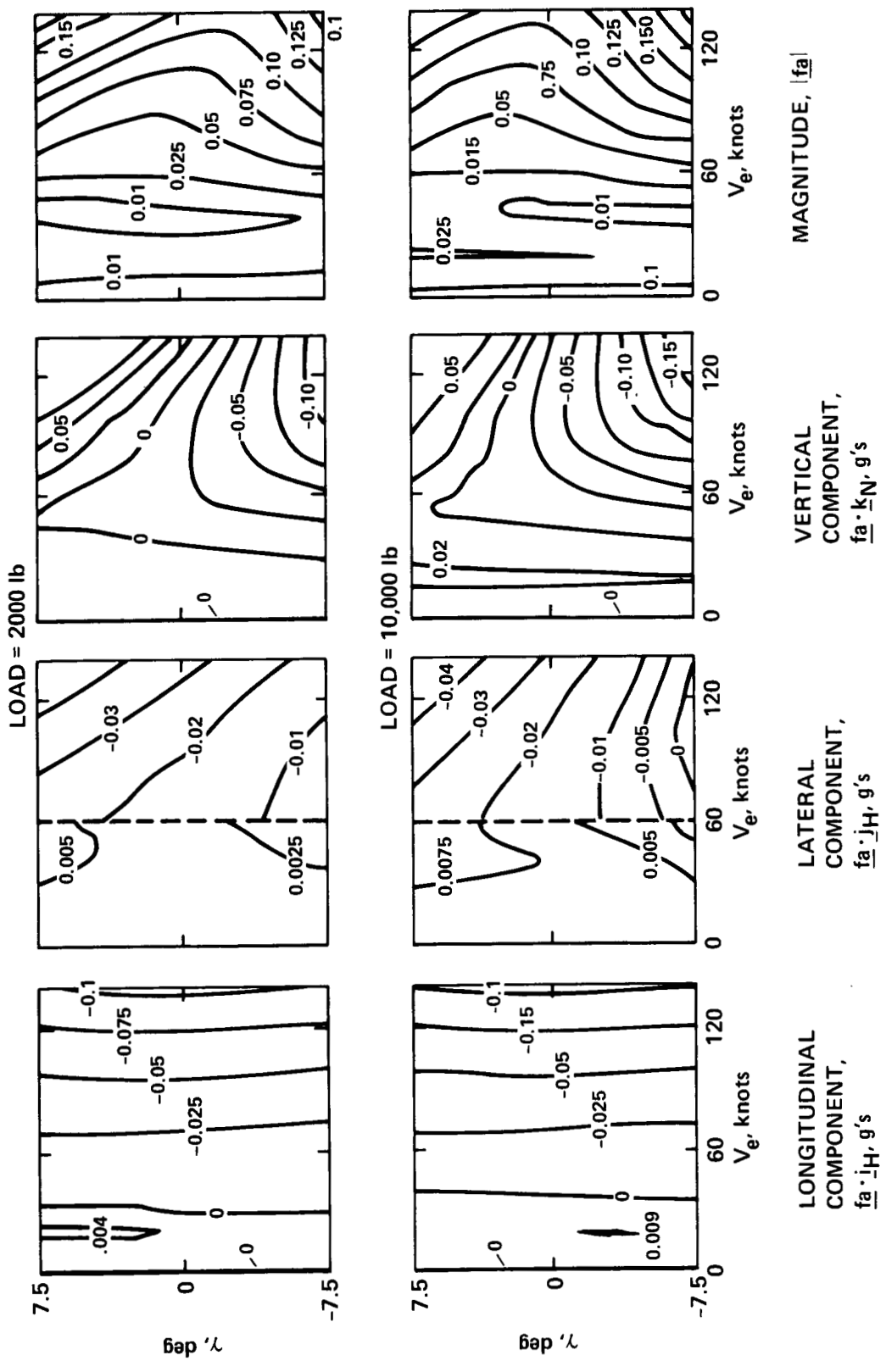


Figure 4.1.- UH-60 aerodynamic specific force in static equilibrium flight,  
 $Fa_H/W_h: W_h = 12,000 \text{ lb.}$

reference 17, gave the same trends, and those trends are expected to characterize other helicopters and load attachment geometries generally. Thus, the helicopter aerodynamic specific force depends weakly on the thrust magnitudes and tether forces, but this dependence can be neglected in solving equations (3.1) since these forces are generally small (of the order of 0.1 g) over the velocity range of interest; as a result, inaccuracies in the present analytical results owing to the neglect of this dependence are not significant. Further, the helicopter aerodynamic forces have no effect on the system below the tethers in the results derived later.

### Load Aerodynamic Forces

The physical characteristics of external loads that might be transported by helicopters vary substantially and the loads are of uncertain stability in forward flight before system testing. In general, a given load and suspension system will be stable beneath helicopters in static equilibrium flight over some speed range. This stability-limited speed range can be determined empirically in wind-tunnel and flight tests, and it can be significantly smaller than the power-limited speed range of the helicopters depending on suspension-system design properties (restraints in yaw, pitch, and pendulum motion, and characteristic lengths) and load properties (aerodynamic force and moment characteristics, weight, c.g. location). Test data are available for single helicopter suspensions (refs. 8-10, 19-21, and the 1976 survey article, reference 22), but not for the dual-lift suspension of this study. Here, the lack of yaw restraint and long pendulum length are unfavorable factors, and the lower bound on load weight (assumed to exceed the single-helicopter payload) is favorable for a given load shape and size. It is beyond our purpose to evaluate the load-speed range combinations that satisfy the load stability assumptions of this paper. However, it is reasonable to assume for the present that the dual-lift and single-cable suspensions have similar load stability boundaries, since both lack yaw restraint. This boundary is noted in references 10 and 19 as being 40 to 65 knots for various difficult but typical loads (e.g., boxes, vehicles, and bridge sections); reference 21 identifies four general categories of military loads and notes maximum operational speeds of 40 to 100 knots, depending on category.

Measurements of the static aerodynamics of some typical loads are given in references 23 and 24 (containers of sizes 8x8x8 ft, 8x8x20 ft (MILVAN), and 8x8x40 ft; a bulldozer; and the M109 self-propelled 155-mm howitzer). These loads are convenient examples for the examination of maximum aerodynamic specific forces and exemplify trim behavior for a large group of loads. For brevity, we omit a load trim analysis based on these data and infer trim attitudes and maximum stable speeds from the literature on single helicopters with single cable suspensions (ref. 22). The elongated boxes of reference 23, and other elongated loads with a definite major axis and weak directional stability when aligned with the wind, generally stabilize broadside to the free stream in a maximum drag heading with small or negligible lift and side forces. The cubic box, and other loads which are axisymmetric about the cable, generally rotate continually over their stable speed range. The aerodynamic force is again principally drag, which is nearly independent of yaw angle. Last, the M109 is a dense load with some degree of weathervane stability at the minimum

drag heading. Flight observations are not available, but a similar load (the M110 self-propelled 203-mm howitzer) trims longitudinally up to 120 knots, and then trims broadside for the remainder of its stable speed range.

The wind-tunnel measurements in references 23 and 24 are given for force/Q, which is assumed independent of Q. The equilibrium aerodynamic specific force on the load can be written as

$$\underline{fa\ell} = \left( \frac{Fa\ell}{Q} \right)_{\text{trim}} \frac{Q_{\ell}}{W_{\ell}} \underline{i}_a \quad (4.4a)$$

where  $fa\ell$  and  $\underline{i}_a$  are the magnitude and direction of the static aerodynamic force vector, and vary with  $\alpha_{\ell}$ ,  $\beta_{\ell}$ . The trim force is dominated by drag for all the example loads and other loads with the same trim attitude behavior:

$$\underline{fa\ell} \approx - \left( \frac{D}{Q} \right)_{\text{trim}} \frac{Q_{\ell}}{W_{\ell}} \underline{i}_{Va\ell} \quad (4.4b)$$

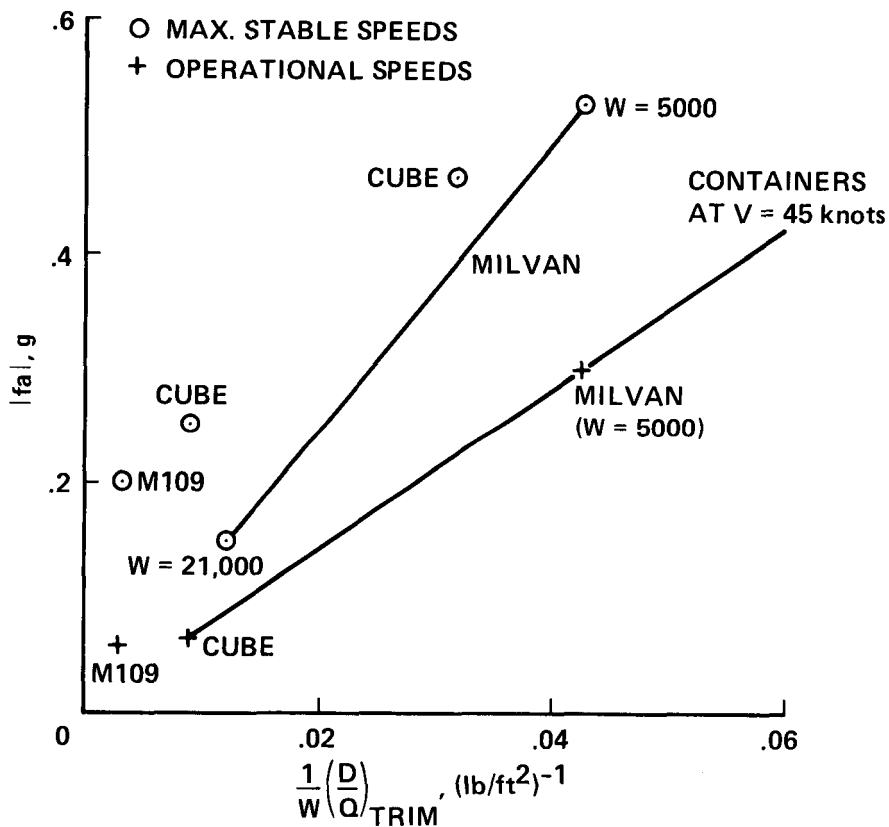
where  $D$ ,  $\underline{i}_{Va\ell}$  are the load's drag and air velocity direction, respectively. The loads can be characterized by the proportionality factor,  $(1/W)(D/Q)_{\text{trim}}$ , which is the drag specific force per unit dynamic pressure, and indicates how rapidly specific force increases with airspeed. Data for the example loads are given in figure 4.2, including maximum stable speeds (critical speed), operational speeds, and the corresponding specific forces. These speeds are typical or approximate values from wind-tunnel or flight tests for the same or a similar load.

The MILVAN's maximum stable speed appears to be independent of weight, so that the maximum specific force to which it is subjected decreases with weight along a straight line (fig. 4.2(b)) over the range 0.145 g to 0.525 g. Maximum specific forces for the other loads fall within this range. The M109 has a much lower drag-specific-force rate than the MILVAN and is subjected to much lower specific force at a given speed, with values below 0.1 g at all speeds below 100 knots, and correspondingly less influence of load aerodynamics on the system equilibrium. Specific forces at operational speeds are also shown. Since the same speed is assigned to all containers, these fall along a straight line in figure 4.2(b) and are below 0.3 g for the MILVAN at all weights.

These data give the maximum specific forces for the example loads cited above and indicate bounds for other other similar loads with drag-specific-force rate in the same range. The discussion also indicates that most stable slung loads are subjected to aerodynamic forces that are dominated by drag and that are, at most, a moderate fraction of 1 g. A load is unlikely to be stable if the specific force approaches 1 g. Further, later sections of this report indicate that unacceptable equilibrium geometry is required if the combined load aerodynamic force and acceleration is sufficiently large (approaches 2 g).

LOAD	$\left(\frac{D}{Q}\right)_{TRIM}$ , ft <sup>2</sup>	W, lb	$\frac{1}{W} \left(\frac{D}{Q}\right)_{TRIM}$ , (lb/ft <sup>2</sup> ) <sup>-1</sup>	V <sub>CRITICAL</sub> , knots	fa  <sub>max</sub> , g	V <sub>OP'L</sub> , knots	fa  <sub>OP'L</sub> , g
M109	85	43,500	0.003	140	0.20	75	0.06
8 × 8 × 8' BOX	79	2,500	0.032	65	0.46	45	0.22
		9,000	0.009	90	0.25	45	0.06
8 × 8 × 20' BOX	216	5,000	0.043	60	0.525	45	0.30
		21,000	0.012	60	0.145	45	0.08

(a) DATA FOR EXAMPLE LOADS



(b) EQUILIBRIUM SPECIFIC FORCE

Figure 4.2.- Maximum equilibrium load aerodynamic specific force (refs. 22-24).

## 5. RESULTS FROM THE LOAD EQUATION

The following results are obtained from the first of equations (3.1):

$$\underline{j}_t \cdot \underline{f}_l = 0 \quad (5.1)$$

$$F_{35} = 0.5 m_l f_l \cos(\delta - \epsilon_l) / \cos \delta \sin \delta \quad (5.2)$$

$$F_{45} = 0.5 m_l f_l \cos(\delta + \epsilon_l) / \cos \delta \sin \delta \quad (5.3)$$

$$\rho_b = F_{35}/F_{45} = \cos(\delta - \epsilon_l) / \cos(\delta + \epsilon_l) \quad (5.4)$$

$$F_{35}, F_{45} > 0 \quad \text{IFF} \quad |\epsilon_l| < \pi/2 - \delta \quad (5.5)$$

$$F_{35} = F_{45} \quad \text{IFF} \quad \epsilon_l = 0 \quad (5.6)$$

These results readily follow from analysis of the dot products of the load equation with  $\underline{i}_t$ ,  $\underline{j}_t$ ,  $\underline{k}_t$  after expressing the cable directions,  $\underline{u}_{35}$ ,  $\underline{u}_{45}$ , in triangle axes (refer to fig. 2.1). These results show the following.

First, since  $\underline{j}_t$  is perpendicular to the triangle it follows from equation (5.1) that the specific apparent suspended load  $\underline{f}_l$  is necessarily in the plane of the triangle at all times. In that case,

$$\lambda_l = 0 \quad (5.7)$$

and

$$\underline{u}_{lt} = (-\sin \epsilon_l, 0, \cos \epsilon_l)$$

This reflects the assumption that the cables are straight lines which support no side force. As a result,  $\epsilon_l$  is the pitch angle of the spreader bar from the plane perpendicular to  $\underline{f}_l$ ; the spreader bar is level relative to  $\underline{f}_l$  when  $\epsilon_l = 0$ .

Second, it follows from equations (5.2) and (5.3) that

$$F_{35} > 0 \quad \text{IFF} \quad -\pi/2 + \delta < \epsilon_l < \pi/2 + \delta$$

$$F_{45} > 0 \quad \text{IFF} \quad -\pi/2 - \delta < \epsilon_l < \pi/2 - \delta$$

Combining these gives the result in equation (5.5) for the range of spreader-bar tilt relative to  $\underline{f}_l$  for which the bridle cables do not collapse. For  $\delta = 60^\circ$ , this is a range of  $\pm 30^\circ$ . At the extremes of  $\epsilon_l$ , one of the bridle cables is parallel to  $\underline{f}_l$  and carries the entire suspended load,  $m_l f_l$ , whereas the other collapses. It will be seen later that the tether cables do not collapse at any  $\epsilon_l$  so that equation (5.5) gives the range of  $\epsilon_l$  for which equations (3.1) are valid.

Third, the bridle-cable tension ratio, equation (5.4), depends only on the spreader-bar tilt,  $\epsilon_l$ . Equal tension requires that the spreader bar be

perpendicular to the apparent suspended load (be level relative to  $\underline{fl}$ ). It will be shown later that, assuming optimum choice of tether angle, the tether-tension ratio is very nearly the same as  $\rho_b$ , and equal loading of the helicopters requires that  $\epsilon_L$  be nearly zero.

Last, the variations of cable forces and force ratio with  $\epsilon_L, \delta$  are shown in figures 5.1 and 5.2.

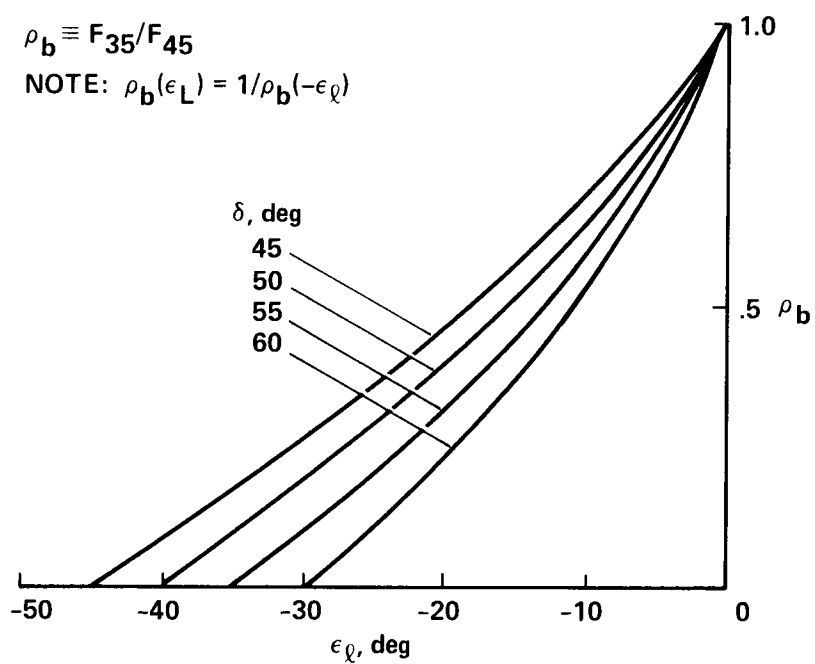


Figure 5.1.- Pendant cable force ratio:  $\rho_p \equiv F_{35}/F_{45}$ .

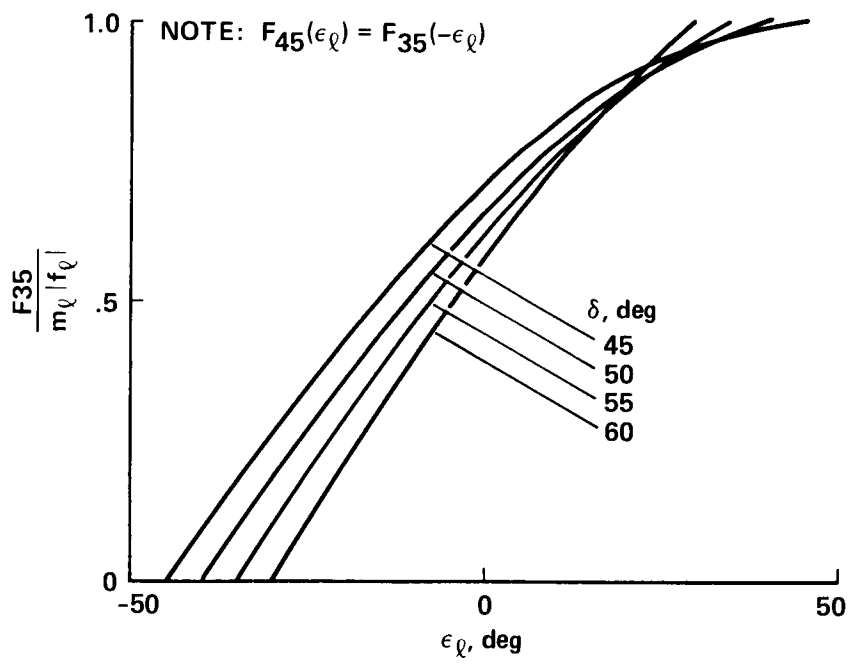


Figure 5.2.- Pendant cable forces.

## 6. BRIDLE TRIANGLE ATTITUDE

The triangle attitude is defined by its body-axis Euler angles,  $\phi_t, \theta_t, \psi_t$ , where  $\psi_t, \theta_t$  are the spreader-bar heading and pitch, and  $\phi_t$  is the load roll or swing angle about the spreader bar from the vertical plane. These angles can be given in terms of  $\psi_v, \beta_t, \epsilon_\ell$ , and  $u\ell_H$  (the direction of  $\underline{f\ell}$ ) from the following identities:

$$\text{and} \quad \psi_t = \psi_v + \beta_t \quad (6.1)$$

$$u\ell_t = T_{t,H} u\ell_H$$

or

$$\begin{pmatrix} -\sin \epsilon_\ell \\ 0 \\ \cos \epsilon_\ell \end{pmatrix} = E_1(\phi_t) E_2(\theta_t) E_3(\beta_t) \begin{pmatrix} u\ell_x \\ u\ell_y \\ u\ell_z \end{pmatrix} \quad (6.2)$$

where  $(u\ell_x, u\ell_y, u\ell_z)$  are the known components of  $u\ell_H$ . Equation (6.1) gives  $\psi_t$  in terms of  $\psi_v, \beta_t$ . Equation (6.2) imposes the conditions that  $\underline{u\ell}$  be in the triangle plane and that it be tilted, relative to the spreader bar, by the angle  $\epsilon_\ell$ . This yields the following relations for the spreader-bar pitch and load swing angles (derivation omitted):

$$\sin \phi_t = (u\ell_x \sin \beta_t - u\ell_y \cos \beta_t) / \cos \epsilon_\ell \quad (6.3)$$

$$\sin (\theta_t - \Sigma) = \sin \epsilon_\ell \cos \Sigma / u\ell_z \quad (6.4)$$

where

$$\tan \Sigma = (u\ell_x \cos \beta_t + u\ell_y \sin \beta_t) / u\ell_z$$

Equations (6.1), (6.3), and (6.4) give the load swing and inertial spreader-bar attitude to be maintained by the helicopters for equilibrium flight as a function of flight condition  $(u\ell_H, \psi_v)$  and the selected values of  $\epsilon_\ell, \beta_t$ .

### Solution Existence Conditions

Equations (6.3) and (6.4) yield a solution for  $\phi_t, \theta_t$ , provided their right-hand sides have magnitudes less than 1. Necessary and sufficient conditions for this are

$$(\phi_t, \theta_t) \text{ exist IFF } [u\ell_z^2 + (u\ell_x \cos \beta_t + u\ell_y \sin \beta_t)^2]^{1/2} > |\sin \epsilon_\ell| \quad (6.5a)$$

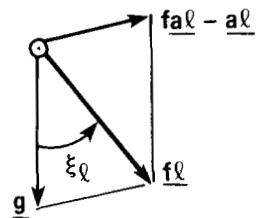
Further restrictions are needed to ensure that the triangle is right side up ( $|\phi_t|, |\theta_t| < \pi/2$ ) at any choice of  $\beta_t$ :

$$(\phi_t, \theta_t) \text{ exist at any } \beta_t \text{ and } |\phi_t|, |\theta_t| < \pi/2 \text{ IFF } u_{\ell z} > |\sin \epsilon_\ell| \quad (6.5b)$$

or at any choice of  $\beta_t, \epsilon_\ell$ :

$$(\phi_t, \theta_t) \text{ exist at any } \beta_t \text{ and } |\epsilon_\ell| < \pi/2 - \delta \text{ and } |\phi_t|, |\theta_t| < \pi/2 \text{ IFF } u_{\ell z} > \cos \delta \quad (6.5c)$$

These are progressively more restrictive conditions on  $\underline{u}_\ell$  which allow for satisfactory solutions over progressively larger domains of the independent variables. It is expected that the narrowest condition, equation (6.5c), is satisfied in dual-lift operations; that is, that  $u_{\ell z} > \cos \delta$ . Then a solution exists for any choice of  $\beta_t$  and any admissible  $\epsilon_\ell$  with the triangle right side up. Note that  $u_{\ell z}$  is defined by the angle between the apparent suspended load and the true vertical, denoted  $\xi_\ell$  in the sketch, and that the condition in equation (6.5c) can be written as



$$\xi_\ell < \delta$$

or

$$\frac{(\underline{fl} \cdot \underline{i}_H^2 + \underline{fl} \cdot \underline{j}_H^2)^{1/2}}{\underline{fl} \cdot \underline{k}_N} < \tan \delta$$

The angle  $\xi_\ell$  depends entirely on the combination  $\underline{fal} - \underline{al}$ : it increases, for example, with load drag, centrifugal acceleration, or load lift (provided  $\underline{fl} \cdot \underline{i}_H$  or  $\underline{fl} \cdot \underline{j}_H$  is nonzero), and it reaches  $60^\circ$  if, for example, the horizontal component of the apparent load is  $1.73 g$ . This condition provides general limits on  $\underline{al}$  and on the load aerodynamic specific force for which it can be appropriate to use the present mode of transport. It is expected that within the stated limits of interest in  $\underline{al}$ , and for load aerodynamic specific forces encountered with stable slung loads (principally moderate drag force with little lift) that the condition in equation (6.5c) is met, and this is assumed to be the case hereinafter.

## Results

To examine the variation of the triangle pitch and roll attitude with flight condition along a trajectory, it is convenient to express the direction  $\underline{u}_{\ell H}$ , in terms of direction angles. This can be done in several ways.

First,  $u_{lH}$  can be given in terms of  $\xi_{\ell}, \beta_{u\ell}$ , where

$$u_{lH} = \begin{pmatrix} u_{lx} \\ u_{ly} \\ u_{lz} \end{pmatrix} = \begin{pmatrix} \sin \xi_{\ell} \cos \beta_{u\ell} \\ \sin \xi_{\ell} \sin \beta_{u\ell} \\ \cos \xi_{\ell} \end{pmatrix} \quad (6.6)$$

or, inversely,

$$\sin \xi_{\ell} = (u_{lx}^2 + u_{ly}^2)^{1/2} \quad 0 < \xi_{\ell} < \pi/2$$

$$(\sin \beta_{u\ell}, \cos \beta_{u\ell}) = (u_{lx}, u_{ly}) / (u_{lx}^2 + u_{ly}^2)^{1/2} \quad -\pi < \xi_{\ell} < \pi$$

Here,  $\xi_{\ell}$  is the angular offset of  $\underline{u\ell}$  from the vertical, as sketched above, and indicates the net effect of trajectory acceleration or significant aerodynamic force on the direction of the apparent suspended load. It can reach magnitudes of 20° to 30° for the regime of interest here. The angle  $\beta_{u\ell}$  is the heading of  $\underline{f\ell}$  and  $\underline{fa\ell} - \underline{a\ell}$  relative to the ground track. Although  $\beta_{u\ell}$  is undefined when  $\underline{f\ell}$  is vertical (when  $\xi_{\ell} = 0$ ) there is no computational difficulty because  $\phi_t, \theta_t$  are independent of  $\beta_{u\ell}$  in this case. The results in equations (6.3) and (6.4) can now be written as

$$\left. \begin{aligned} \sin \phi_t &= \sin \xi_{\ell} \sin(\beta_t - \beta_{u\ell}) / \cos \epsilon_{\ell} & |\phi_t| < \pi/2 \\ \sin(\theta_t - \Sigma) &= \sin \epsilon_{\ell} \cos \Sigma / \cos \xi_{\ell} & |\theta_t - \Sigma| < \pi/2 \\ \tan \Sigma &= \tan \xi_{\ell} \cos(\beta_t - \beta_{u\ell}) & |\Sigma| < \pi/2 \end{aligned} \right\} \quad (6.7)$$

These give the triangle attitude in terms of three variables,  $\xi_{\ell}, \beta_t - \beta_{u\ell}$ , and  $\epsilon_{\ell}$ , where  $\beta_t - \beta_{u\ell}$  is the spreader-bar heading relative to the heading of the apparent suspended load.

The required spreader-bar pitch, equation (6.7), has the following properties:

$$|\Sigma| \leq \xi_{\ell}$$

$$\theta_t = \begin{cases} \Sigma & \text{if } \epsilon_{\ell} = 0 \\ \Sigma + A & \text{if } \epsilon_{\ell} \neq 0 \end{cases}$$

where

$$|\sin A| = |\sin \epsilon_{\ell} \cos \Sigma / \cos \xi_{\ell}| \geq |\sin \epsilon_{\ell}|$$

The required load roll about the spreader bar in equation (6.7) can be made zero at all times along a trajectory by continually aligning the spreader-bar

heading with that of the apparent load and varying the spreader-bar pitch with  $\underline{fal} - \underline{al}$  as required; that is,

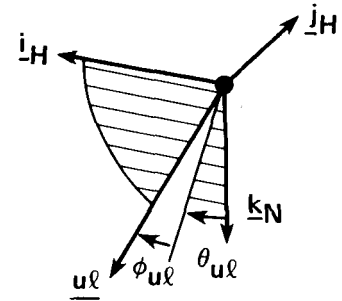
$$\text{if: } \beta_t = \beta_{u\ell}, \quad \text{then: } \phi_t = 0, \quad \theta_t = \epsilon_\ell + \xi_\ell$$

Similarly, in the case of equal bridle-cable loading,  $\theta_t$  can be made zero at all times by aligning the spreader bar perpendicular to  $\beta_{u\ell}$ ; and then the load swing varies with  $\underline{fal} - \underline{al}$  as required. That is,

$$\text{if: } \epsilon_\ell = 0 \quad \text{and} \quad \beta_t = \beta_{u\ell} \pm \pi/2, \quad \text{then: } |\phi_t| = \xi_\ell, \quad \theta_t = 0$$

Thus, it is possible to fly the system such that either  $\phi_t$  or  $\theta_t$  is invariant along a trajectory by maintaining a fixed spreader-bar heading relative to  $\beta_{u\ell}$ . However, note that  $\beta_{u\ell}$  undergoes large changes at turn entries and exits and at other transitions between steady flight segments so that flying the system with invariant load swing or spreader bar pitch appears impractical. Plots of the map  $(\xi_\ell, \beta_t - \beta_{u\ell}; \epsilon_\ell) \rightarrow (\phi_t, \theta_t)$  are given in figure 6.1 for  $\epsilon_\ell = 0$  ( $\rho_b = 1$ ) and  $\epsilon_\ell = 10^\circ$  ( $\rho_b = 1.9$  if  $\delta = 60^\circ$ ). The trends noted above are evident for the lines corresponding to  $|\beta_t - \beta_{u\ell}| \in \{0, \pm 90^\circ, 180^\circ\}$ .

Second, an alternative form for  $u\ell_H$  can be given in terms of pitch and roll angles relative to level-heading axes,  $\theta_{u\ell}, \phi_{u\ell}$ , (see sketch) where  $\theta_{u\ell}$  is a rotation about  $\underline{j}_H$  from the vertical which reflects acceleration and aerodynamic force along the ground track and  $\phi_{u\ell}$  is a roll angle which reflects acceleration and aerodynamic force lateral to the ground track. For these angles:

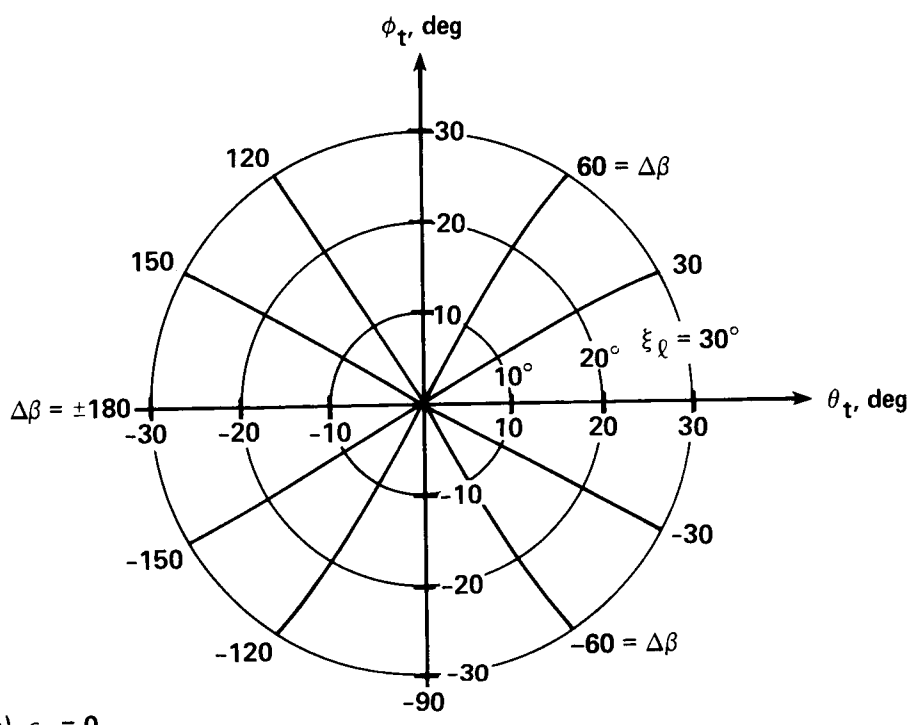


$$u\ell_H = \begin{pmatrix} u\ell_x \\ u\ell_y \\ u\ell_z \end{pmatrix} = \begin{pmatrix} \cos \phi_{u\ell} \sin \theta_{u\ell} \\ -\sin \phi_{u\ell} \\ \cos \phi_{u\ell} \cos \theta_{u\ell} \end{pmatrix} \quad (6.8)$$

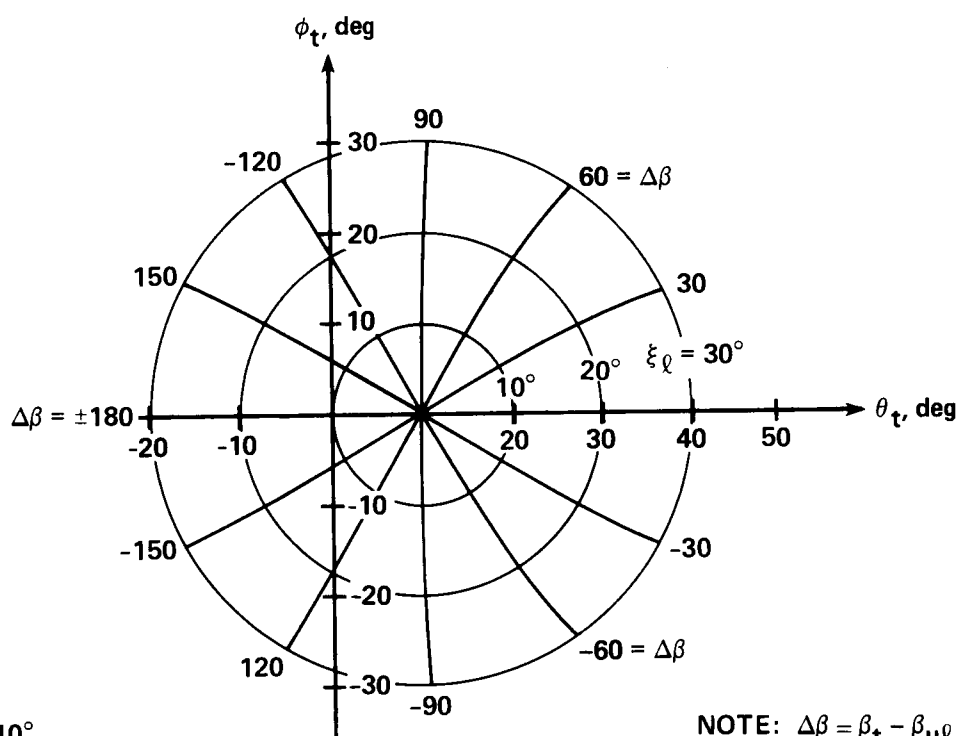
or, inversely:

$$\begin{aligned} \sin \phi_{u\ell} &= -u\ell_y & |\phi_{u\ell}| < \pi/2 \\ \tan \theta_{u\ell} &= u\ell_x / u\ell_z & |\theta_{u\ell}| < \pi/2 \end{aligned}$$

The range of these angles encountered in quasi-steady flight over the operational domain is examined in figure 6.2(a) for the MILVAN, with equilibrium aerodynamic force calculated from equation (4.5). First, results are shown for speeds and turn rates over their ranges of interest for the MILVAN, with the remaining flight condition variables ( $\gamma, \dot{v}$ , wind) taken as zero. The angle  $\theta_{u\ell}$  decreases from  $0^\circ$  to  $-10^\circ$  with airspeed because of load drag, and  $\phi_{u\ell}$  varies with turn rate over a range that increases to  $\pm 14^\circ$  with speed. Second, the remaining variables expand the ranges of  $(\theta_{u\ell}, \phi_{u\ell})$  encountered in quasi-steady flight to the boundary shown in figure 6.2(a) when taken over their maximum ranges of interest. Flightpath angle



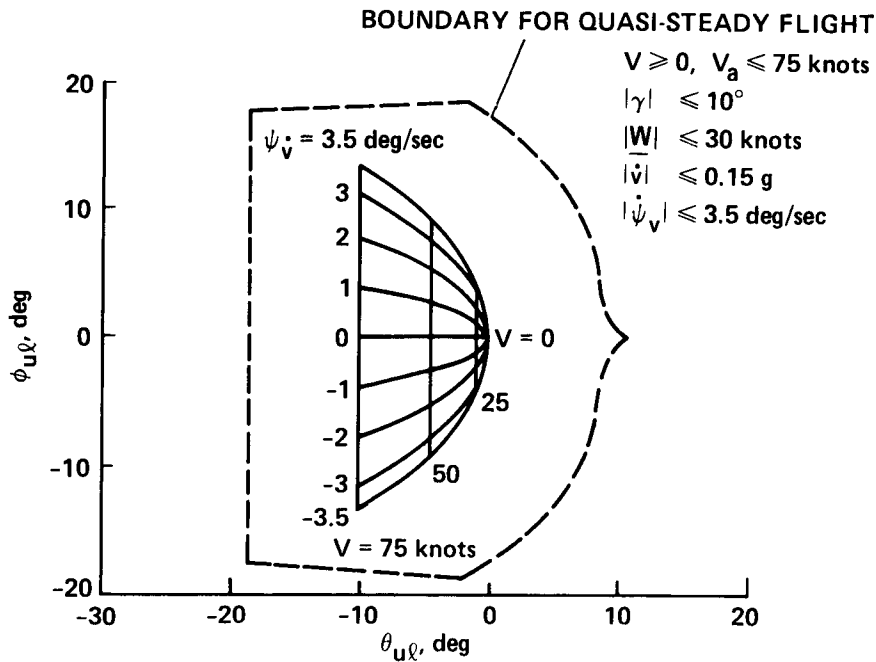
(a)  $\epsilon_\ell = 0$



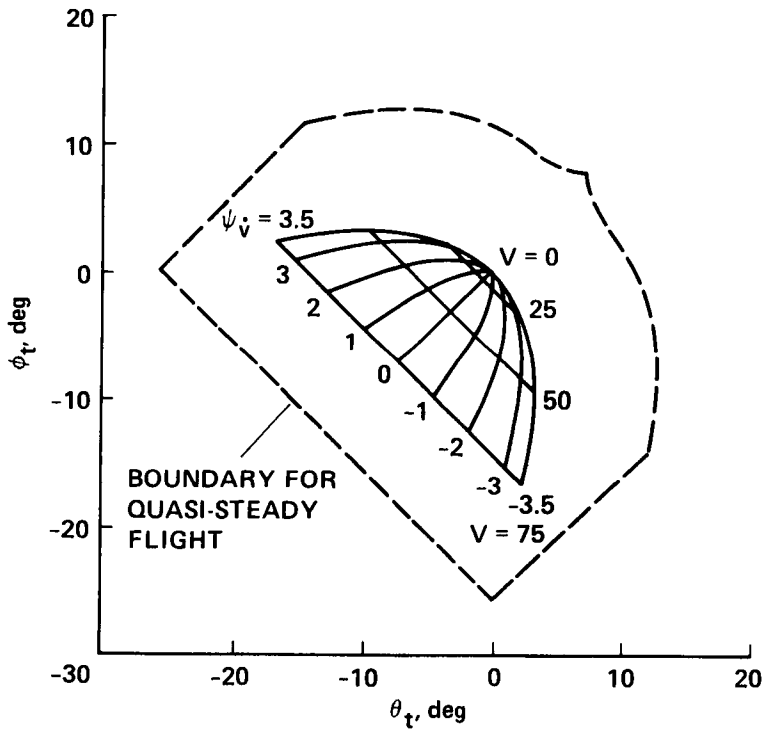
(b)  $\epsilon_\ell = 10^\circ$

NOTE:  $\Delta\beta = \beta_t - \beta_{u\ell}$

Figure 6.1.- Triangle attitude:  $(\phi_t, \theta_t)$  vs  $(\epsilon_\ell, \beta_t - \beta_{u\ell})$ .



(a) DIRECTION ANGLES OF APPARENT LOAD



(b) TRIANGLE ATTITUDE:  $\beta_t = 45^\circ, \epsilon_\ell = 0$

Figure 6.2.- Apparent-load direction angles and triangle attitude in quasi-steady flight for the MILVAN ( $W_\ell = 15,000 \text{ lb}$ ).

has no significant effect, whereas  $\dot{v}$  moves the figure left or right, and the wind acts to change the drag vector, depending on wind direction and magnitude; these effects collectively expand the direction angle ranges of interest to  $-20^\circ$  to  $10^\circ$  and  $\pm 20^\circ$  for  $\theta_{u\ell}$  and  $\phi_{u\ell}$ , respectively. Last, it is noted that the apparent-load magnitude,  $f\ell$  (not shown), is insensitive in these variations in flight condition and is within the range of 0.99-1.1 g for the entire set of flight conditions.

The triangle attitude angles can be given from equations (6.8), (6.3), and (6.4) as

$$\begin{aligned}\sin \phi_t &= (\cos \phi_{u\ell} \sin \theta_{u\ell} \sin \beta_t + \sin \phi_{u\ell} \cos \beta_t) / \cos \epsilon_\ell \\ \tan \Sigma &= \tan \theta_{u\ell} \cos \beta_t - \tan \phi_{u\ell} \sin \beta_t / \cos \theta_{u\ell} \\ \sin(\theta_t - \Sigma) &= \sin \epsilon_\ell \cos \Sigma / \cos \phi_{u\ell} \cos \theta_{u\ell}\end{aligned}\tag{6.9}$$

This form of the results is convenient for examining the variation in triangle attitude along a trajectory when the system is flown with fixed formation angle,  $\beta_t$ . Plots of the map  $(\phi_{u\ell}, \theta_{u\ell}; \epsilon_\ell, \beta_t) \rightarrow (\phi_t, \theta_t)$  are given in figure 6.3. For the longitudinal formation ( $\beta_t = 0$ ), the map is an identity in the case of equal bridle-cable loading ( $\epsilon_\ell = 0$ ); the load roll angle changes with turn rate and aerodynamic force lateral to the ground track, while the spreader-bar pitch is nearly fixed, and the spreader-bar pitch changes with speed and longitudinal aerodynamic force while the load-roll angle is nearly fixed. The reverse trends occur for the transverse formation; that is, spreader-bar pitch changes for turns (outside helicopter up) or side force, and the load swings backward/forward to accelerate/decelerate or in response to load drag. For the  $45^\circ$  formation angle, spreader-bar pitch and load-roll angle both change for turns and speed changes or as a result of load drag. This is further illustrated in figure 6.2(b) which shows the triangle attitude for steady turns and the boundary of the region required for quasi-steady flight in the case of the MILVAN with  $\beta_t = 45^\circ$  and  $\epsilon_\ell = 0$ . This boundary is defined as shown in figure 6.2(a) and encloses a range of  $-26^\circ$  to  $8^\circ$  in both  $\theta_{u\ell}$  and  $\phi_{u\ell}$ . At other values of  $\beta_t$  and  $\epsilon_\ell$ , the figure rotates and translates on the plot with corresponding changes in the angle range required in quasi-steady flight.

All of these variations of triangle attitude with maneuvering and aerodynamic forces are defined by the basic properties stated in equations (6.1) and (6.2); (1) the triangle necessarily contains  $\underline{f\ell}$ , (2) the spreader-bar tilt relative to  $\underline{f\ell}$  is  $\epsilon_\ell$ , and (3) the spreader-bar heading from the ground track is  $\beta_t$ .

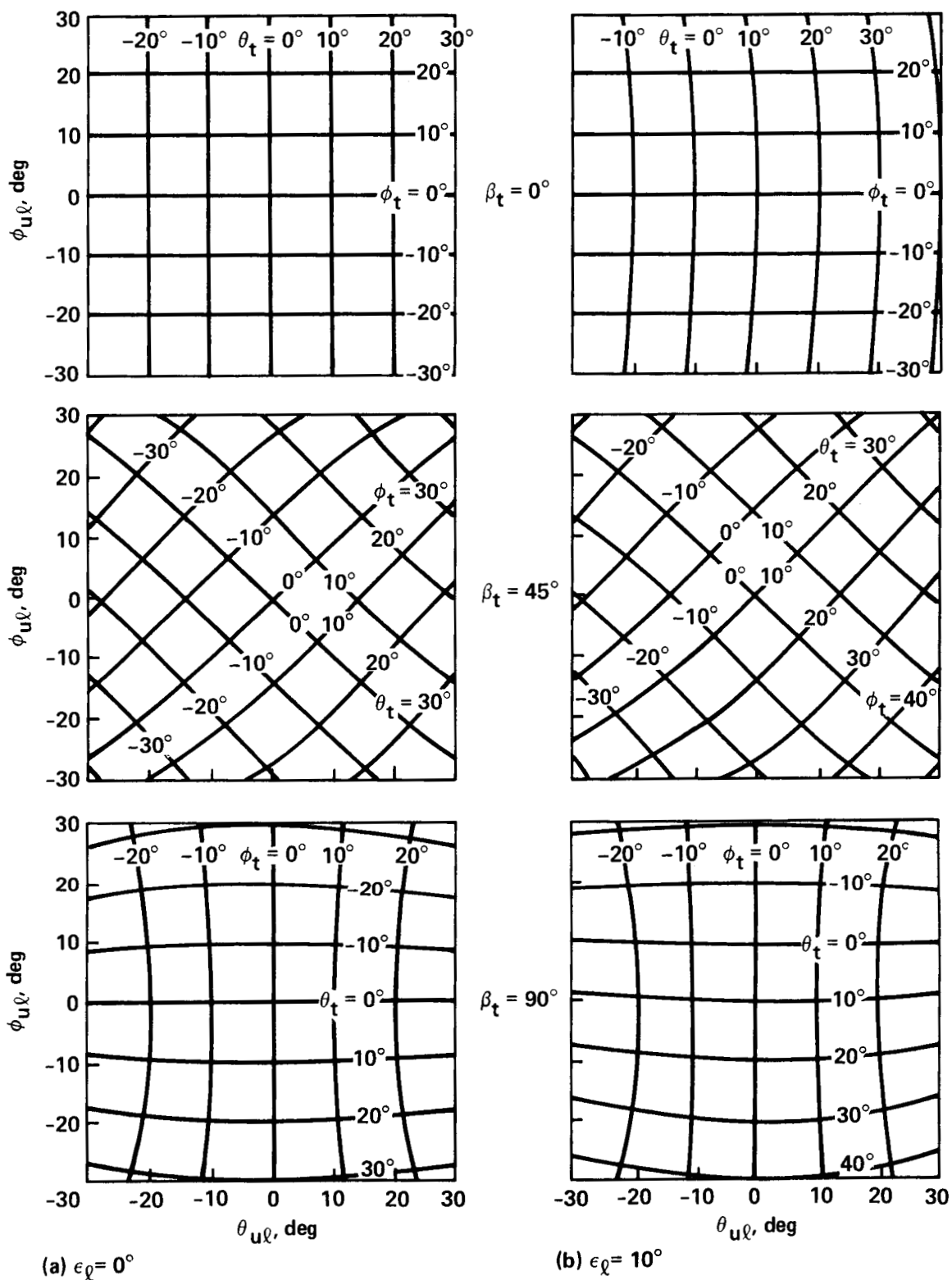


Figure 6.3.- Triangle attitude map:  $(\phi_t, \theta_t)$  vs  $(\phi_{u\ell}, \theta_{u\ell}; \epsilon_l, \beta_t)$ .

## 7. SPREADER-BAR AND HELICOPTER EQUATIONS: GENERAL RESULTS

The tether forces can be obtained from the spreader-bar equations in equations (3.1) and from the previous results for F35, F45 (eq. (5.1)). First, it is convenient to separate the bridle-cable forces into a term parallel to  $\underline{f}_l$  and a remainder:

$$\begin{aligned} F35 \underline{u35} &= \mu m_l \underline{f}_l - A \underline{i}_t \\ F45 \underline{u45} &= (1 - \mu) m_l \underline{f}_l + A \underline{i}_t \end{aligned} \tag{7.1}$$

where

$$\begin{aligned} \mu &\triangleq 0.5 \cos(\delta - \epsilon_l) / \cos \delta \cos \epsilon_l \\ A &\triangleq 0.5 m_l \underline{f}_l \cos(\delta - \epsilon_l) \cos(\delta + \epsilon_l) / \sin \delta \cos \delta \cos \epsilon_l \end{aligned}$$

The terms with coefficients  $\mu$ ,  $1 - \mu$ , are the apparent suspended load,  $\underline{f}_l$ , distributed to the endpoints of the spreader bar in the same ratio as the bridle-cable tensions; that is,  $0 \leq \mu \leq 1$  for  $\epsilon_l$  in its admissible range, and  $\mu/(1 - \mu) = \rho_b$ . The remaining terms in A are forces along the spreader bar in opposite directions, and produce the spreader-bar compression caused by the bridle-cable forces. Using equations (7.1) in the spreader-bar equations yields the tether forces:

$$\begin{aligned} F13 \underline{u13} &= \underline{F13}^0 - B \underline{i}_t \\ F24 \underline{u24} &= \underline{F24}^0 + B \underline{i}_t \end{aligned} \tag{7.2}$$

where

$$\begin{aligned} \underline{F13}^0 &\triangleq 0.5 m_l \underline{f}_3 + \mu m_l \underline{f}_l \\ \underline{F24}^0 &\triangleq 0.5 m_l \underline{f}_4 + (1 - \mu) m_l \underline{f}_l \\ B &\triangleq F34 + A \end{aligned}$$

Here,  $\underline{F13}^0$ ,  $\underline{F24}^0$  are the tether forces for the special case that the spreader-bar compression is due entirely to the suspended load (by means of the bridle cables) with no effect from the helicopters (by means of the tethers); that is, for the case in which  $B = 0$  and  $F34 = -A$ . The superscript ( )<sup>0</sup> will hereinafter refer to quantities corresponding to this special configuration, which can be obtained by appropriate choice of tether angle.

Equations (7.2) provide six scalar equations containing seven unknowns ( $F34$  or  $B$  and the tether-force components). The analysis is simpler if  $B$  is treated

as the independent variable, but this is equivalent to treating  $F_{34}$  or  $\epsilon_{13}$  or  $\epsilon_{24}$  as independent.

The tethers can always be placed in tension at any given  $B$  by locating the helicopters relative to the spreader bar such that

$$\begin{aligned} \underline{u}_{13} &= (\underline{F}_{13}^0 - B \underline{i}_t) / |\underline{F}_{13}^0 - B \underline{i}_t| \\ \underline{u}_{24} &= (\underline{F}_{24}^0 + B \underline{i}_t) / |\underline{F}_{24}^0 + B \underline{i}_t| \end{aligned}$$

and then  $F_{13}, F_{24} > 0$ . However, interest is limited to the case in which this can be done with the helicopters on the side of the spreader bar opposite the suspended load; that is, to cases for which  $\underline{u}_{13} \cdot \underline{k}_t, \underline{u}_{24} \cdot \underline{k}_t > 0$ , or, equivalently,  $\underline{F}_{13}^0 \cdot \underline{k}_t, \underline{F}_{24}^0 \cdot \underline{k}_t > 0$ . From equation (7.1),

$$\text{if: } f_{3k}, f_{4k} > 0, \quad \text{then: } F_{13k}^0, F_{24k}^0 > 0 \quad \text{for all } |\epsilon_\ell| < \frac{\pi}{2} - \delta \quad (7.3)$$

Attention is called to the notation  $( )_i, ( )_j, ( )_k$  to denote the  $t$ -axes components of a vector here and in the remaining analyses; for example,  $f_{3t} = (f_{3i}, f_{3j}, f_{3k}) = (\underline{f}_3 \cdot \underline{i}_t, \underline{f}_3 \cdot \underline{j}_t, \underline{f}_3 \cdot \underline{k}_t)$ . A simpler, more conservative condition than equation (7.3) can be given by writing  $f_{3k}, f_{4k}$  in terms of the apparent-load differences:

$$\begin{aligned} f_{3k} &= (\underline{f}_3 - \underline{f}_\ell + f_\ell \underline{u}_\ell) \cdot \underline{k}_t = (\underline{f}_3 - \underline{f}_\ell) \cdot \underline{k}_t + f_\ell \cos \epsilon_\ell \\ f_{4k} &= (\underline{f}_4 - \underline{f}_\ell + f_\ell \underline{u}_\ell) \cdot \underline{k}_t = (\underline{f}_4 - \underline{f}_\ell) \cdot \underline{k}_t + f_\ell \cos \epsilon_\ell \end{aligned}$$

and then

$$\text{if: } \frac{|\underline{f}_3 - \underline{f}_\ell|}{f_\ell}, \frac{|\underline{f}_4 - \underline{f}_\ell|}{f_\ell} < \sin \delta, \quad \text{then: } F_{13k}^0, F_{24k}^0 > 0 \quad \text{at all } |\epsilon_\ell| < \frac{\pi}{2} - \delta \quad (7.4)$$

Or even more conservatively,

$$\left. \begin{aligned} \text{if: } & \frac{|\underline{ab} - \underline{al}| + |\underline{\Delta f}| + |\underline{fal} - \underline{fab}|}{f_\ell} < \sin \delta \\ \text{then: } & F_{13k}^0, F_{24k}^0 > 0 \quad \text{at all } |\epsilon_\ell| < \frac{\pi}{2} - \delta \end{aligned} \right\} \quad (7.5)$$

In the present context  $|\underline{ab} - \underline{al}|, |\underline{\Delta f}| \ll f_\ell$ , and if the aerodynamic force difference satisfies  $|\underline{fal} - \underline{fab}| < f_\ell \sin \delta - |\underline{ab} - \underline{al}| - |\underline{\Delta f}|$  (that is, is below about 0.7 g) then the conditions in equations (7.3) to (7.5) are met. In that case, equation (7.2) yields the following results for the tether angles relative to the triangle and the tensions:

$$\left.
\begin{aligned}
\tan \epsilon_{13} &= (B - F13_i^0)/(F13_j^0{}^2 + F13_k^0{}^2)^{1/2} \\
\tan \epsilon_{24} &= -(B + F24_i^0)/(F24_j^0{}^2 + F24_k^0{}^2)^{1/2} \\
\tan \lambda_{13} &= F13_j^0/F13_k^0 \\
\tan \lambda_{24} &= F24_j^0/F24_k^0 \\
F13 &= [(F13_i^0 - B)^2 + F13_j^0{}^2 + F13_k^0{}^2]^{1/2} \\
F24 &= [(F24_i^0 + B)^2 + F24_j^0{}^2 + F24_k^0{}^2]^{1/2}
\end{aligned}
\right\} \quad (7.6)$$

These solutions for the angles follow from their relations with components of  $u_{13_t}, u_{24_t}$ , defined previously in figure 2.1. All angles are below  $90^\circ$ , and  $F13, F24 > 0$ , provided the conditions in equations (7.3), (7.4), or (7.5) are met. The above results are listed in the equation summary, figure 7.1, along with alternative expressions for some variables in terms of  $\epsilon_{13}, \epsilon_{24}$ . Either of these angles or  $F34$  or  $B$  can be taken as the independent variable.

The required helicopter thrust vectors in triangle axes can now be obtained from the last two of equations (3.1) and the above results for tether forces:

$$\left.
\begin{aligned}
\underline{T1} &= \underline{T1^0} + B \underline{i_t} \\
\underline{T2} &= \underline{T2^0} - B \underline{i_t}
\end{aligned}
\right\} \quad (7.7)$$

where

$$\begin{aligned}
\underline{T1^0} &= -\underline{F13^0} - m_1 \underline{f1} \\
\underline{T2^0} &= -\underline{F24^0} - m_2 \underline{f2}
\end{aligned}$$

The thrust-direction vectors  $\underline{u1}, \underline{u2}$  are defined as

$$\left.
\begin{aligned}
\underline{u1} &\triangleq -\underline{T1}/T1 \\
\underline{u2} &\triangleq -\underline{T2}/T2
\end{aligned}
\right\} \quad (7.8)$$

The negative sign is adopted in equations (7.8) so that the direction angles of  $\underline{u1}, \underline{u2}$  relative to triangle axes will tend to be small. To obtain angles below  $90^\circ$  (thrust directed away from the spreader bar) we require  $T1_k, T2_k < 0$ , and this is obtained at all admissible  $\epsilon_k$ , provided  $f1_k, f2_k, f3_k, f4_k > 0$ , or, more simply and more conservatively,

**DEFINITIONS:**

$$\mu = 0.5 \cos(\delta - \epsilon_{\rho}) / \cos \delta \cos \epsilon_{\rho}$$

$$\underline{F13}^0 = 0.5 m_b \underline{f3} + \mu m_{\rho} \underline{f\ell}$$

$$\underline{F24}^0 = 0.5 m_b \underline{f4} + (1 - \mu) m_{\rho} \underline{f\ell}$$

$$\underline{T1}^0 = -\underline{F13}^0 - m_1 \underline{f1}$$

$$\underline{T2}^0 = -\underline{F24}^0 - m_2 \underline{f2}$$

$$\alpha_1 = (\underline{T1}_j^0{}^2 + \underline{T1}_k^0{}^2)^{1/2}$$

$$\alpha_2 = (\underline{T2}_j^0{}^2 + \underline{T2}_k^0{}^2)^{1/2}$$

$$\alpha_3 = (\underline{F13}_j^0{}^2 + \underline{F13}_k^0{}^2)^{1/2}$$

$$\alpha_4 = (\underline{F24}_j^0{}^2 + \underline{F24}_k^0{}^2)^{1/2}$$

$$A = 0.5 m_{\rho} \underline{f\ell} \cos(\delta - \epsilon_{\rho}) \cos(\delta + \epsilon_{\rho}) / \sin \delta \cos \delta \cos \epsilon_{\rho}$$

$$B = F34 + A$$

**ASSUMPTIONS:**

$\underline{f\ell}_t, \underline{f1}_t, \underline{f2}_t, \underline{f3}_t, \underline{f4}_t, F34$  OR  $\epsilon_{13}$  OR  $\epsilon_{24}, m_{\rho}, m_b, m_1, m_2, \delta$  ARE KNOWN

$$|\epsilon_{\rho}| < \pi/2 - \delta$$

$\underline{fb}_k, \underline{f1}_k, \underline{f2}_k > 0$  OR (MORE CONSERVATIVELY)  $|\underline{f1} - \underline{f\ell}|, |\underline{f2} - \underline{f\ell}|, |\underline{f3} - \underline{f\ell}|, |\underline{f4} - \underline{f\ell}| < \underline{f\ell} \sin \delta$

**TETHER DIRECTIONS AND FORCES:**

$$F13 \underline{u13} = \underline{F13}^0 - B \underline{i}_t$$

$$F24 \underline{u24} = \underline{F24} + B \underline{i}_t$$

$$|\epsilon_{13}|, |\lambda_{13}|, |\epsilon_{24}|, |\lambda_{24}| < \pi/2$$

$$\tan \epsilon_{13} = (B - F13_i^0) / \alpha_3$$

$$\tan \epsilon_{24} = -(B + F24_i^0) / \alpha_4 = -(F13_i^0 + F24_i^0 + \alpha_3 \tan \epsilon_{13}) / \alpha_4$$

$$\tan \lambda_{13} = F13_j^0 / F13_k^0$$

$$\tan \lambda_{24} = F24_j^0 / F24_k^0$$

Figure 7.1.- Equation summary; spreader bar, tether, and thrust forces.

$$F_{13} = [(B - F_{13i}^0)^2 + \alpha_3^2]^{1/2} = \alpha_3 / \cos \epsilon_{13}$$

$$F_{24} = [(B + F_{24i}^0)^2 + \alpha_4^2]^{1/2} = \alpha_4 / \cos \epsilon_{24}$$

**SPREADER-BAR FORCE:**

$$F_{34} = -A + B$$

$$F_{34} = \alpha_3 \tan \epsilon_{13} - 0.5 m_\rho f_l \cos(\delta - \epsilon_\rho) / \sin \delta + 0.5 m_b f_{3i}$$

$$F_{34} = -\alpha_4 \tan \epsilon_{24} - 0.5 m_\rho f_l \cos(\delta + \epsilon_\rho) / \sin \delta - 0.5 m_b f_{4i}$$

**THRUST DIRECTIONS AND MAGNITUDES:**

$$\underline{T}_1 = -0.5 m_b \underline{f}_3 - \mu m_\rho \underline{f}_l - m_1 \underline{f}_1 + B_{i_t} = \underline{T}_1^0 + B_{i_t}$$

$$\underline{T}_2 = -0.5 m_b \underline{f}_4 - (1 - \mu) m_\rho \underline{f}_l - m_2 \underline{f}_2 - B_{i_t} = \underline{T}_2^0 - B_{i_t}$$

$$\underline{T}_1 + \underline{T}_2 = -m_\rho \underline{f}_l - m_b \underline{f}_b - m_1 \underline{f}_1 - m_2 \underline{f}_2$$

$$\underline{u}_1 = -\underline{T}_1 / T_1$$

$$\underline{u}_2 = -\underline{T}_2 / T_2$$

$$|\epsilon_1|, |\lambda_1|, |\epsilon_2|, |\lambda_2| < \pi/2$$

$$\tan \epsilon_1 = (T_1^0 + B) / \alpha_1 = (\alpha_3 \tan \epsilon_{13} - m_1 f_{1i}) / \alpha_1$$

$$\tan \epsilon_2 = (T_2^0 - B) / \alpha_2 = (\alpha_4 \tan \epsilon_{24} - m_2 f_{2i}) / \alpha_2$$

$$\tan \lambda_1 = T_{1j}^0 / T_{1k}^0$$

$$\tan \lambda_2 = T_{2j}^0 / T_{2k}^0$$

$$T_1 = [(T_1^0 + B)^2 + \alpha_1^2]^{1/2} = \alpha_1 / \cos \epsilon_1$$

$$T_2 = [(T_2^0 - B)^2 + \alpha_2^2]^{1/2} = \alpha_2 / \cos \epsilon_2$$

$$\Sigma T = T_1 + T_2 > |m_\rho \underline{f}_l + m_b \underline{f}_b + m_1 \underline{f}_1 + m_2 \underline{f}_2|$$

$$\delta_T = \frac{T_1}{T_2} = \frac{\alpha_1 \cos \epsilon_2}{\alpha_2 \cos \epsilon_1}$$

Figure 7.1.- Concluded.

$$\left. \begin{array}{l} \text{if: } \frac{|f_1 - f_l|}{f_l}, \frac{|f_2 - f_l|}{f_l}, \frac{|f_3 - f_l|}{f_l}, \frac{|f_4 - f_l|}{f_l} < \sin \delta, \\ \text{then: } T_{1k}, T_{2k} < 0 \quad \text{at all } |\epsilon_l| < \frac{\pi}{2} - \delta \end{array} \right\} \quad (7.9)$$

These results, along with expressions for the thrust direction angles and magnitudes, the thrust ratio, and thrust-sum are listed in figure 7.1. Alternative expressions in terms of the thrust angles  $\epsilon_{13}, \epsilon_{24}$  are given for some variables, and these show many similarities of form to the tether force results.

The following remarks pertain to figure 7.1.

1. The out-of-plane tether angles,  $\lambda_{13}, \lambda_{24}$ , depend only on the trajectory (on  $f_l, f_b$ ) and on the value of  $\epsilon_l$  and are independent of  $F_{34}$  or  $B$ . Since  $m_b f_3, m_b f_4 \ll m_l f_l$  then  $\lambda_{13}, \lambda_{24}$  are small angles at all  $|\epsilon_l| < \pi/2 - \delta$ , except possibly near the extremes of  $\epsilon_l$ , where one of the tethers is nearly unloaded, and

$$\tan \lambda_{13} \rightarrow f_{3j}/f_{3k} \quad \text{or} \quad \tan \lambda_{24} \rightarrow f_{4j}/f_{4k}$$

In general, the tethers lie in the plane of the triangle if  $f_{3j} = f_{4j} = 0$  (e.g., at windless hover) and otherwise lie out of the plane by small angles.

2. The spreader-bar force is given in terms of  $B$  or in terms of the tether direction angles,  $\epsilon_{13}$  or  $\epsilon_{24}$ , and conversely. Any of the three can be regarded as the independent variable. The expression for  $F_{34}$  contains three terms owing to, respectively, the tether direction, the suspended load, and the spreader bar. At the extremes of  $\epsilon_l$  (at  $|\epsilon_l| = \pi/2 - \delta$ ),  $F_{34}$  is independent of the load.

3. The expressions for the required thrust,  $T_1, T_2$ , have four terms which show that each helicopter carries its own apparent load plus very nearly half the spreader-bar apparent load ( $f_3, f_4$  differ negligibly from  $f_b$ ), plus a fraction of the apparent suspended load determined by  $\epsilon_l$ , plus mutually canceling terms of arbitrary magnitude along the spreader bar. At the extremes of  $\epsilon_l$  one helicopter carries the entire suspended load,  $m_l f_l$ , and the terms in  $f_l$  for the other are zero. At  $\epsilon_l = 0$ , the suspended load terms are the same for both helicopters.

4. The out-of-plane thrust angles,  $\lambda_1, \lambda_2$ , are independent of  $B$  or  $F_{34}$  or tether direction angles. In general, the thrust vectors lie in the triangle plane if  $m_b f_{3j} + 2m_1 f_{1j} = m_b f_{4j} + 2m_2 f_{2j} = 0$  (e.g., at windless hover) and otherwise lie out of the plane, principally to balance  $f_{1j}$  or  $f_{2j}$ .

5. The thrust sum and corresponding fuel requirements vary with  $B$  and can be minimized with respect to  $B$ . Solutions for this optimum configuration are given in the next section. At other values of  $B$ , only the mutually canceling components of  $T_1, T_2$  along the spreader bar (along  $i_t$ ) vary.

6. The vector sum  $T_1 + T_2$  is invariant with  $B$  and equals the sum of all apparent loads, as is expected from the force balance of the entire system. Therefore, the magnitude of the apparent-load sum is a lower bound for the

thrust-magnitude sum,  $\Sigma T$ . The lower bound is obtained only if the system can be flown with T1 and T2 parallel to the apparent-load sum.

## 8. SPREADER-BAR AND HELICOPTER EQUATIONS: TETHER-ANGLE OPTIMIZATION

The tether angle  $\epsilon_{13}$  (or, equivalently,  $\epsilon_{24}$  or F34 or B) is an independent variable in the general results (fig. 7.1) and can be selected to optimize some dependent function, such as thrust margin or fuel rate. The system thrust margin

$$M_T = (T1_{\max} - T1) + (T2_{\max} - T2) = (T1_{\max} + T2_{\max}) - \Sigma_T \quad (8.1)$$

is maximized at the minimum thrust sum.

Fuel-rate dependence on thrust was examined empirically for the UH-60 as an example case. First, test-stand data for its engines (two GE-T700s) indicate that fuel rate is very nearly linear and increasing with power output, and is accurately modeled in the form

$$\dot{w}_f = a + bP$$

where  $a$  and  $b$  vary with ambient air conditions and Mach number (see fig. 8.1). Second, the required power is nonlinear in thrust, but the nonlinearity is usually weak over the thrust range of interest. A simulation model of the UH-60 (refs. 13 and 16) was trimmed in various static equilibrium flight conditions for a range of weights in order to obtain power required versus thrust output. The results (fig. 8.2) show that the required power increases with thrust at all flight conditions except in the region of high-speed descending flight where it is insensitive to thrust. In addition, it is adequately approximated as linear in thrust over the

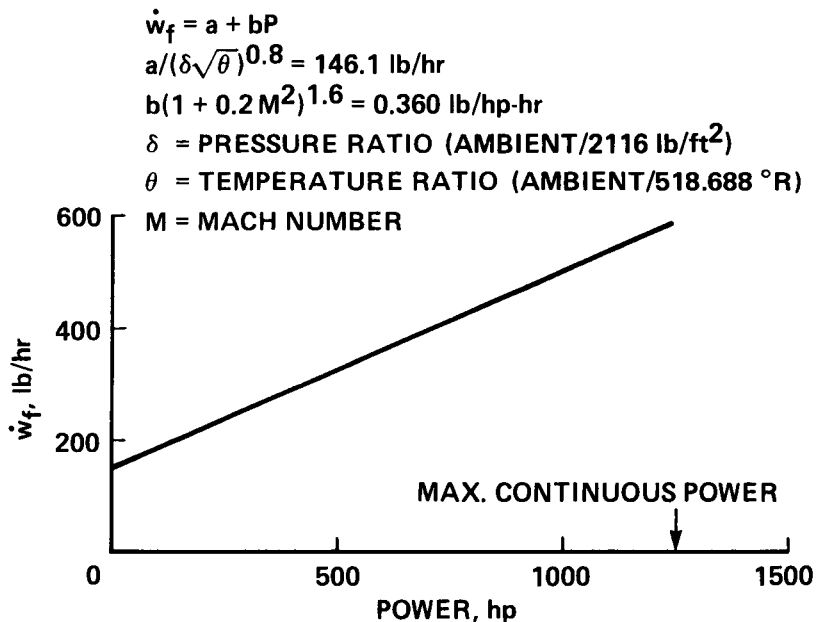


Figure 8.1.- Fuel rate versus power: GE-T700 engine.

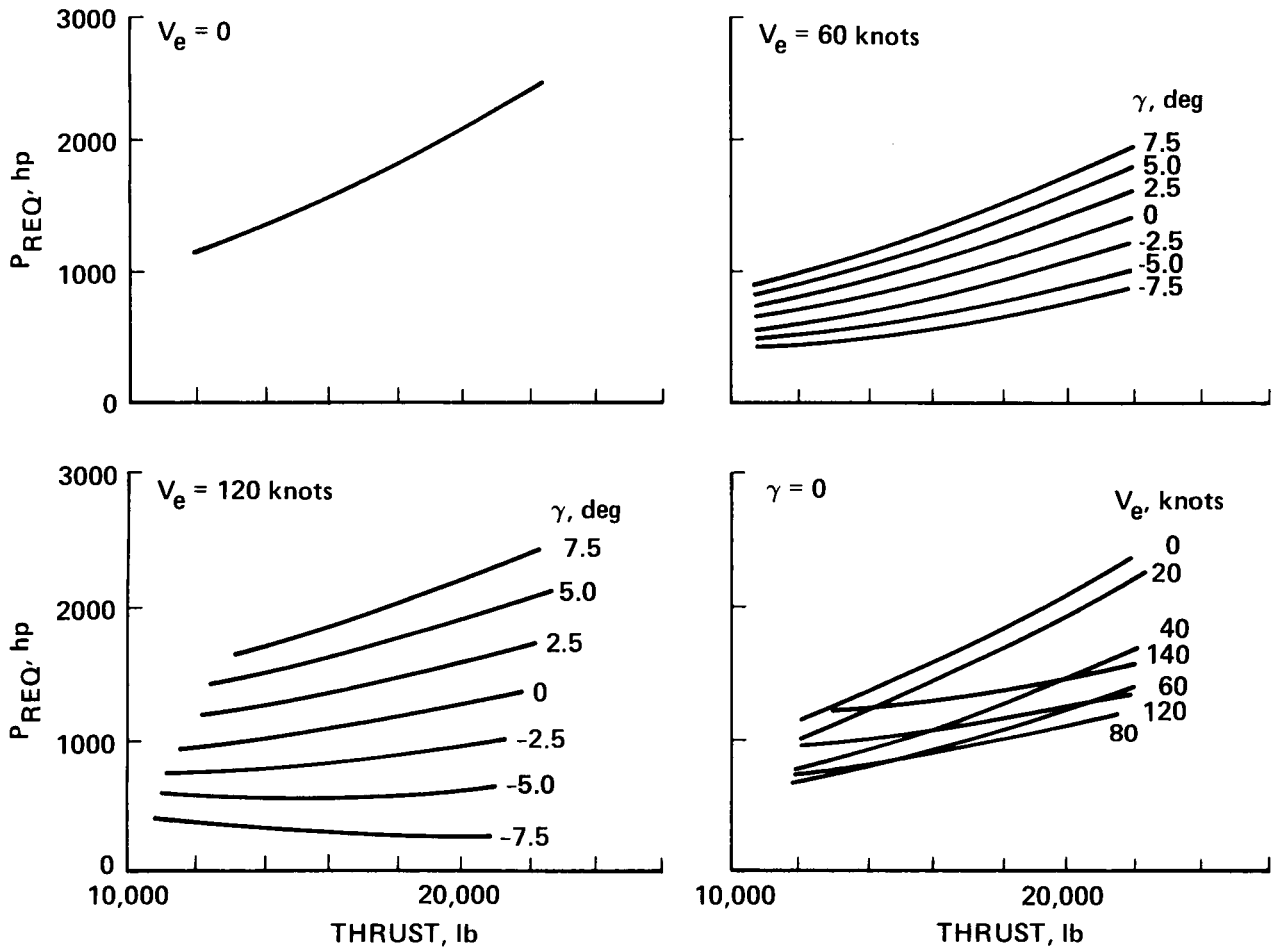


Figure 8.2.- Power required versus thrust in unaccelerated flight: UH-60.

range of flight conditions and thrust shown in the figure; that is, the required power for the UH-60 is of the form

$$P = c + dT$$

where the coefficients  $c$  and  $d$  vary with flight conditions. Then, fuel rate and thrust are linearly related:

$$\dot{w}_f = A + BT$$

The same degree of linearity and trends for the slope  $d$  are expected to characterize other engines and helicopters so that, in general, the dual-lift fuel rate sum is approximately linearly related to thrust:

$$\Sigma \dot{w}_f = (A_1 + A_2) + B_1 T_1 + B_2 T_2 \quad (8.2)$$

For flight conditions with positive  $B_1$  and  $B_2$ , the minimum fuel is obtained by minimizing the thrust-sum (weighted thrust-sum) in the case of identical (nonidentical) helicopters.

We select the tether angle to minimize the thrust-sum in this study. This choice yields the maximum system thrust margin in all cases and, for identical helicopters, it is expected that the corresponding fuel requirements will be minimized or insensitive to thrust and tether angle at all flight conditions. In addition, results are given for the configuration in which the apparent suspended load is distributed to the two helicopters in the same ratio as the bridle-cable force ratio; this yields simple general results for tether angles and thrust, and also minimizes the thrust-sum in the commonest cases of interest (at hover and for identical helicopters with equal load sharing).

We remark that the thrust-sum varies with three independent configuration variables ( $\epsilon_\ell$ ,  $\beta_t$ ,  $\epsilon_{13}$ ), and that it can be minimized with respect to all three variables. However, it is demonstrated below that the minimum given with respect to  $\epsilon_{13}$  alone is at the absolute lower bound given by the apparent load-sum in the commonest cases of interest and otherwise is within 1% of this lower bound for a large set of empirical examples. Thus,  $\epsilon_\ell$  and  $\beta_t$  can be selected as desired with no significant effect on thrust requirements.

In the analysis below it is convenient to minimize with respect to  $B$ , but this is equivalent to using either tether angle or  $F_{34}$  as the independent variable.

#### A Suboptimum Configuration

A near-optimum choice of  $B$  with simple results is obtained if we select  $B = 0$ . In this case, equations (7.2) and (7.7) give the tether and thrust forces as  $\underline{F13}^\circ$ ,  $\underline{F24}^\circ$ ,  $\underline{T1}^\circ$ , and  $\underline{T2}^\circ$ . These are repeated here for convenience.

if:  $B = 0$ , then:  $F_{34} = -A$

$$\begin{aligned} \underline{F13} \underline{u13} &= \underline{F13}^\circ = 0.5 m_b \underline{f3} + \mu m_\ell \underline{f\ell} \\ \underline{F24} \underline{u24} &= \underline{F24}^\circ = 0.5 m_b \underline{f4} + (1 - \mu) m_\ell \underline{f\ell} \\ \underline{T1} &= \underline{T1}^\circ = -0.5 m_b \underline{f3} - \mu m_\ell \underline{f\ell} - m_1 \underline{f1} \\ \underline{T2} &= \underline{T2}^\circ = -0.5 m_b \underline{f4} - (1 - \mu) m_\ell \underline{f\ell} - m_\ell \underline{f2} \end{aligned} \quad (8.3)$$

where

$$\begin{aligned} \mu &= 0.5 \cos(\delta - \epsilon_\ell) / \cos \delta \cos \epsilon_\ell \\ A &= 0.5 m_\ell \underline{f\ell} \cos(\delta - \epsilon_\ell) \cos(\delta + \epsilon_\ell) / \cos \epsilon_\ell \cos \delta \sin \delta \end{aligned}$$

The results for any other choice of  $B$  are related to these by adding the term  $B \underline{i}_t$  along the spreader bar as given previously in equations (7.2) and (7.7).

The results for this configuration are denoted by the superscript  $( )^\circ$  and are readily characterized:  $F_{34}$  depends only on the apparent suspended load but is independent of  $\underline{f}_1$ ,  $\underline{f}_2$ ,  $\underline{f}_3$ , and  $\underline{f}_4$ ; the apparent loads appear linearly in the tether and thrust forces; the suspended load is distributed to the tethers and the helicopters in the ratio  $\mu/(1 - \mu)$ , which depends only on  $\epsilon_g$  and is identical to the bridle-cable force ratio (fig. 5.1); and the spreader-bar load is distributed very nearly equally to the two helicopters. The tether tensions and directions are independent of the helicopter apparent loads and are generally aligned nearly parallel to  $\underline{f}_l$  (except for the unloaded tether when  $\epsilon_g$  is an extreme and  $\mu$  or  $(1 - \mu)$  is zero), and the thrust for each helicopter is independent of the other helicopter.

As is shown below, this simple configuration also minimizes  $\Sigma T$  in two cases of common interest. More generally, its thrust sum exceeds the minimum. Recalling the lower bound given by the apparent-load-sum (fig. 7.1), then the minimum thrust-sum, denoted  $\Sigma T^*$ , is bracketed by

$$\Sigma L \leq \Sigma T^* \leq \Sigma L^\circ \quad (8.4)$$

where

$$\Sigma T^\circ = T_{10} + T_{20}$$

$$\underline{\Sigma L} = m_g \underline{f}_l + m_b \underline{f}_b + m_1 \underline{f}_1 + m_2 \underline{f}_2$$

$$\Sigma L = |\underline{\Sigma L}|$$

#### Minimum Thrust-Sum Configuration

The thrust sum is given in figure 7.1 as a sum of positive functions of  $B$ , each with a single minimum:

$$\Sigma T = [(T_{1i}^\circ + B)^2 + \alpha_1^2]^{1/2} + [(T_{2i}^\circ - B) + \alpha_2^2]^{1/2}$$

where  $T_{1i}^\circ$ ,  $T_{2i}^\circ$ ,  $\alpha_1$ , and  $\alpha_2$  are defined in figure 7.1. The value of  $B$  that minimizes  $\Sigma T$  is (algebra omitted):

$$B^* = (\alpha_1 T_{2i}^\circ - \alpha_2 T_{1i}^\circ) / (\alpha_1 + \alpha_2) \quad (8.5)$$

Then,

$$\Sigma T^* = [(T_{1i}^\circ + T_{2i}^\circ)^2 + (\alpha_1 + \alpha_2)^2]^{1/2}$$

This result is derived assuming that  $\underline{f1}$ ,  $\underline{f2}$  do not vary with tether direction or rotor thrust. This assumption is not strictly satisfied, since the helicopter aerodynamic forces vary with thrust, but these variations are negligible.

Some functional properties of the minimum  $\Sigma T$  configuration can also be given. The minimum point for each thrust is

$$\min(T1) = \alpha_1 \quad \text{at} \quad B = -T1_i^0$$

$$\min(T2) = \alpha_2 \quad \text{at} \quad B = T2_i^0$$

and then

$$\Sigma T^* \geq \alpha_1 + \alpha_2 \quad \text{and} \quad B^* \quad \text{is between} \quad -T1_i^0 \quad \text{and} \quad T2_i^0$$

These properties indicate that  $B^*$  lies between the minimum points for the two thrust functions, and, in general, neither  $T1$  nor  $T2$  is minimized at  $B^*$ .

Expressions for the corresponding values of thrust, tether directions, and other variables that depend on  $B$  are listed in figure 8.3. For the minimum  $\Sigma T$  configuration,  $B^*$  and the other variables depend on all the apparent loads of the system. If  $B^* = 0$ , then the optimum configuration is given by equations 8.3. This occurs if  $\underline{T1}^0$  and  $\underline{T2}^0$  have identical tilt angles relative to the spreader bar (when  $T1_i^0/\alpha_1 = T2_i^0/\alpha_2$ ); for example, when (1)  $\epsilon_L = 0$  and  $m_1 \underline{f1} = m_2 \underline{f2}$  (identical helicopters, equal loading) or (2) the apparent loads  $\underline{f1}$ ,  $\underline{f2}$ ,  $\underline{f3}$ ,  $\underline{f4}$  are all parallel (e.g., at hover).

The general results in figure 8.3 indicate that the optimum thrust angles  $\epsilon_1^*$ ,  $\epsilon_2^*$  are equal (equal tilt from the spreader bar); however, the thrust vectors are not necessarily parallel, since their angles out-of-the-plane of the triangle,  $\lambda_1, \lambda_2$ , can differ. In addition,

$$|\tan \epsilon_1^*| = \frac{|\Sigma L_i|}{a_1 + a_2} \leq \frac{|\Sigma L_i|}{(\Sigma L_j^2 + \Sigma L_k^2)^{1/2}} = |\tan \epsilon_L|$$

and then

$$|\epsilon_1^*| < |\epsilon_L|$$

This inequality follows from the definitions of  $\alpha_1, \alpha_2$ , and the identity,  $\underline{T1}^0 + \underline{T2}^0 = -\Sigma L$ ; the result states that  $|\epsilon_1^*|$  is less than the tilt of  $\Sigma L$  from the spreader bar,  $\epsilon_L$ . The thrust ratio  $\rho_T^*$  depends on  $\epsilon_L$  and the apparent loads, and can be controlled by choosing  $\epsilon_L$  appropriately.

These results are difficult to characterize with respect to several properties of interest, such as (1) the optimum tether directions, and (2) the effects of load, spreader-bar and helicopter aerodynamics, and apparent loads on the solutions.

DEFINITIONS:<sup>a,b</sup>

$$\underline{\Sigma L} = m_\ell \underline{f\ell} + m_b \underline{fb} + m_1 \underline{f1} + m_2 \underline{f2}$$

SPREADER-BAR COMPRESSION:

$$B^* = (\alpha_1 T2_i^0 - \alpha_2 T1_i^0) / (\alpha_1 + \alpha_2)$$

$$B^* = 0.5 m_\ell f\ell \sin \delta \left( \frac{\alpha_1 - \alpha_2}{\alpha_1 + \alpha_2} - \tan \delta \tan \epsilon_\ell \right) - 0.5 m_b fb_i \frac{\alpha_1 - \alpha_2}{\alpha_2 - \alpha_1} - \frac{\alpha_1 m_2 f2_i - \alpha_2 m_1 f1_i}{\alpha_1 + \alpha_2}$$

$$F34^* = -A + B^*$$

THRUST FORCES:<sup>c</sup>

$$T1_t^* = T1_t^0 + B^*(1, 0, 0)^T = \left( -\frac{\alpha_1 \Sigma L_i}{\alpha_1 + \alpha_2}, T1_j^0, T1_k^0 \right)^T$$

$$T2_t^* = T2_t^0 - B^*(1, 0, 0)^T = \left( -\frac{\alpha_2 \Sigma L_i}{\alpha_1 + \alpha_2}, T2_j^0, T2_k^0 \right)^T$$

$$\tan \epsilon_1^* = \tan \epsilon_2^* = -\Sigma L_i / (\alpha_1 + \alpha_2)$$

$$T1^* = \alpha_1 / \cos \epsilon_1^*$$

$$T2^* = \alpha_2 / \cos \epsilon_1^*$$

$$\Sigma T^* = [\Sigma L_i^2 + (\alpha_1 + \alpha_2)^2]^{1/2}$$

$$P_T^* = \alpha_1 / \alpha_2$$

TETHER FORCES:<sup>c</sup>

$$F13^* u13_t^* = F13_t^0 - B^*(1, 0, 0)^T = \left( \frac{\alpha_1 \Sigma L_i}{\alpha_1 + \alpha_2} - m_1 f1_i, F13_j^0, F13_k^0 \right)^T$$

$$F24^* u24_t^* = F24_t^0 + B^*(1, 0, 0)^T = \left( \frac{\alpha_2 \Sigma L_i}{\alpha_1 + \alpha_2} - m_2 f2_i, F24_j^0, F24_k^0 \right)^T$$

$$\tan \epsilon_{13}^* = (\alpha_1 \tan \epsilon_1^* + m_1 f1_i) / \alpha_3$$

$$\tan \epsilon_{24}^* = (\alpha_2 \tan \epsilon_2^* + m_2 f2_i) / \alpha_4$$

$$F13^* = \alpha_3 / \cos \epsilon_{13}^*$$

$$F24^* = \alpha_4 / \cos \epsilon_{24}^*$$

<sup>a</sup>  $\mu, A, F13^0, F24^0, T1^0, T2^0, \alpha_1, \alpha_2, \alpha_3, \alpha_4$  ARE DEFINED IN FIG. 7.1.

<sup>b</sup> ASSUMPTIONS LISTED IN FIG. 7.1 ARE MADE HERE.

<sup>c</sup>  $\lambda_1, \lambda_3, \lambda_{13}, \lambda_{24}$  ARE INDEPENDENT OF  $\epsilon_{13}$  AND ARE GIVEN IN FIG. 7.1.

Figure 8.3.- Minimum thrust-sum configuration: tether and thrust forces.

However, two special cases for which the minimum  $\Sigma T$  configuration is given by equation (8.3) are more easily interpreted and are considered next.

### Results for Identical Helicopters and Equal Load Sharing

It is expected that the most common dual-lift case will be the one in which the helicopters are identical and there is equal load sharing. Results can be derived from the equations given in figure 8.3 using the following assumptions:

$$m_1 = m_2 = m_h$$

$$\underline{f}_1 = \underline{f}_2 = \underline{f}_h$$

$$\underline{f}_3 = \underline{f}_4 = \underline{f}_b$$

$$\epsilon_\ell = 0$$

The equal helicopter masses are denoted  $m_h$ . Equal apparent helicopter loads, denoted  $\underline{f}_h$ , can be assumed for identical helicopters with equal loading, but it suffices that their difference be negligible ( $|\underline{f}_1 - \underline{f}_2| \ll 0.1 g$ ). The differences  $|\underline{f}_3 - \underline{f}_b| = |\underline{f}_4 - \underline{f}_b| = |\underline{\Delta f}|$  are zero in static equilibrium and generally negligible over the maneuvering domain of interest. Last, the spreader bar is set level relative to the apparent suspended load ( $\epsilon_\ell = 0$ ), and this results in equal helicopter loading ( $\mu = 0.5, T1^* = T2^*$ ).

These assumptions result in considerable simplification of the equations given in figure 8.3 because  $\alpha_1 = \alpha_2$ , and  $\alpha_3 = \alpha_4$ . In addition,  $B^* = 0$ , so that the optimum configuration is given by equation (8.3) for this case. Results for the tether and thrust force variables are given in figure 8.4. Results are also given in terms of the dimensionless apparent-load difference vectors,  $\underline{\ell}_b, \underline{\ell}_h$ , in order to indicate the effects of aerodynamic forces, where

$$\underline{\ell}_b = m_b(\underline{f}_b - \underline{f}_\ell)/m_\ell f_\ell = m_b(\underline{f}_{ab} - \underline{f}_{a\ell} + \underline{a}_\ell - \underline{a}_b)/m_\ell f_\ell$$

$$\underline{\ell}_h = m_h(\underline{f}_h - \underline{f}_\ell)/m_\ell f_\ell = m_h(\underline{f}_{ah} - \underline{f}_{a\ell} + \underline{a}_\ell - \underline{a}_h)/m_\ell f_\ell$$

These differences are due to differences in aerodynamic specific forces and accelerations, and, in view of the discussion in section 4, are negligible at hover and low speeds, and are dominated by aerodynamics at higher speeds (principally as drag differences). As shown below, the tether and thrust directions depart from the direction of  $\underline{f}_\ell$  in proportion to these differences. Note that for  $m_b \ll m_\ell$ , then  $|\underline{\ell}_b| \ll 1$  in all circumstances within the assumptions of figure 7.1. The following properties are seen in figure 8.4(a):

1. The optimum tether directions are parallel; each tether carries half the apparent load attributable to the suspended load and spreader bar and is parallel to

**ASSUMPTIONS:**

$$e_\ell = 0$$

$$m_1 = m_2 = m_h$$

$$\underline{f}_1 = \underline{f}_2 = \underline{f}_h \quad \text{OR} \quad |\underline{f}_1 - \underline{f}_2| \ll 0.1 \text{ g}$$

$$\underline{f}_3 = \underline{f}_4 = \underline{f}_b \quad \text{OR} \quad |\underline{\Delta f}| \ll 0.1 \text{ g}$$

**DEFINITIONS:**

$$\underline{\ell}_b = m_b(\underline{f}_b - \underline{f}_\ell)/m_\ell f_\ell$$

$$\underline{\ell}_h = m_h(\underline{f}_h - \underline{f}_\ell)/m_\ell f_\ell$$

**RESULTS:**

$$|\lambda_n|, |\epsilon_n^*| < \pi/2 \quad n \in \{1, 2, 13, 24\}$$

$$F_{34}^* = -0.5 m_\ell f_\ell \text{Ctn} \delta$$

$$\tan \lambda_{13} = \tan \lambda_{24} = \frac{m_b f_{b_j}}{m_\ell f_\ell + m_b f_{b_k}} = \frac{\ell b_j}{1 + m_b/m_\ell + \ell b_k}$$

$$\tan \epsilon_{13}^* = \tan \epsilon_{24}^* = \frac{-m_b f_{b_i}}{\sqrt{(m_b f_{b_j})^2 + (m_\ell f_\ell + m_b f_{b_k})^2}} = \frac{-\ell b_j}{\sqrt{\ell b_j^2 + (1 + m_b/m_\ell + \ell b_k)^2}}$$

$$\underline{F}_{13}^* = \underline{F}_{24}^* = 0.5(m_\ell f_\ell + m_b \underline{f}_b)$$

$$\tan \lambda_1 = \tan \lambda_2 = \frac{m_b f_{b_j} + 2m_h f_{h_j}}{m_\ell f_\ell + m_b f_{b_k} + 2m_h f_{h_k}} = \frac{\ell b_j + 2\ell h_j}{1 + m_b/m_\ell + 2m_h/m_\ell + \ell b_k + 2\ell h_k}$$

$$\begin{aligned} \tan \epsilon_1^* = \tan \epsilon_2^* &= \frac{-m_b f_{b_i} - 2m_h f_{h_i}}{\sqrt{(m_b f_{b_j} + 2m_h f_{h_j})^2 + (m_\ell f_\ell + m_b f_{b_k} + 2m_h f_{h_k})^2}} \\ &= \frac{-\ell b_i - 2\ell h_i}{\sqrt{(\ell b_j + 2\ell h_j)^2 + (1 + m_b/m_\ell + 2m_h/m_\ell + \ell b_k + 2\ell h_k)^2}} \end{aligned}$$

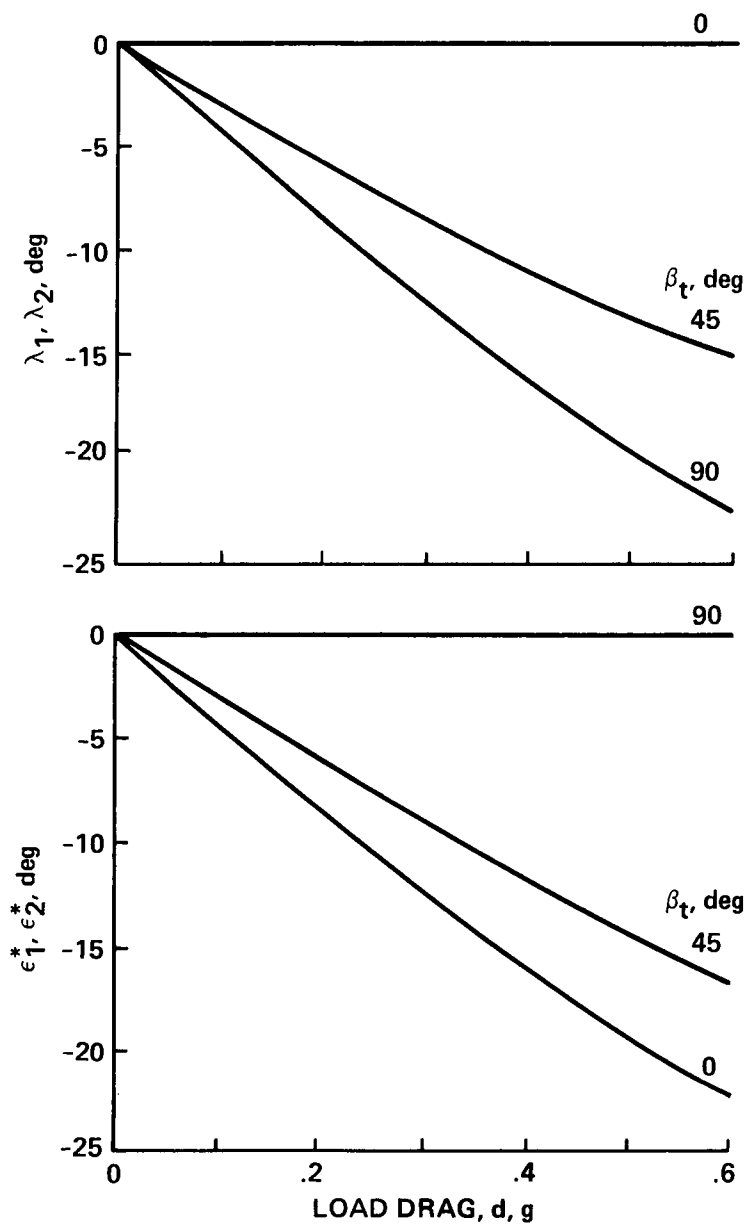
$$\underline{T}_1^* = \underline{T}_2^* = -0.5 m_\ell f_\ell - 0.5 m_b \underline{f}_b - m_h \underline{f}_h$$

$$\Sigma T^* = |m_\ell f_\ell + m_b \underline{f}_b + 2m_h \underline{f}_h|$$

$$\rho_T^* = 1$$

**(a) EQUATION SUMMARY**

Figure 8.4.- Minimum thrust-sum configuration: identical helicopters, equal load sharing.



(b) EFFECT OF LOAD DRAG ON THRUST DIRECTION ANGLES:

$$(\epsilon_\rho, \delta, m_b, m_h) = (0, 60^\circ, 0.1m_\rho, 1.5m_\rho)$$

$$\underline{fab} = \underline{fah} = \underline{ao} = 0$$

$$\underline{fa\ell} = -d i_H$$

Figure 8.4.- Concluded

this load vector-sum. This tether direction is independent of the helicopter apparent loads. The tether angles,  $\lambda_{13}$ ,  $\epsilon_{13}^*$ , are also given in terms of the spreader-bar load-difference vector,  $\underline{lb}_t$ . Since  $|\underline{lb}| \ll 1$ , these angles are small (approximately  $\underline{lb}_j$ ,  $\underline{lb}_i$ , respectively) and the tethers are close to  $\underline{k}_t$  and  $\underline{ul}$  (nearly in the triangle plane and nearly perpendicular to the spreader bar). These angles increase with the spreader-bar mass ratio  $m_b/m_\ell$ .

2. The required helicopter thrust vectors are parallel; each equals half the total apparent load and is directed opposite this vector-sum. The thrust-sum equals the lower bound given by the magnitude of the total apparent loads so that  $\Sigma L = \Sigma_T^* = \Sigma_T^0$  for this case. The thrust direction angles relative to triangle axes,  $\lambda_1$ ,  $\epsilon_1^*$ , are also given in terms of the difference vectors,  $\underline{lb}_t$ ,  $\underline{lh}_t$ . These angles are small, and the thrust direction is nearly aligned with  $\underline{k}_t$  provided  $|\underline{lh}| \ll 1$ . However, moderate differences in aerodynamics,  $|\underline{fah} - \underline{fal}|/f_\ell$ , can occur and can result in larger angles between  $\underline{k}_t$  and  $\underline{u1}^*$ ,  $\underline{u2}^*$ . This is illustrated in figure 8.4(b) by the effect of load drag on these angles for various values of  $\beta_t$ .

#### Results for Parallel Apparent Loads

For the parallel apparent-loads case the apparent loads of all bodies in the system are parallel; that is,

$$\text{Parallel apparent loads: } \underline{f1} = f1 \underline{ul}, \underline{f2} = f2 \underline{ul}, \underline{f3} = f3 \underline{ul}, \underline{f4} = f4 \underline{ul} \quad (8.6a)$$

Windless hover is a case of general interest which satisfies equation (8.6a) and for which the specific apparent loads are also equal in magnitude:

$$\text{Windless hover: } \underline{fal} = \underline{fab} = \underline{fa1} = \underline{fa2} = 0$$

$$\underline{\omega v} = 0$$

(8.6b)

$$\underline{al} = \underline{ab} = \underline{a1} = \underline{a2} = 0$$

and then

$$\underline{f\ell} = \underline{f1} = \underline{f2} = \underline{f3} = \underline{f4} = g \underline{k}_N$$

For parallel apparent loads,  $B^* = 0$  and the optimum configuration is again given by equation (8.3). Results for all variables that depend on  $B$  are listed in figure 8.5, including values at the extremes of  $\epsilon_\ell$  and at  $\epsilon_\ell = 0$ . In addition, graphical results are given figure 8.6. These show the following properties of the minimum  $\Sigma_T$  configuration for this case:

1. The tethers and thrust vectors are aligned parallel to the apparent suspended load vector,  $\underline{f\ell}$ , at all  $\epsilon_\ell$ . This is always in the plane of the triangle and at an angle  $\epsilon_\ell$  from the perpendicular to the spreader bar, and the system is coplanar.

**ASSUMPTIONS:**

$$\underline{f1} = f1 \underline{u\ell}, \underline{f2} = f2 \underline{u\ell}, \underline{f3} = f3 \underline{u\ell}, \underline{f4} = f4 \underline{u\ell}$$

**DIRECTIONS:**

$$\underline{u13}^* = \underline{u24}^* = \underline{u1}^* = \underline{u2}^* = \underline{u\ell}$$

$$\epsilon_{13}^* = \epsilon_{24}^* = \epsilon_1^* = \epsilon_2^* = \epsilon_\ell$$

$$\lambda_{13} = \lambda_{24} = \lambda_1 = \lambda_2 = 0$$

**FORCES:**

SYMBOL	GENERAL FORM	VALUES AT		
		$\epsilon_\ell = -\pi/2 + \delta$	$\epsilon_\ell = 0$	$\epsilon_\ell = \pi/2 - \delta$
F34*	$0.5 m_\ell f\ell \frac{\cos(\delta - \epsilon_\ell) \cos(\delta + \epsilon_\ell)}{\cos \delta \cos \epsilon_\ell}$	0	$-0.5 m_\ell f\ell \text{ctn } \delta$	0
$\mu$	$0.5 \cos(\delta - \epsilon_\ell) / \cos \delta \cos \epsilon_\ell$	0	0.5	1
F13*	$\mu m_\ell f\ell + 0.5 m_b f3$	$0.5 m_b f3$	$0.5(m_\ell f\ell + m_b f3)$	$m_\ell f\ell + 0.5 m_b f3$
F24*	$(1 - \mu) m_\ell f\ell + 0.5 m_b f4$	$m_\ell f\ell + 0.5 m_b f4$	$0.5(m_\ell f\ell + m_b f4)$	$0.5 m_b f4$
T1*	$\mu m_\ell f\ell + 0.5 m_b f3 + m_1 f1$	$0.5 m_b f3 + m_1 f1$	$0.5(m_\ell f\ell + m_b f3) + m_1 f1$	$m_\ell f\ell + 0.5 m_b f3 + m_1 f1$
T2*	$(1 - \mu) m_\ell f\ell + 0.5 m_b f4 + m_2 f2$	$m_\ell f\ell + 0.5 m_b f4 + m_2 f2$	$0.5(m_\ell f\ell + m_b f4) + m_1 f2$	$0.5 m_b f4 + m_2 f2$
$\Sigma T$	$m_\ell f\ell + m_b fb + m_1 f1 + m_2 f2$			

Figure 8.5.- Minimum thrust-sum configuration: parallel apparent loads.

2. The spreader bar is in compression at all  $|\epsilon_\ell| < \pi/2 - \delta$ . The compression is zero at the extremes of  $\epsilon_\ell$  and maximum at  $\epsilon_\ell = 0$ . This maximum is proportional to  $\text{ctn } \delta$  and decreases with  $\delta$ .

3. Each tether supports half the spreader-bar apparent load plus a fraction of the suspended load determined by  $\epsilon_\ell$ . At the extremes of  $\epsilon_\ell$ , one tether supports the entire load, and at  $\epsilon_\ell = 0$  the tethers support the load equally.

4. Each helicopter supports its own apparent load plus that portion of the spreader bar and suspended apparent loads carried by its tether cable.

5. The thrust-sum equals the sum of apparent loads,  $m_\ell f\ell + m_b fb + m_1 f1 + m_2 f2$ , at all  $\epsilon_\ell$ .

Thus, for parallel apparent loads, the optimum geometry is simple; the entire system is coplanar, with tether- and thrust-force vectors parallel to the apparent loads, and with thrust requirements at the lower bound,  $\Sigma L$ .

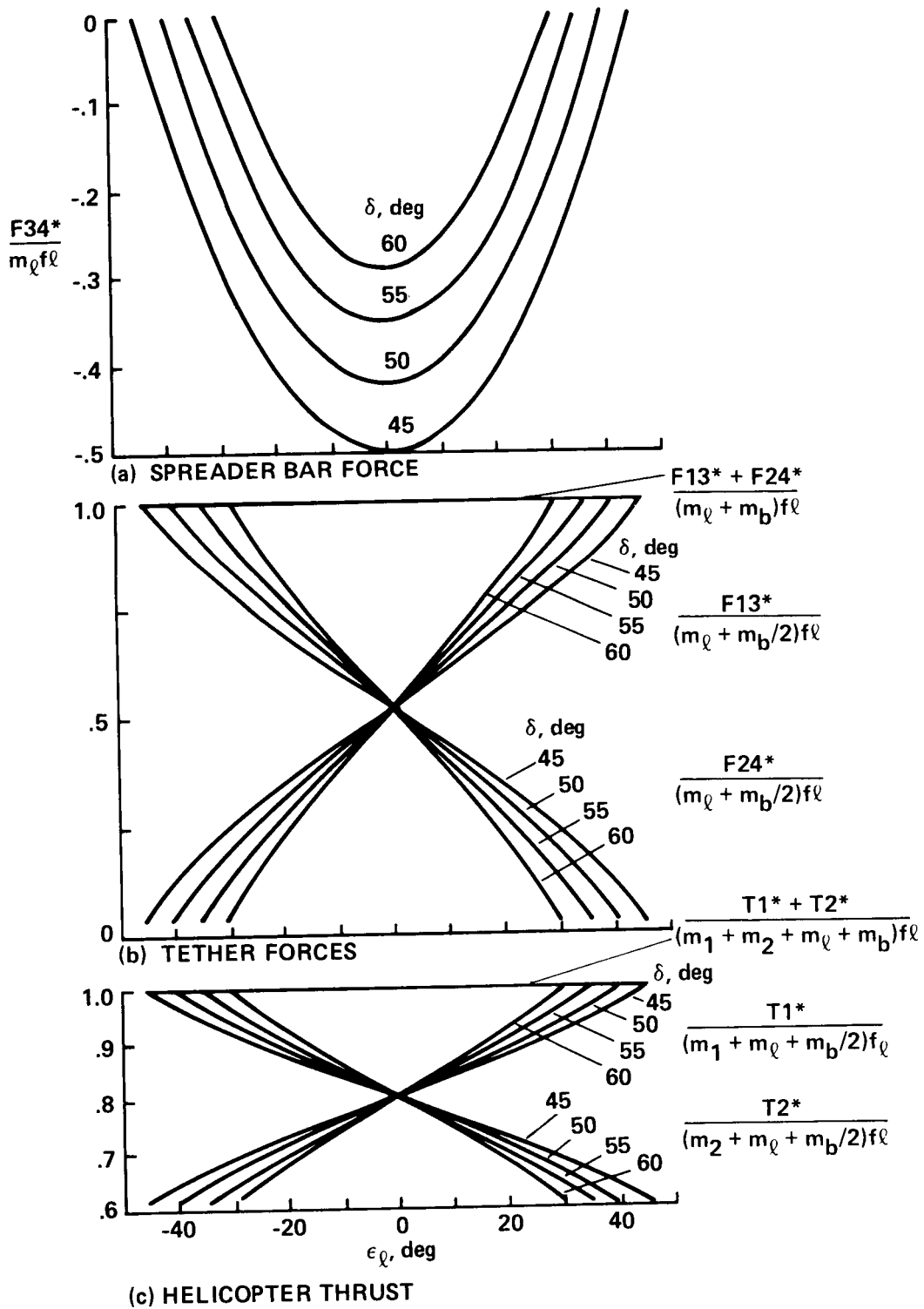


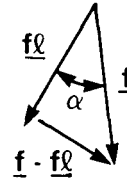
Figure 8.6.- Minimum thrust-sum configuration: results for equal specific apparent loads ( $f_1 = f_2 = f_3 = f_4 = f_\ell$ ),  $(m_b, m_1, m_2) = (0.1, 1.5, 1.5)m_\ell$ ,  $\delta = 60^\circ$ .

## General Results for Minimum Thrust-Sum Configuration

Parallel loads are obtained at hover and result in the simple geometry noted above. It can be shown that if the angles between these vectors are small, or if the apparent load is small compared to  $m_k f_l$ , then the properties given above for parallel apparent loads approximately characterize the minimum thrust-sum configuration.

The spreader-bar apparent load is always small ( $m_b f_b \ll m_k f_l$ ) in the present context so that significant departures from the results in figure 8.5 require significant angles between the apparent loads of the helicopters and cargo. In most circumstances, these angles are small in equilibrium flight. Referring to the sketch, the angle between  $\underline{f}$ ,  $\underline{f}_l$  satisfies

$$|\sin \alpha| \leq \frac{|\underline{f} - \underline{f}_l|}{f_l} = \frac{|\underline{f}_a - \underline{f}_a l + \underline{a} l - \underline{a}|}{f_l}$$



where  $\underline{f}$ ,  $\underline{f}_a$ , and  $\underline{a}$  are associated with either helicopter. The differences in specific apparent loads are due to differences in aerodynamic forces and c.g. accelerations. The discussion in section 4 indicates that acceleration differences are of the order of 0.1 g or less on all segments of the trajectory for the maneuver domain and system sizes of interest here, and the aerodynamic forces are dominated by drag and tend to be parallel so that differences,  $|\underline{f}_a - \underline{f}_a l|$ , of the order of 0.1 g require sufficiently large airspeeds, and are unlikely to exceed 0.5 g at any speed. Thus, the properties noted in figure 8.5 provide a good approximate characterization of the minimum  $\Sigma T$  configuration to moderate airspeeds, of the order of 50 knots.

Computations were made to indicate the variation in configuration geometry with apparent-load differences. The algorithm used to compute the configuration is given in figure 8.7 and comprises a solution of the restricted trim problem stated in section 3. The input quantities consist of system parameters, the formation angle, and spreader-bar tilt, and the specific aerodynamic forces and reference trajectory acceleration. Simplifying approximations are made in computing the apparent loads; that is, differences in c.g. accelerations of the constituent masses and the spreader-bar rotation effect  $\Delta \underline{f}$  are neglected. Accurate calculation of these quantities and the input aerodynamic forces requires solution of the general trim problem outlined in section 3, but reasonable approximations can be made for the present illustrative calculations based on section 4. The remaining equations are taken from equations (6.3) and (6.4) and figures 7.1 and 8.3; these are valid for any equilibrium configuration except that the parameter  $B$  is computed to minimize  $\Sigma T$ .

Cargo drag is the principal aerodynamic force in equilibrium, and results were obtained for its effects on the configuration; that is, for the case in which

**INPUTS:<sup>a</sup>**

$$m_{\rho}, m_b, m_1, m_2, \delta, \epsilon_{\rho}, \beta_t$$

$$fa_{lH}, fab_H, fa1_H, fa2_H, ao_H$$

**SPECIFIC APPARENT LOADS, LEVEL-HEADING AXES:<sup>b</sup>**

$$fl_H = g_H + fa_{lH} - ao_H$$

$$fb_H = g_H + fab_H - ao_H$$

$$f3_H = fb_H$$

$$f4_H = fb_H$$

$$f1_H = g_H + fa1_H - ao_H$$

$$f2_H = g_H + fa2_H - ao_H$$

**TRANSFORMATION OF TRIANGLE AXES:**

$$fl = |fl_H|$$

$$u1_H = fl_H/fl$$

$$\phi_t = \sin^{-1} [(ul_x \sin \beta_t - ul_y \cos \beta_t)/\cos \epsilon_{\rho}] \quad |\phi_t| < \pi/2$$

$$\Sigma = \tan^{-1} [(ul_x \cos \beta_t + ul_y \sin \beta_t)/ul_z] \quad |\Sigma| < \pi/2$$

$$\theta_t = \Sigma + \sin^{-1} (\sin \epsilon_{\rho} \cos \Sigma / ul_z) \quad |\theta_t - \Sigma| < \pi/2$$

$$T_{t,H} = E_1(\phi_t) E_2(\theta_t) E_3(\beta_t)$$

**SPECIFIC APPARENT LOADS, TRIANGLE AXES:**

$$fl_t = fl (-\sin \epsilon_{\rho}, 0, \cos \epsilon_{\rho})$$

$$f1_t = T_{t,H} f1_H$$

$$f2_t = T_{t,H} f2_H$$

$$f3_t = T_{t,H} f3_H$$

$$f4_t = T_{t,H} f4_H$$

**AUXILLIARY QUANTITIES:**

$$\mu = 0.5 \cos(\delta - \epsilon_{\rho}) / \cos \delta \cos \epsilon_{\rho}$$

$$F13_t^0 = 0.5 m_b f3_t + \mu m_{\rho} fl_t$$

$$F24_t^0 = 0.5 m_b f4_t + (1 - \mu) m_{\rho} fl_t$$

$$T1_t^0 = -F13_t^0 - m_1 f1_t$$

$$T2_t^0 = -F24_t^0 - m_2 f2_t$$

Figure 8.7.- Restricted trim algorithm: minimum  $\Sigma_T$  configuration.

$$\alpha_1 = (T1_j^0{}^2 + T1_k^0{}^2)^{1/2}$$

$$\alpha_2 = (T2_j^0{}^2 + T2_k^0{}^2)^{1/2}$$

**BRIDLE-CABLE TENSIONS:**

$$F35 = 0.5 m_{\rho} f_{\ell} \cos(\delta - \epsilon_{\rho}) / \cos \delta \sin \delta$$

$$F45 = 0.5 m_{\rho} f_{\ell} \cos(\delta + \epsilon_{\rho}) / \cos \delta \sin \delta$$

**SPREADER-BAR COMPRESSION, MINIMUM  $\Sigma T$  CONFIGURATION:**

$$B^* = (\alpha_1 T2_i^0 - \alpha_2 T1_i^0) / (\alpha_1 + \alpha_2)$$

$$B = B^*$$

$$F34 = B - 0.5 m_{\rho} f_{\ell} \cos(\delta - \epsilon_{\rho}) \cos(\delta + \epsilon_{\rho}) / \cos \epsilon_{\rho} \cos \delta \sin \delta$$

**THRUST AND TETHER FORCES:<sup>c</sup>**

$$T1_t = T1_t^0 + B(1, 0, 0)$$

$$T2_t = T2_t^0 - B(1, 0, 0)$$

$$F13_t = F13_t^0 - B(1, 0, 0)$$

$$F24_t = F24_t^0 + B(1, 0, 0)$$

<sup>a</sup> ASSUMPTIONS LISTED IN SECTION 2 ARE MADE HERE.

<sup>b</sup> DIFFERENCES IN C.G. ACCELERATIONS AND  $\Delta f$  ARE NEGLECTED.

<sup>c</sup> F13, F24 ARE TETHER FORCES AS APPLIED TO SPREADER BAR.

Figure 8.7.- Concluded.

$$\underline{fa}_{\ell} = -d \underline{i}_H$$

$$\underline{fab} = \underline{fa1} = \underline{fa2} = 0$$

where drag is represented as a force along the ground-track direction for these computations (this assumes zero wind and  $\gamma$  for simplicity). Computations were made for

$$d \in [0, 0.6] g$$

$$|\epsilon_{\rho}| < \pi/2 - \delta$$

$$\beta_t \in [0^{\circ}, 90^{\circ}]$$

and for both static equilibrium and turns ( $\underline{a} = 0$  and  $\underline{a} = 0.3 \text{ g } \underline{1}_H$  for all bodies), and for both identical and nonidentical helicopters ( $m_1 = m_2 = 1.5 m_\ell$  and  $m_1 = m_\ell, m_2 = 2m_\ell$ ). Some results are presented in figure 8.8 for the case of identical helicopters, static equilibrium, and  $\beta_t = 45^\circ$ .

Results for tether- and thrust-direction angles (fig. 8.8(a)) show that  $|\lambda_{13}|$  increases with cargo drag at all  $\epsilon_\ell$  but is small (under  $5^\circ$ ) except when the tether is unloaded ( $\epsilon_\ell = -30^\circ$ ); that is, tether No. 1 is always nearly in the triangle plane except in the extreme case in which it is unloaded. The thrust angle  $|\lambda_1|$  increases with cargo drag to moderate angles ( $15^\circ - 20^\circ$ ) at all  $\epsilon_\ell$ , so that the thrust vector is more noticeably inclined from the triangle plane as drag increases. The tether and thrust tilt angles,  $\epsilon_{13}^*$  and  $\epsilon_1^*$ , are shown versus  $\epsilon_\ell$ . For zero drag, these directions are parallel to  $\underline{f}_\ell$  ( $\epsilon_{13}^* = \epsilon_1^* = \epsilon_\ell$ ) as expected; for nonzero drag these angles depart from this simple relationship increasingly with drag. This departure becomes large near the extreme case in which the tether is unloaded. These conclusions apply to both tethers and thrust vectors in all cases calculated.

Additional results in figure 8.8 show that the angles between the two tethers and the two thrust vectors,  $\angle(\underline{u}_{13}^*, \underline{u}_{24}^*)$ ,  $\angle(\underline{T}_1^*, \underline{T}_2^*)$ , are zero for (1)  $\epsilon_\ell = 0$  independent of drag and (2)  $d = 0$  independent of  $\epsilon_\ell$ . That is, these are parallel vector pairs for the cases of (1) identical helicopters with equal load sharing and (2) parallel apparent loads, as previously noted in figures 8.4 and 8.5. In other cases, these are not parallel, and moderate mutual tether and thrust angles must be maintained by the helicopters as a function of drag, helicopter masses,  $\beta_t$  and  $\epsilon_\ell$ .

The angle between  $\underline{T}_1^*$  and apparent-load-sum was computed (not shown). The thrust vectors are necessarily along  $-\underline{\Sigma L}$  whenever  $\underline{\Sigma T}^*$  is at the lower bound,  $\underline{\Sigma L}$ . This angle was found to be zero for  $\epsilon_\ell = 0$  or  $d = 0$  and otherwise increases with drag but is under  $10^\circ$  in all cases calculated. In addition, the required thrust-sum and its lower and upper bounds (eq. (8.4)) were also computed. These were within 1% of each other in all cases computed; that is, both  $\underline{\Sigma T}^*$  and  $\underline{\Sigma T}^\circ$  were within 1% of the absolute lower bound on thrust requirements given by  $\underline{\Sigma L}$ .

In general,  $\underline{\Sigma T}^*$  varies with the independent configuration variables not included in the optimization,  $\beta_T$  and  $\epsilon_\ell$ , but the present empirical results and special-case analytical results above demonstrate that the variation is weak or nonexistent. The possibility of variations in the aerodynamics and, hence, in the apparent loads,  $\underline{f}_\ell$ ,  $\underline{f}_b$ ,  $\underline{f}_1$ , and  $\underline{f}_2$ , with  $\beta_t, \epsilon_\ell$  is not considered in the preceding statement since the apparent loads enter the problem as parameters in this report. However, it can be assumed that these variations are negligible for the load and helicopters and that the spreader-bar aerodynamic force may vary strongly with  $\beta_t$  but always satisfies  $|\underline{F}_{ab}|/W_\ell \ll 1$ ; therefore, its variations are negligible in the sums  $\underline{\Sigma L}, \underline{\Sigma T}^*$ . Thus,  $\underline{\Sigma T}^*$  is very nearly invariant with  $\beta_t$  and  $\epsilon_\ell$ , and no significant further reductions are available by minimizing  $\underline{\Sigma T}^*$  with respect to these variables.

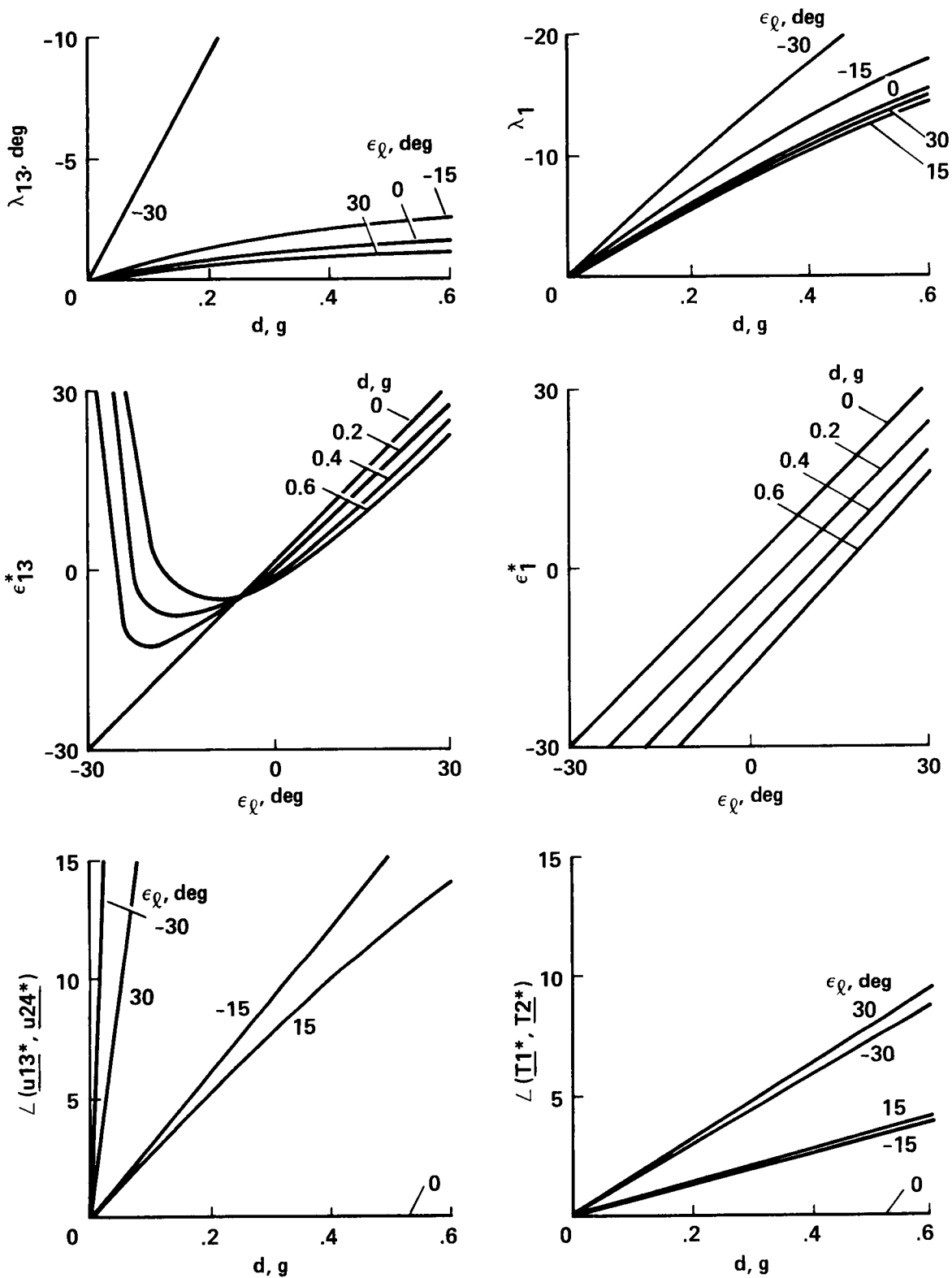


Figure 8.8.- Effect of cargo drag on minimum thrust-sum configuration:  $\beta_t = 45^\circ$ ,  $\delta = 60^\circ$ ,  $(m_b, m_1, m_2) = (0.1, 1.5, 1.5)m_g$ ,  $\underline{fa} = d \underline{i}_H$ .

## 9. LOAD DISTRIBUTION

In this section, load distribution refers to the apportioning of the thrust requirement  $\Sigma T^*$  to the two helicopters. This can be controlled within a range of values by selecting the spreader-bar tilt,  $\epsilon_\ell$ , appropriately within its admissible range for no cable collapse. However, each helicopter has a thrust limit,  $T1_{\max}$ ,  $T2_{\max}$ , which further restricts the range of load distributions that can be flown to those for which all thrust margins are positive; that is,  $\epsilon_\ell$  can be flown provided that

$$\begin{aligned} M_1(\epsilon_\ell) &= T1_{\max} - T1^*(\epsilon_\ell) > 0 \\ M_2(\epsilon_\ell) &= T2_{\max} - T2^*(\epsilon_\ell) > 0 \\ M_T(\epsilon_\ell) &= \Sigma T_{\max} - \Sigma T^*(\epsilon_\ell) > 0 \end{aligned} \tag{9.1}$$

where

$$\Sigma T_{\max} \triangleq T1_{\max} + T2_{\max}$$

To examine the corresponding limits on load sharing, consider the space of thrust combinations (see fig. 9.1) and let  $p$  be the locus of thrust combinations for the minimum  $\Sigma T$  configuration generated as  $\epsilon_\ell$  varies over its admissible range:

$$p = [(T1^*, T2^*): -\pi/2 + \delta < \epsilon_\ell < \pi/2 - \delta] \tag{9.2}$$

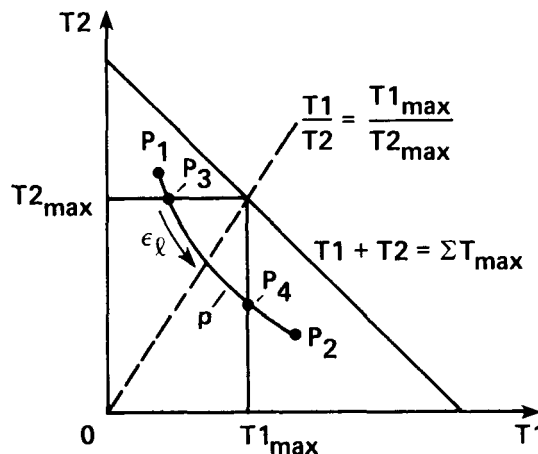


Figure 9.1.- Available and required thrust combinations.

Assume two properties of  $p$ :

A1.  $T1^*$  increases with  $\epsilon_\ell$

A2.  $T2^*$  decreases with  $\epsilon_\ell$

The endpoints of this curve-segment,  $p_1, p_2$ , correspond to the extremes of  $\epsilon_\ell$

$$\epsilon_{\ell_1} = -\pi/2 + \delta$$

$$\epsilon_{\ell_2} = \pi/2 - \delta$$

Next, consider the helicopter thrust limits  $T1_{\max}, T2_{\max}$ , and the region of thrust combinations given by (see fig. 9.1):

$$\mathcal{F} \triangleq [0, T1_{\max}] \times [0, T2_{\max}]$$

Every combination in this region satisfies the requirements for positive thrust margins (eq. (9.1)), and every point outside does not. Therefore, only that subsegment of  $p$  inside this region, if any, can be used in selecting  $\epsilon_\ell$ . Assume that the use of dual lift is restricted to suspended loads that cannot be carried by a single helicopter. Then,  $T1_{\max}, T2_{\max}$  must be less than the maximum values of  $T1^*, T2^*$  at the endpoints of  $p$  since these correspond to unloading one of the helicopters. In addition, assume that dual lift is possible; that is, that  $p$  intersect the required region. For this, it suffices that  $\Sigma T^*$  be less than  $\Sigma T_{\max}$  at all  $\epsilon_\ell$ . This requires that  $p$  be below the boundary  $T1 + T2 = \Sigma T_{\max}$  in figure 9.1. This is not an unduly restrictive assumption since  $\Sigma T^*$  is very nearly invariant with  $\epsilon_\ell$  for all the special and empirical cases discussed in section 8. Thus, for situations in which dual lift is both necessary and possible, assume

$$A3. \quad T1_{\max} < T1^*(\epsilon_\ell), \quad T2_{\max} < T2^*(\epsilon_\ell) \quad (\text{dual lift is necessary})$$

$$A4. \quad \Sigma T^*(\epsilon_\ell) < \Sigma T_{\max} \quad \text{for} \quad \epsilon_{\ell_1} < \epsilon_\ell < \epsilon_{\ell_2} \quad (\text{dual lift is possible})$$

The assumptions, A1 - A4, suffice for  $p$  to have some nontrivial subsegment within the required region:

$$p' = [(T1^*, T2^*): \epsilon_{\ell_3} < \epsilon_\ell < \epsilon_{\ell_4}] \quad (9.3a)$$

where the endpoints of this segment,  $p_3, p_4$  (see fig. 9.1) correspond to tilt angles,  $\epsilon_{\ell_3}, \epsilon_{\ell_4}$ , defined by

$$T2^*(\epsilon_{\ell_3}) = T2_{\max} \quad (9.3b)$$

$$T1^*(\epsilon_{\ell_4}) = T1_{\max}$$

Then the available range of the thrust ratio,  $T1^*/T2^*$ , is

$$\rho_T^*(\epsilon_{\ell_3}) = \frac{\Sigma T^*}{T2_{\max}} - 1 < \rho_T^* < \rho_T^*(\epsilon_{\ell_4}) = \frac{T1_{\max}}{\Sigma T^* - T2_{\max}} \quad (9.3c)$$

A suitable choice of thrust ratio is given by the thrust limits:

$$\rho_{Tx} \stackrel{\Delta}{=} T1_{\max}/T2_{\max} \quad (9.4)$$

This occurs at  $\epsilon_{\ell}$  corresponding to the intersection of the locus,  $p$ , with the line  $T1/T2 = T1_{\max}/T2_{\max}$  in figure 9.1, and it is always a possible choice (it is always in the subsegment,  $p'$ ) for the present assumptions. Note that this choice is also mandatory when the load equals the system's maximum load-carrying capacity (when  $\Sigma T^* = \Sigma T_{\max}$ ), since the only such point in the region of non-negative thrust margins in figure 9.1 occurs at  $(T1_{\max}, T2_{\max})$ . Thus, only when the suspended load is significantly below the system's maximum payload is there any significant range of choice of  $\rho_T^*$  other than  $\rho_{Tx}$ . The thrust margins for this choice are in the same ratio; if

$$\text{if: } \rho_T^* = \rho_{Tx}, \quad \text{then: } M_1/M_2 = \rho_{Tx}$$

The conditions A1 - A4 suffice for a solution to exist that has positive thrust margins. The results for parallel apparent loads (figs. 8.5 and 8.6) satisfy A1, A2, assuming that the apparent loads are constant or that they vary negligibly with  $\epsilon_{\ell}$ . In addition,  $\Sigma T^* = \Sigma L$  and is invariant with  $\epsilon_{\ell}$  for this case; the locus  $p$  is the straight line  $T1 + T2 = \Sigma L$ ; and the condition A4 requires simply  $\Sigma L < \Sigma T_{\max}$  for a solution to exist.

The conditions A1 and A2 and the insensitivity of  $\Sigma T^*$  to  $\epsilon_{\ell}$  are difficult to verify analytically for arbitrary apparent loads. However, these conditions are satisfied by all the empirical cases discussed in section 8, and at flight conditions in which the apparent loads are nearly parallel, which encompasses low-speed flight and is expected to encompass most flight conditions and helicopter-load combinations of interest.

Further, it can be shown that if the configuration is selected to obtain  $B = 0$ , then  $T1^\circ$  and  $T2^\circ$  are, respectively, increasing and decreasing with  $\epsilon_{\ell}$ . Thus, conditions analogous to A3 and A4 suffice for solutions with positive thrust margins for this configuration also.

Finally, assuming that  $\epsilon_{13}$  is selected to minimize  $\Sigma T$ , then the value of  $\epsilon_{\ell}$  corresponding to any choice of  $\rho_T^*$  can be calculated from the general equations in figure 8.3:

$$\rho_T^* = \frac{a_1}{a_2}$$

$$= \left[ \frac{(0.5m_b f_{3j} + m_1 f_{1j})^2 + [0.5m_b f_{3k} + m_1 f_{1k} + 0.5m_\ell f_\ell \cos(\delta - \epsilon_\ell)/\cos \delta]^2}{(0.5m_b f_{4j} + m_2 f_{2j})^2 + [0.5m_b f_{4k} + m_2 f_{2k} + 0.5m_\ell f_\ell \cos(\delta + \epsilon_\ell)/\cos \delta]^2} \right]^{1/2}$$

(9.5)

Empirical inversion appears necessary in general (note that the triangle axes components of  $\underline{f}_1$ , etc., vary with  $\epsilon_\ell$ ), but a closed-form solution can be given for the case of parallel apparent loads from the results in figure 8.5:

$$\tan \epsilon_\ell = \operatorname{ctn} \delta \left[ \frac{\rho_T^* - 1}{\rho_T^* + 1} \frac{\Sigma L}{m_\ell f_\ell} + \frac{m_2 f_2 - m_1 f_1 + m_b \Delta f}{m_\ell f_\ell} \right]$$

## 10. GENERAL EQUILIBRIUM CONFIGURATIONS

The general equilibrium results for arbitrary tether angles given in figure 7.1 are reconsidered in this section to determine (1) the variation in system geometry and thrust requirements with the tether tilt angle  $\epsilon_{13}$ , and (2) the sensitivity of the geometry and thrust requirements to variations in the tilt angle from its optimum (minimum  $\Sigma T$ ) value. The previous results can be rearranged in terms of values at the optimum configuration and the effect of variations of the No. 1 tether tilt angle. Results are listed in figure 10.1 along with derivatives to indicate local sensitivity of the equilibrium configuration. The results are also illustrated graphically in figure 10.2 for an example case with unequal helicopters and drag forces on all bodies.

The general variations in tether force and thrust vectors with tether angle are readily characterized from the analytical results (fig. 10.1); only their components along the spreader bar vary with tether angle, and these variations are identical in magnitude to the variation in spreader-bar force for all four forces with opposite signs for the two tether forces and the two thrust vectors. In addition, the following properties of the variations can be seen.

First, the spreader-bar force increases linearly with the tilt-angle variation, expressed as  $\tan \epsilon_{13} - \tan \epsilon_{13}^*$ . Its proportionality factor  $\alpha_3$  is an increasing function of  $\epsilon_{13}$ ; that is, sensitivity to variation of the No. 1 tether tilt increases as the tether carries more of the cargo in the optimum configuration. At  $\epsilon_{13} = -\pi/2 + \delta$ , the No. 1 tether is unloaded and  $\alpha_3 \ll m_1 f l$ , whereas at  $\epsilon_{13} = \pi/2 - \delta$  the No. 1 tether carries the entire load and sensitivity increases an order of magnitude to  $\alpha_3 = m_1 f l \sin \delta$ . This variation in sensitivity with  $\epsilon_{13}$  is evident in figure 10.2(a) and also occurs for the other variables (e.g., figs. 10.2(b) and 10.2(d)). When expressed in terms of tilt-angle variations of the No. 2 tether,  $\tan \epsilon_{24} - \tan \epsilon_{24}^*$ , (fig. 10.1),  $F_{34}$  is found to be linear in this variation with proportionality factor,  $\alpha_4$ , which decreases with  $\epsilon_{13}$ ; that is, sensitivity to  $\epsilon_{24}$  increases with increased loading of the No. 2 tether.

The results (figs. 10.1 and 10.2(a)) also indicate that the spreader bar can be placed in tension for sufficiently large tilt-angle variations and that  $F_{34}$  becomes arbitrarily large at any  $\epsilon_{13}$  as  $|\epsilon_{13}|$  approaches  $\pi/2$ . However, the realizable range of  $F_{34}$ , tether angles, and system forces in equilibrium is limited by the helicopters' maximum thrust capabilities.

Second, the No. 2 tether angle,  $\tan \epsilon_{24}$ , varies linearly with  $\tan \epsilon_{13}$ ; its proportionality factor,  $-\alpha_3/\alpha_4$ , is negative [that is,  $\epsilon_{13}$  and  $\epsilon_{24}(\epsilon_{13})$  vary in opposite directions from the optimum configuration ( $\epsilon_{13}^*$ ,  $\epsilon_{24}(\epsilon_{13}^*)$ )] and increases with  $\epsilon_{13}$ . At  $\epsilon_{13} = -\pi/2 + \delta$  the No. 1 tether is nearly unloaded,  $\alpha_3/\alpha_4 \ll 1$ , and even large variations of  $\epsilon_{13}$  require very little change in  $\epsilon_{24}$  (fig. 10.2(b)). However, at  $\epsilon_{13} = \pi/2 - \delta$ , the sensitivity is very large,  $\alpha_3/\alpha_4 \gg 1$ , and the required angle  $|\epsilon_{24}|$  is driven to values near  $\pi/2$  by even small variations,  $\epsilon_{13} - \epsilon_{13}^*$ .

VARIABLE	GENERAL FORMULA	DERIVATIVES, $\left(\frac{d( )}{d \tan \epsilon_{13}}\right)^*$
F13 <u>u13</u>	$F13^* \underline{u13}^* - (F34 - F34^*) i_t$	$-\alpha_3 i_t$
F24 <u>u24</u>	$F24^* \underline{u24}^* + (F34 - F34^*) i_t$	$\alpha_3 i_t$
<u>T1</u>	$\underline{T1}^* + (F34 - F34^*) i_t$	$\alpha_3 i_t$
<u>T2</u>	$\underline{T2}^* - (F34 - F34^*) i_t$	$-\alpha_3 i_t$
F34	$F34^* + \alpha_3(\tan \epsilon_{13} - \tan \epsilon_{13}^*)$ $F34^* + \alpha_4(\tan \epsilon_{24} - \tan \epsilon_{24}^*)$	$\alpha_3$
$\tan \epsilon_{24}$	$\tan \epsilon_{24}^* - \frac{\alpha_3}{\alpha_4} (\tan \epsilon_{13} - \tan \epsilon_{13}^*)$	$-\frac{\alpha_3}{\alpha_4}$
F13	$F13^* \cos \epsilon_{13}^* / \cos \epsilon_{13}$	$\alpha_3 \sin \epsilon_{13}^*$
F24	$F24^* \cos \epsilon_{24}^* / \cos \epsilon_{24}$	$-\alpha_3 \sin \epsilon_{24}^*$
$\Sigma F$	$F13 + F24$	$\alpha_3(\sin \epsilon_{13}^* - \sin \epsilon_{24}^*)$
$\tan \epsilon_1$	$\tan \epsilon_1^* + \frac{\alpha_3}{\alpha_1} (\tan \epsilon_{13} - \tan \epsilon_{13}^*)$	$\frac{\alpha_3}{\alpha_1}$
$\tan \epsilon_2$	$\tan \epsilon_2^* - \frac{\alpha_3}{\alpha_2} (\tan \epsilon_{13} - \tan \epsilon_{13}^*)$	$-\frac{\alpha_3}{\alpha_2}$
T1	$T1^* \cos \epsilon_1^* / \cos \epsilon_1$	$\alpha_3 \sin \epsilon_1^*$
T2	$T2^* \cos \epsilon_2^* / \cos \epsilon_2$	$-\alpha_3 \sin \epsilon_2^*$
$\Sigma T$	$T1 + T2$	0

DEFINITIONS:

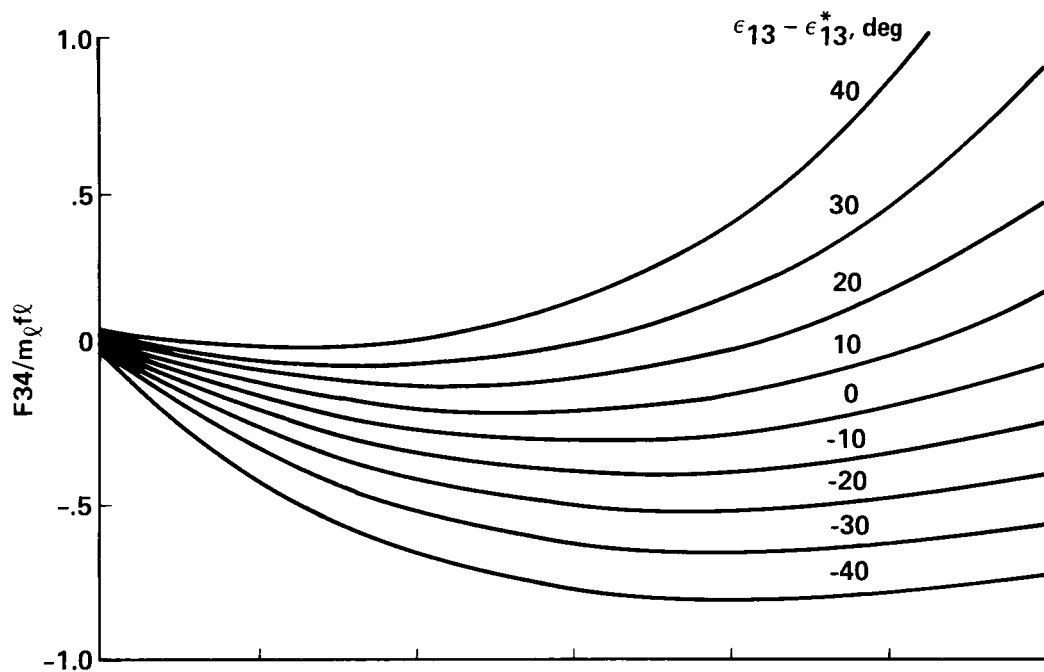
$$\alpha_1 = 0.5 \left\{ (m_b f_{3j} + m_1 f_{1j})^2 + [m_b f_{3k} + m_1 f_{1k} + m_\rho f_\rho \cos(\delta - \epsilon_\rho) / \cos \delta]^2 \right\}^{1/2}$$

$$\alpha_2 = 0.5 \left\{ (m_b f_{4j} + m_2 f_{2j})^2 + [m_b f_{4k} + m_2 f_{2k} + m_\rho f_\rho \cos(\delta + \epsilon_\rho) / \cos \delta]^2 \right\}$$

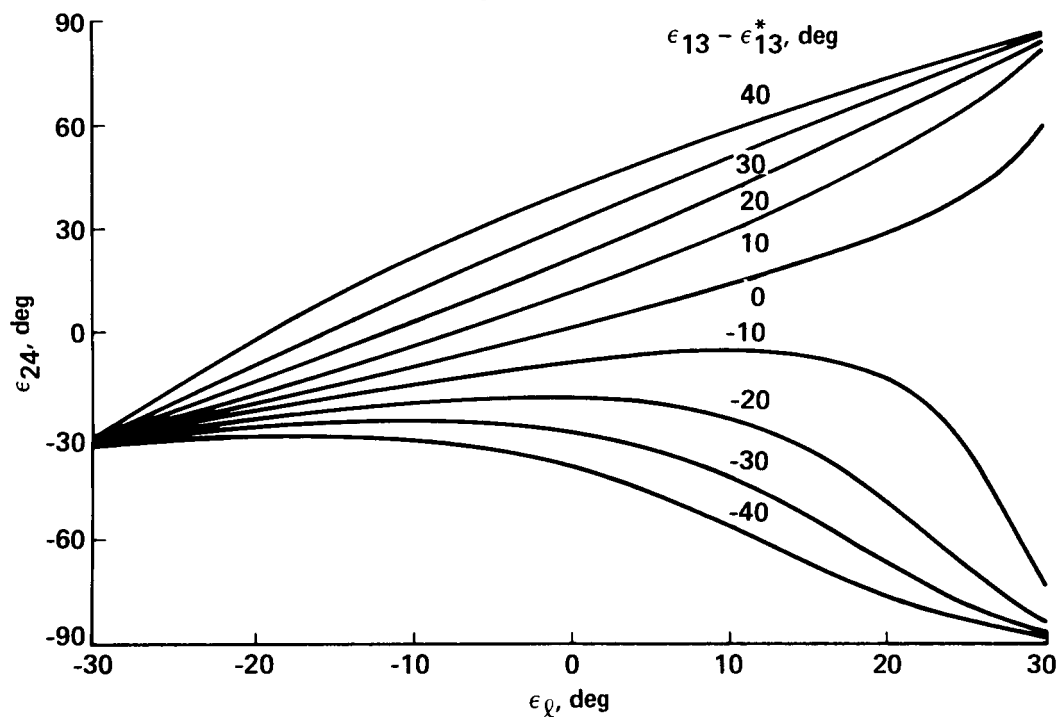
$$\alpha_3 = 0.5 \left\{ (m_b f_{3j})^2 + [m_b f_{3k} + m_\rho f_\rho \cos(\delta - \epsilon_\rho) / \cos \delta]^2 \right\}^{1/2}$$

$$\alpha_4 = 0.5 \left\{ (m_b f_{4j})^2 + [m_b f_{4k} + m_\rho f_\rho \cos(\delta + \epsilon_\rho) / \cos \delta]^2 \right\}^{1/2}$$

Figure 10.1.- Equilibrium configuration with tethers misaligned from the direction for minimum  $\Sigma T$ .

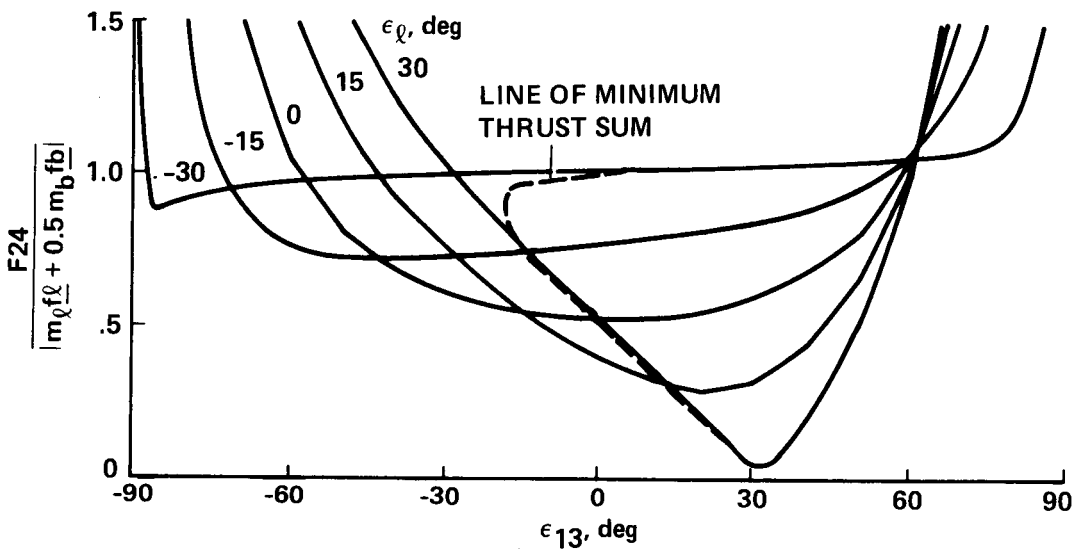
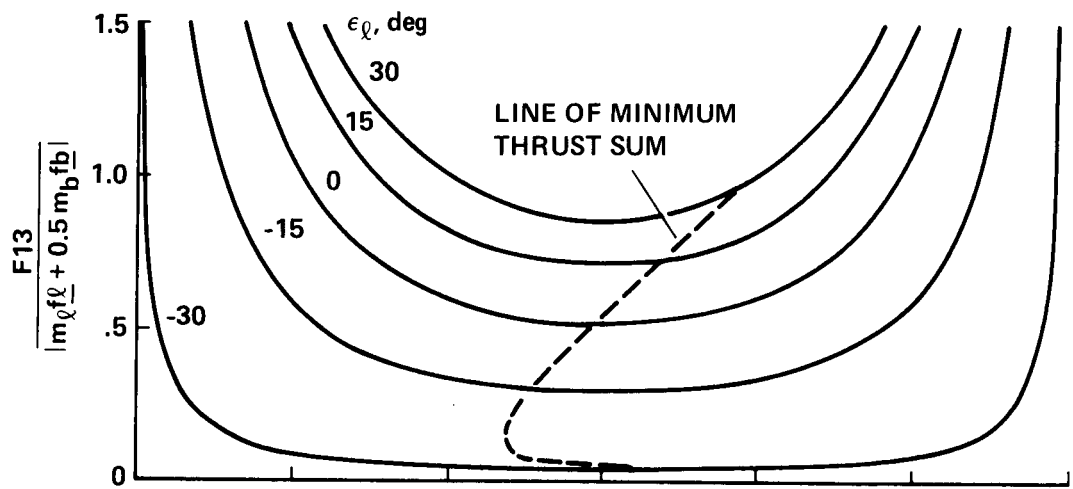


(a) SPREADER BAR FORCE



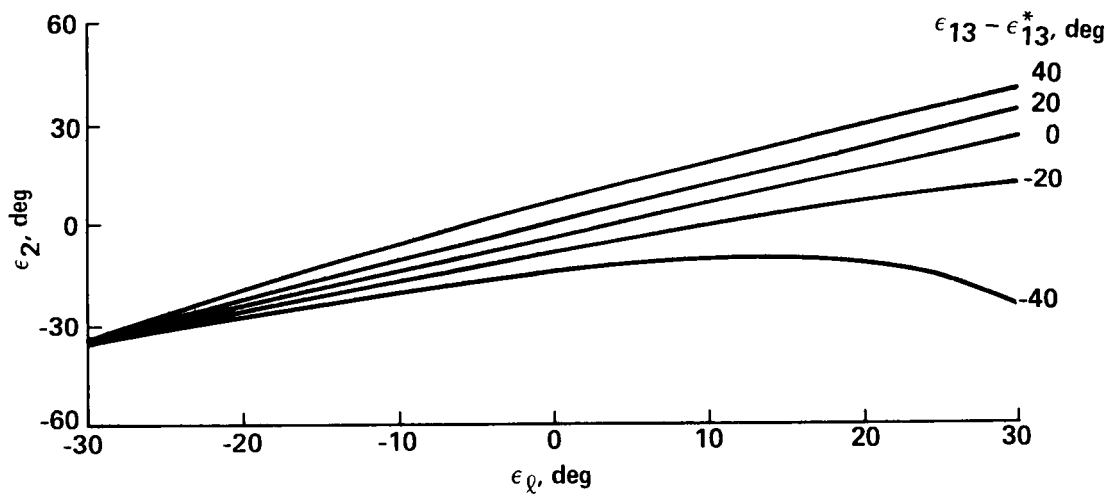
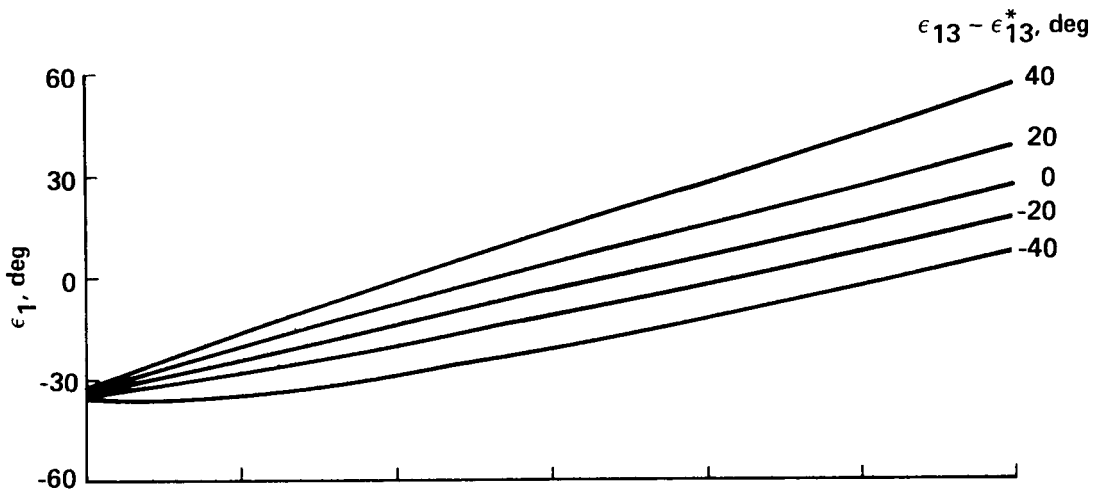
(b) TETHER TILT ANGLE - NO. 2 HELICOPTER

Figure 10.2.- Effect of non-optimum tether alignment ( $\epsilon_{13} - \epsilon_{13}^*$ ) on equilibrium characteristics:  $\delta = 60^\circ$ ,  $(m_b, m_1, m_2) = (0.1, 1, 2)m_L$ ,  $\underline{fa}_L = -0.25 \underline{l}_H$ ,  $\underline{fab} = -0.3 \underline{l}_H$ ,  $\underline{fa1} = \underline{fa2} = -0.1 \underline{l}_H$ ,  $\beta_t = 45^\circ$ .



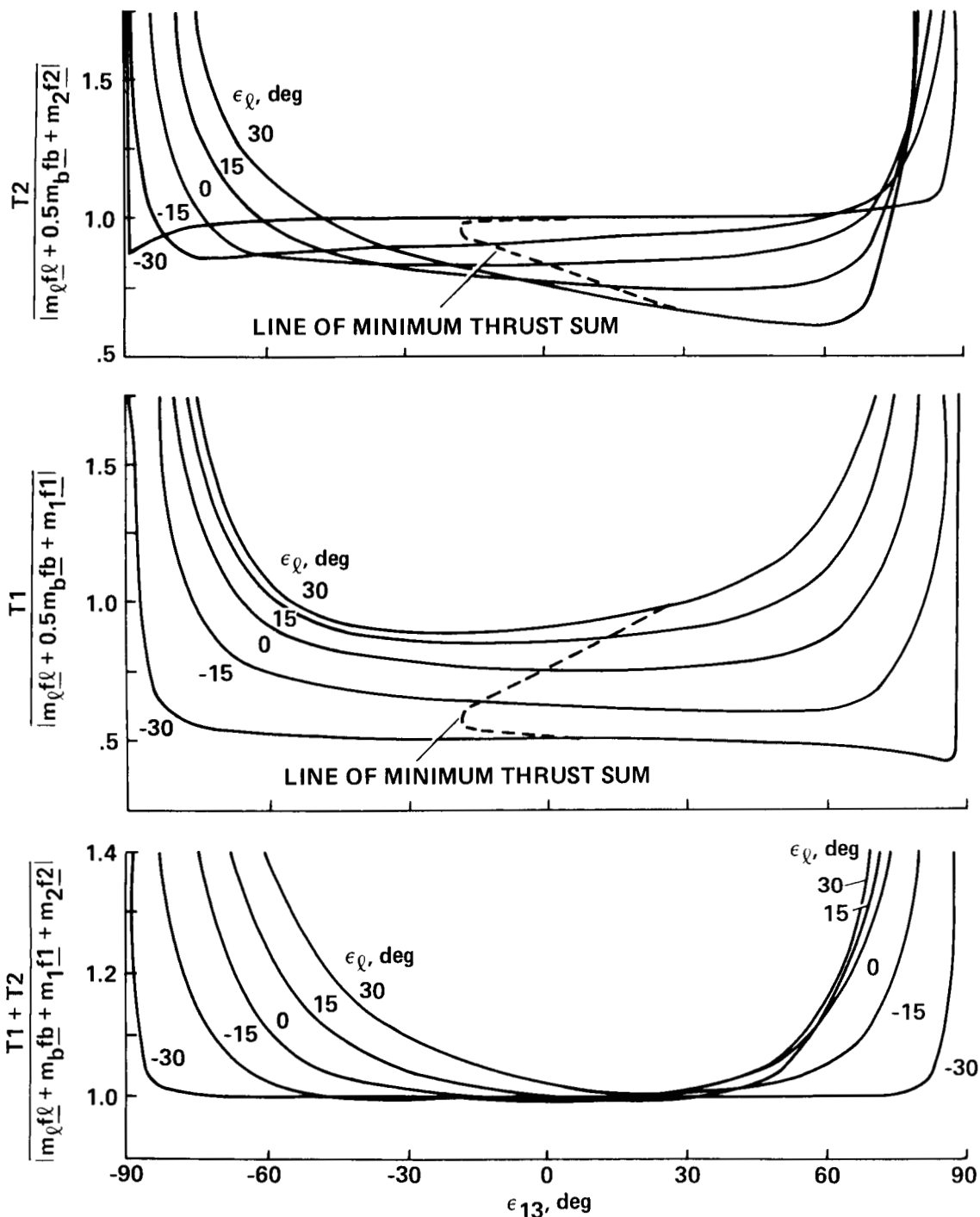
(c) TETHER CABLE TENSIONS

Figure 10.2.- Continued.



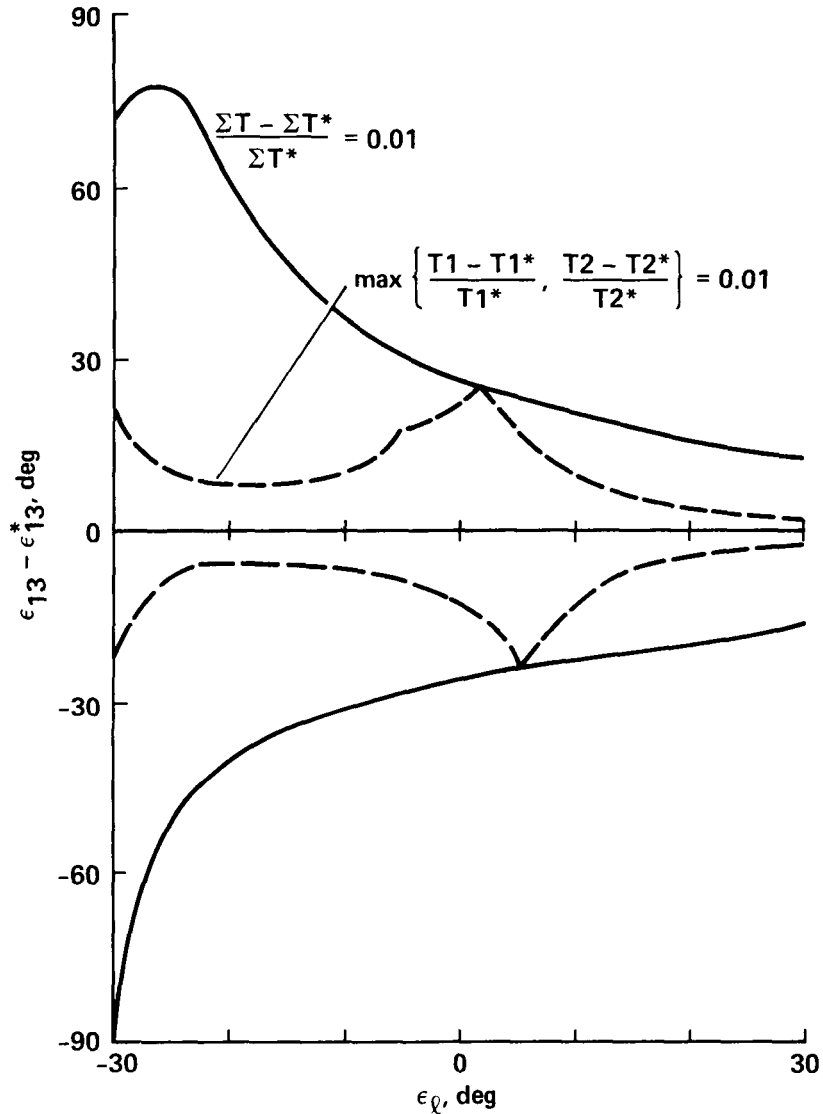
(d) HELICOPTER THRUST ANGLES

Figure 10.2.- Continued.



(e) HELICOPTER THRUST MAGNITUDES

Figure 10.2.- Continued.



(f) HELICOPTER THRUST SENSITIVITY: TETHER MISALIGNMENT FOR 1% PENALTY

Figure 10.2.- Concluded.

If  $\epsilon_{13}$  is given in terms of the misalignment of the No. 2 tether,

$$\tan \epsilon_{13} = \tan \epsilon_{13}^* - \frac{\alpha_4}{\alpha_3} (\tan \epsilon_{24} - \tan \epsilon_{24}^*)$$

it is seen that the reciprocal proportionality and the reverse sensitivity trend with  $\epsilon_l$  occurs. Thus, near the extremes of load sharing, the lightly loaded tether is required to undergo large variations in tether angle between  $\pm 90^\circ$  to maintain equilibrium in the presence of even small changes in the direction of the heavily loaded tether.

Third, the general variations of tether tensions are more easily anticipated from their relations with F34:

$$F13 = [(F34 + A - F13_0)^2 + \alpha_3^2]^{1/2}$$

$$F24 = [(F34 + A + F24_0)^2 + \alpha_4^2]^{1/2}$$

These are positive functions of F34 with a single minimum point and with arbitrarily large values as  $|F34| \rightarrow \infty$  or, equivalently, as  $|\epsilon_{13}| \rightarrow \pi/2$ . This behavior is seen in figure 10.2(c). The line of optimum configurations is included in the figure. It coincides with the minimum points of F13 and F24 when their derivatives are zero (fig. 10.1); this occurs at  $\epsilon_{13}^* = \epsilon_{24}^* = 0$  (e.g., at hover with  $\epsilon_\ell = 0$ ) and is very nearly obtained when these angles are both small (identical helicopters with  $\epsilon_\ell = 0$ ). More generally, these derivatives have opposite signs whenever  $\epsilon_{13}^*, \epsilon_{24}^*$  have the same signs, and (locally) one tension increases and the other decreases with  $\epsilon_{13} - \epsilon_{13}^*$ .

The derivatives of the tether-tension-sum (fig. 10.1) are zero and the tether-tension-sum is minimized at the optimum configuration simultaneously with  $\Sigma T$  whenever  $\epsilon_{13}^* = \epsilon_{24}^*$ ; this occurs at hover and for identical helicopters with  $\epsilon_\ell = 0$ .

Fourth, the thrust angles,  $\tan \epsilon_1, \tan \epsilon_2$ , vary linearly with the  $\tan \epsilon_{13}$  and in mutually opposite directions (fig. 10.1). Their sensitivities to tilt variations (fig. 10.2(d)) increase with  $\epsilon_\ell$  and are both smaller at nearly all  $\epsilon_\ell$  than the sensitivity of  $\epsilon_{24}$  (compare figs. 10.2(d) and 10.2(b)) because of the influence of the helicopter apparent loads in defining the required thrust-vector directions.

Last, the helicopter thrust magnitudes are positive functions with a single minimum and arbitrarily large values at  $|\epsilon_{13}| = \pi/2$ . This is seen in figure 10.2(e) for the example case. In general, the derivatives of T1 and T2 are equal and opposite at the optimum configuration (fig. 10.1) so that locally one thrust increases and the other decreases. This occurs because the optimum  $\epsilon_{13}^*$  always falls between the values of  $\epsilon_{13}$ , which minimize T1 and T2 separately. These derivatives are zero, and T1 and T2 are minimized, as well as  $\Sigma T$ , whenever  $\epsilon_1^* = 0$  or, equivalently, when the spreader bar is perpendicular to  $\Sigma L$  (when  $\Sigma L_1 = 0$ ); this occurs at  $\epsilon_\ell = 4^\circ$  for the example case, and usually occurs at small  $\epsilon_\ell$ . These derivatives are small (relative to  $m_\ell f_\ell$  per radian) when  $\epsilon_1^*$  is small (when  $|\Sigma L_1| \ll (\alpha_1 + \alpha_2)$ ).

The thrust-sum derivative is zero at the optimum configuration by construction, and its sensitivity to tilt variations is small in the example (fig. 10.2(e)). Sensitivity is examined further in figure 10.2(f), which shows the boundary of misalignments corresponding to a thrust-sum penalty of 1%. This encloses a region that narrows with  $\epsilon_\ell$  (from  $\pm 25^\circ$  at  $\epsilon_\ell = 0$  to  $-18^\circ, +12^\circ$  at  $\epsilon_\ell = 30^\circ$ ) and indicates a moderate increase in sensitivity with increased loading of the No. 1 tether. Similar calculations were made for each helicopter thrust, and the boundary for which both variations are under 1% of the optimum thrust is included in figure 10.2(f). This boundary is inside the corresponding boundary for  $\Sigma T$  at

all  $\epsilon_\lambda$ ; it meets that boundary in the vicinity of  $\epsilon_\lambda = 4^\circ$  where the derivatives of  $T_1$  and  $T_2$  are zero, and it narrows considerably to  $-3^\circ, +2^\circ$  at  $\epsilon_\lambda = 30^\circ$ .

These results indicate a broad optimum with respect to the choice of tether angle at and near equal load sharing and that the thrust requirements ( $T_1, T_2, \Sigma T$ ) are not sensitive to tether-tilt variations,  $\epsilon_{13} - \epsilon_{13}^*$  or  $\epsilon_{24} - \epsilon_{24}^*$  in this case. Thus, the configuration corresponding to  $B = 0$  with simpler formulas than the optimum (eq. (8.3); fig. 8.3) can be used for system flight coordination with little penalty. More generally, it is found that the sensitivity of system geometry and forces to misalignment of a tether from its optimum direction varies in proportion to the fraction of the apparent load that it carries, and that sensitivity to one or the other tether angles,  $\epsilon_{13}$  or  $\epsilon_{24}$ , increases with unequal load sharing. Near the extremes of  $\epsilon_\lambda$ , the equilibrium direction of the unloaded tether becomes very sensitive to variations in the direction of the loaded tether. This suggests difficulty in flying a system if the load distribution differs by as much as an order of magnitude.

## 11. CONCLUSIONS

The characteristics of a dual-lift helicopter system in equilibrium flight along any reference trajectory within its operational domain were examined. The system consists of two helicopters with a spreader-bar suspended below the helicopters on cables and the cargo suspended by cables from the ends of the spreader-bar.

System characteristics (suspension geometry and forces, thrust-vector requirements) are obtained by solving the force-balance equations at various points on the configuration, assuming that the c.g. accelerations and aerodynamic forces on the component bodies of the system are known. It can be shown that these quantities can be determined exactly, or to a good approximation, from the reference trajectory and from the force and moment descriptions of the bodies independent of solving the force-balance equations. Closed-form solutions of the force-balance equations can then be given with the c.g. accelerations and aerodynamic forces appearing parametrically. For each body, these quantities appear only as the combination of weight, inertia reaction, and aerodynamic force, which in this report is termed the apparent load ( $m\mathbf{f} = m(\mathbf{g} - \mathbf{a}) + \mathbf{F}_a$ ).

The detailed analytical results are summarized in the restricted trim algorithm (shown in fig. 8.7) and in the following conclusions:

1. At any given flight condition, the force-balance equations have multiple solutions corresponding to three redundant configuration angles which can be selected by the pilot or autopilot. These can be taken as the spreader-bar heading relative to the ground track (formation angle,  $\beta_t$ ); the spreader-bar tilt relative to the apparent suspended load vector ( $\epsilon_\lambda$ ), which determines load distribution; and the tilt of the No. 1 helicopter's tether relative to the spreader bar ( $\epsilon_{13}$ ), which determines the thrust-sum requirements. In equilibrium flight along a reference trajectory, the relative positions of the system's bodies are fixed or very nearly fixed (relative to axes attached to the load-spreader bar triangle) on any quasi-steady flight segment, with movement to new relative positions during transient maneuvering between these segments. This assumes the redundant configuration variables are maintained invariant on these segments.

2. Some limits on the parameters of the problem are required for the existence of solutions with appropriate properties. First, one bridle cable becomes slack if the other is aligned with the apparent suspended load, and both bridle cables are in tension only if the tilt  $|\epsilon_\lambda|$  is less than  $\pi/2 - \delta$ , where  $\delta$  is the angle between the spreader bar and either bridle cable. Second, the triangle is right side up at any  $\beta_t$  and at any admissible  $\epsilon_\lambda$  if the angle between the apparent suspended load and the vertical is less than  $\delta$ . This limits the combined c.g. acceleration and aerodynamic specific force of the suspended load for which the suspension is appropriate. Third, the tethers are in tension with the helicopters on the opposite side of the spreader bar from the cargo and their thrust is directed away from the spreader bar if the specific apparent load differences between the cargo and the other bodies are bounded; that is, if  $|\underline{f}_1 - \underline{f}_\lambda|$ ,  $|\underline{f}_2 - \underline{f}_\lambda|$ ,  $|\underline{f}_b - \underline{f}_\lambda| < f_\lambda \sin \delta$ .

3. The inertial orientation of the triangle formed by the spreader bar and the suspended load varies along a reference trajectory and is defined by the condition that it always contain the apparent suspended load at the selected values of  $\beta_t, \epsilon_\ell$ . It is expected that the system will be flown with a fixed or slowly varying formation angle. The required spreader-bar pitch and load-swing variations with maneuvering and load aerodynamic force depend principally on  $\beta_t$ ; if the formation is longitudinal or transverse to the ground track, then turns or speed-change maneuvers and lateral or longitudinal aerodynamic forces correspond to decoupled variations in bar pitch or load swing from their attitude in unaccelerated low-speed flight. For intermediate formation angle, the required load swing and bar tilt are coupled.

4. The required thrust-sum depends on the tether angle and is very nearly invariant with  $\epsilon_\ell$  and  $\beta_t$ . The tether angle can be selected for minimum thrust-sum; this maximizes the system thrust margin and also minimizes fuel rate at most flight conditions in the case of identical helicopters. A lower bound on the required thrust-sum is given by the magnitude of the sum of apparent loads:  
$$\Sigma L = |m_\ell \underline{f}_\ell + m_b \underline{f}_b + m_1 \underline{f}_1 + m_2 \underline{f}_2|$$
. This value is reached for special cases of interest (for identical helicopters with equal loading and at hover) and the corresponding thrust vectors are along  $-\underline{\Sigma L}$ . More generally, in empirical results for a comprehensive set of cases, the minimum required thrust-sum was found to be within 1% of this lower bound with small angles between  $-\underline{\Sigma L}$  and the thrust directions.

5. The tether directions for the minimum thrust-sum configuration are as follows. For identical helicopters with equal load sharing, the two tethers must be parallel to the sum of the apparent loads owing to the suspended load and spreader bar, and very nearly perpendicular to the spreader bar. More generally, if the apparent loads are all parallel, the entire system is coplanar with tethers and thrust vectors parallel to the common direction; this occurs at hover and is nearly obtained at low speeds for any flight condition, helicopter pair, or load distribution. At higher speeds, these directions become nonparallel and noncoplanar to moderate angles; principally because of the differences between the cargo and helicopter specific aerodynamic forces; however, the tethers are always close to the plane of the triangle except near the extreme case of an unloaded tether.

6. The ratio of thrust requirements for the two helicopters depends solely on the spreader-bar tilt, assuming that the tether directions are selected to minimize the thrust-sum. A suitable choice for this ratio is given by the helicopters' thrust limits,  $T1_{\max}/T2_{\max}$ . This value is required when the cargo weight is the maximum possible for the helicopter pair and is always a possible choice for smaller weights. For identical helicopters, equal loading is obtained with the spreader bar perpendicular to the apparent suspended load.

7. If the tether tilt angle  $\epsilon_{13}$  is selected to be different from the value for minimum thrust-sum, then the corresponding changes in the equilibrium configuration can be summarized as follows. First, thrust and tether force vectors vary only in their components along the spreader bar; these variations equal in magnitude the change in spreader-bar force from its optimum value, but with opposite signs for the two tether forces and the two thrust vectors. Second, spreader-bar force and the

dependent tilt angles vary linearly with the misalignment (with  $\tan \epsilon_{13}$ ), and sensitivity increases with unequal load distribution (with  $|\epsilon_{\lambda}|$ ). Third, the thrust requirements for each helicopter and their sum,  $T_1$ ,  $T_2$ ,  $\Sigma T$ , are simultaneously minimized at the optimum configuration in the special case that the spreader-bar is perpendicular to  $\underline{\Sigma L}$ . For this case and for small values of  $\epsilon_{\lambda}$  the sensitivity of thrust requirements to misalignments is much smaller than  $m_{\lambda} f_{\lambda}$  per radian.

Ames Research Center  
National Aeronautics and Space Administration  
Moffett Field, California 94035  
March 3, 1986

APPENDIX

FORCE BALANCE AT THE SPREADER BAR ENDPOINTS

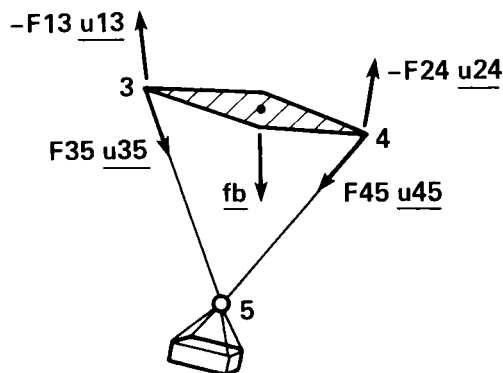
The forces applied to the spreader bar by the cables (see sketch) are

$$\underline{F13} = -F13 \underline{u13}$$

$$\underline{F24} = -F24 \underline{u24}$$

$$\underline{F35} = F35 \underline{u35}$$

$$\underline{F45} = F45 \underline{u45}$$



and the bar's rigid-body equations of motion are

$$\underline{F13} + \underline{F24} + \underline{F35} + \underline{F45} = -m_b \underline{fb} \tag{A1}$$

$$0.5 L34 \underline{i}_t \otimes (\underline{F13} + \underline{F35} - \underline{F24} - \underline{F45}) = \dot{\underline{Hb}} - \underline{Mab}$$

where  $\underline{Mab}$  is the spreader-bar aerodynamic moment about its midpoint, and  $\dot{\underline{Hb}}$  is its angular momentum rate owing to  $\underline{\omega b}, \dot{\underline{\omega b}}$ . These equations contain no information on the spreader-bar compression, so the force-balance equations for its endpoints are written as

$$\underline{F13} + \underline{F35} - F34 \underline{i}_t = \underline{a} \tag{A2}$$

$$\underline{F24} + \underline{F45} + F34 \underline{i}_t = \underline{b}$$

where  $\underline{a}$  and  $\underline{b}$  contain the effects of spreader-bar mass and motion. Appropriate expressions for  $\underline{a}$  and  $\underline{b}$  can be obtained by imposing consistency of equation (A2) with equation (A1); from which

$$\underline{a} + \underline{b} = -m_b \underline{fb}$$

$$0.5 L34 \underline{i}_t \otimes (\underline{a} - \underline{b}) = \dot{\underline{Hb}} - \underline{Mab}$$

and then solving for  $\underline{a}, \underline{b}$ :

$$\underline{a} = -0.5 m_b \underline{fb} - \underline{i}_t \otimes (\dot{\underline{Hb}} - \underline{Mab})/L34 - c \underline{i}_t \tag{A3}$$

$$\underline{b} = -0.5 m_b \underline{fb} + \underline{i}_t \otimes (\dot{\underline{Hb}} - \underline{Mab})/L34 + c \underline{i}_t$$

where  $c$  is arbitrary. However,  $c$  can be combined with  $F_{34}$  in equation (A2) without loss of generality.

The results in equation (A3) appear in equations (3.1) in the text in the form

$$\underline{a} = -0.5 m_b \underline{f3} = -0.5 m_b (\underline{fb} + \underline{\Delta f})$$

$$\underline{b} = -0.5 m_b \underline{f4} = -0.5 m_b (\underline{fb} - \underline{\Delta f})$$

where

$$\underline{\Delta f} = \frac{2}{m_b L_{34}} \underline{i}_t \otimes (\underline{\dot{H}b} - \underline{Mab})$$

or, in scalar form,

$$\Delta f_t = \frac{2}{m_b L_{34}} [0, -(\dot{H}b_k - Mab_k), (\dot{H}b_j - Mab_j)]^T$$

$$\dot{H}b_t = E_1(\phi_t) [Jb \dot{\omega}b_b + S(\omega b_b) Jb \omega b_b]$$

$$\underline{\omega}b = \dot{\psi}_t k_N + \dot{\theta}_t (-\sin \psi_t \underline{i}_N + \cos \psi_t \underline{j}_N)$$

$$T_{b,N} = E_2(\theta_t) E_3(\psi_t)$$
(A4)

and  $\Delta f_t$  can be computed from these equations assuming that  $Mab_t$ ,  $\phi_t$ ,  $\theta_t$ ,  $\psi_t$ ,  $\dot{\theta}_t$ , and  $\dot{\psi}_t$  are known for equilibrium flight.

Last, we note that  $\underline{\Delta f}$  is expected to be negligible (of the order of 0.01 g) in equilibrium at all points on a reference trajectory and can be neglected in computations. To estimate the size of  $\underline{\Delta f}$ , assume that the spreader bar is a body of revolution which is lengthwise symmetric about the midpoint cross-sectional plane and has a lengthwise mass distribution that is constant or that declines with distance from the midpoint. Then,

$$Jb = \text{diag} (I_i)$$

$$\max_i (I_i) \leq m_b L_{34}^2 / 12$$

and

$$|\underline{\Delta f}| \leq \frac{L_{34}}{6} \left( |\underline{\dot{\omega}b}| + \omega b^2 + \frac{|\underline{Mab}|}{I_{\max}} \right)$$
(A5)

where it can be shown for the present context that  $|\underline{\omega}b| \approx |\dot{\psi}_y|$ . We expect, for reference trajectories within the operational domain and for typical spreader-bar lengths and aerodynamics, that equation (A5) yields  $|\underline{\Delta f}| \ll 0.1$  g. However,  $\underline{\Delta f}$  is retained in the analytical results for completeness.

## REFERENCES

1. Carter, E. S.: Implication of Heavy Lift Helicopter Size Effect Trends and Multilift Options for Filling the Need. Proceedings of the Eighth European Rotorcraft Forum, Aix-en-Provence, France, Sept. 1982.
2. Carter, E. S.; Cooper, D. E.; and Knapp, L. G.: Single Rotor Options for Heavy Lift and Potential of Multilift. SAE Paper No. 791087, Dec. 1974.
3. Sherman, P. F.; et al.: Feasibility Study for Multiple Helicopter Heavy Lift Systems. Report R-136, VERTOL Aircraft Corporation, Philadelphia, Pa., Oct. 1957.
4. Maciolek, J. R.; et al.: Preliminary Multilift Feasibility Study. Report SER 64460, Sikorsky Aircraft Company, Stratford, Conn., May 1969.
5. Meek, T.; Chesley, G. B.; et al.: Twin Helicopter Lift System Study and Feasibility Demonstration. Report SER 64323, Sikorsky Aircraft Company, Stratford, Conn., Dec. 1970.
6. Maciolek, J. R.: Master-Slave Controller for Twin Lift Systems. Report SER 6647, Sikorsky Aircraft Company, Stratford, Conn., Dec. 1970.
7. Curtiss, H. C.; and Warburton, F. W.: Stability and Control of the Twin-Lift Helicopter System. J. Am. Helicopter Soc., Apr. 1985. (Also, Proceedings of the 40th Annual National Forum of the American Helicopter Society, 1984.)
8. Wilson, G. J.; and Newton, N. N.: Evaluation, Development, and Advantages of the Helicopter Tandem Dual Cargo Hook System. AGARDograph CP-121, Feb. 1973.
9. Hutto, A. J.: Qualitative Report on Flight Test of a Two-Point External Load Suspension System. Paper No. 473, Proceedings of the 26th Annual National Forum of the American Helicopter Society, June 1970.
10. Sheldon, D. F.: An Appreciation of the Dynamic Problems Associated with the External Transportation of Loads from a Helicopter--The State of the Art. Proceedings of the First European Rotorcraft and Powered Airlift Forum, Southampton, U.K., Sept. 1975. (Also, Vertica, vol. 1, 1977.)
11. Taylor, M. J. H.: Helicopters of the World. Scribner, New York, 1978.
12. Davis, J. M.; Bennett, R. L.; and Blankenship, B. L.: Rotorcraft Flight Simulation with Aeroelastic Rotor and Improved Aerodynamic Representation. Vol. 1, TR-74-10A, U.S. Army Air Mobility Research and Development Laboratory, Ft. Eustis, Va., June 1974.

13. Talbot, P. D.; et al.: A Mathematical Model of a Single Main Rotor Helicopter for Piloted Simulation. NASA TM-84281, 1982.
14. Biggers, J. C.; et al.: Wind Tunnel Tests of Two Full Scale Helicopter Fuselages. NASA D-1548, 1962.
15. Shaughnessy, J. D.; et al.: Development and Validation of a Piloted Simulation of a Helicopter and External Sling Load. NASA TP-1285, 1979.
16. Hilbert, K. B.: A Mathematical Model of the UH-60 Helicopter. NASA TM-85890, 1984.
17. Weber, J. M.; et al.: A Mathematical Simulation Model of a CH-47B Helicopter. NASA TM-84351, 1984.
18. Houck, J. A.; Gibson, L. H.; and Steinmetz, G. G.: A Real-Time Digital Computer Program for the Simulation of a Single Rotor Helicopter. NASA TM X-2872, 1974.
19. Sheldon, D. F.; and Pryor, J.: A Study on the Stability and Aerodynamic Characteristics of Particular Military Loads Underslung from a Helicopter. Report TN-AM/40, Royal Military College of Science, Shrivenham, U.K., Apr. 1973.
20. Pryor, J.; and Sheldon, D. F.: A Wind Tunnel Investigation of Yaw Instabilities of Box-Shaped Loads Underslung from a Helicopter on a Tandem Suspension. Report TN-AM/62, Royal Military College of Science, Shrivenham, U.K., Dec. 1974.
21. Watkins, T. C.; Sinacori, J. B.; and Kesler, D. F.: Stabilization of Externally Slung Helicopter Loads. Report TR-74-22, U.S. Army Air Mobility Research and Development Laboratory, Fort Eustis, Va., Aug. 1974.
22. Matheson, N.: Stability of Helicopter Slung Loads. Aerodynamics Note 364, Department of Defense, Aeronautical Research Laboratories, Melbourne, Australia, Aug. 1976.
23. Laub, G. H.; and Kodani, H. M.: Wind Tunnel Investigation of Aerodynamic Characteristics of Scale Models of Three Rectangular-Shaped Cargo Containers. NASA TM X-62169, 1972.
24. Laub, G. H.; and Kodani, H. M.: Wind Tunnel Investigation of Aerodynamic Characteristics of a Scale Model of a D5 Bulldozer and an M109 Self-Propelled 155-mm Howitzer. NASA TM X-62330, 1974.

1. Report No. NASA TP-2615	2. Government Accession No.	3. Recipient's Catalog No.	
4. Title and Subtitle General Equilibrium Characteristics of a Dual-Lift Helicopter System		5. Report Date July 1986	6. Performing Organization Code
		8. Performing Organization Report No. A-86114	10. Work Unit No.
7. Author(s) L. S. Cicolani and G. Kanning		11. Contract or Grant No.	
		13. Type of Report and Period Covered Technical Paper	
9. Performing Organization Name and Address Ames Research Center Moffett Field, CA 94035		14. Sponsoring Agency Code 505-66-01	
		12. Sponsoring Agency Name and Address National Aeronautics and Space Administration Washington, DC 20546	
15. Supplementary Notes Point of contact: L. S. Cicolani, Ames Research Center, M/S 210-3, Moffett Field, CA 94035, (415)694-5446 or FTS 464-5446			
16. Abstract  The equilibrium characteristics of a dual-lift helicopter system are examined. The system consists of the cargo attached by cables to the endpoints of a spreader bar which is suspended by cables below two helicopters. Results are given for the orientation angles of the suspension system and its internal forces, and for the helicopter thrust vector requirements under general circumstances, including nonidentical helicopters, any accelerating or static equilibrium reference flight condition, any system heading relative to the flight direction, and any distribution of the load to the two helicopters. Optimum tether angles which minimize the sum of the required thrust magnitudes are also determined.  The analysis does not consider the attitude degrees of freedom of the load and helicopters in detail, but assumes that these bodies are stable, and that their aerodynamic forces in equilibrium flight can be determined independently as functions of the reference trajectory. The ranges of these forces for example helicopters and loads are examined and their effects on the equilibrium characteristics are given parametrically in the results.			
17. Key Words (Suggested by Author(s)) Dual lift equilibrium Dual lift Slung loads Helicopters		18. Distribution Statement Unclassified - Unlimited  Subject Category 01	
19. Security Classif. (of this report) Unclassified	20. Security Classif. (of this page) Unclassified	21. No. of Pages 88	22. Price* A03

\*For sale by the National Technical Information Service, Springfield, Virginia 22161